



Wrocław University  
of Science and Technology

## Doctoral Thesis

Synthesis, characterisation, and functionalisation of colloidal semiconductor nanoparticles displaying nonlinear optical activity

Synteza, charakterystyka i funkcjonalizacja koloidalnych nanocząstek półprzewodnikowych wykazujących aktywność nieliniowo optyczną

by Katarzyna Celina Nawrot, Msc Eng.

Wrocław University of Science and Technology  
Faculty of Chemistry  
Advanced Materials Engineering and Modelling Group

Supervisor: Dr. Marcin Nyk Associate Professor

This research was supported by the National Science Centre  
under grant no. UMO- 2018/29/B/ST4/02172.

Wrocław, 2022

# Table of Contents

List of abbreviations .....	3
TPEE – two-photon excited emission.....	3
Abstract.....	4
Abstract in Polish (Streszczenie pracy) .....	5
Wprowadzenie .....	5
Wyniki eksperymentalne i dyskusja .....	8
Podsumowanie .....	20
1. INTRODUCTION .....	22
2. PURPOSE AND SCOPE OF THE WORK.....	26
3. THEORY .....	27
3.1. Excitation and following processes.....	28
3.2. Third-order nonlinear optical processes.....	31
3.2.1. <i>Determining <math>\sigma_2</math> via two-photon excited emission method</i> .....	33
3.2.2. <i>Determining <math>\sigma_2</math> via Z-scan method</i> .....	34
3.3. Materials .....	36
3.3.1. <i>Colloidal semiconductor quantum dots (QDs)</i> .....	37
3.3.2. <i>Two-dimensional semiconductor nanomaterials – colloidal nanoplatelets</i> .....	42
4. EXPERIMENTAL.....	54
4.1. Methods.....	54
4.1.1. Synthesis .....	55
4.1.2. Characterisation .....	56
4.2. Colloidal semiconductor nanomaterials: synthesis, characterisation, and functionalisation.....	60
4.2.1. Cadmium Sulfide QDs.....	61
4.2.2. Cadmium selenide NPLs.....	71
5. CONCLUSION.....	109
References.....	111
Appendix (Achievements) .....	123
Publications included in PhD thesis.....	124
Publications not included in PhD thesis.....	124
Conference presentations .....	125

## List of abbreviations

BSA – bovine serum albumin

EBE – exciton binding energy

EDX – energy dispersive X-ray

GM – Goepfert-Mayer units

HH – heavy hole

LH – light hole

MB – methylene blue

MTT – 3-(4,5-dimethylthiazol-2-yl)-2,5-diphenyltetrazolium bromide

NC(s) – nanocarrier(s)

NLO – nonlinear optical

NPL(s) – nanoplatelet(s)

QD(s) – quantum dot(s)

QLED – quantum light-emitting diode

QY – quantum yield

RGM – refractive Goepfert-Mayer units

TEM – transmission electron microscopy/microscope

TPA – two-photon absorption

TPEE – two-photon excited emission

## Abstract

The dissertation discusses semiconductor nanomaterials, their interaction with light and the impact of their size and shape on the strength of the phenomena occurring within or involving subjected nanomaterials, especially charge separation and NLO properties. Several functionalisation approaches are also presented aimed for enhancement, introduction or inhibition of certain physicochemical properties along with simultaneous preservation of desired behaviour.

In the experimental part, CdS QDs and CdSe NPLs of different thicknesses were synthesised, characterized, and subjected to functionalisation. Hydrophilic penicillamine-capped CdS QDs were decorated with gold nanostructures in order to entrap electrons after light-induced excitation and employ them or separated holes for reduction or oxidation reactions, respectively. The concentration of embedded gold was optimized for preservation of nonlinear optical (NLO) properties with the two-photon absorption (TPA) cross section of  $15.8 \times 10^3$  GM, making the resulting CdS-Au nanohybrids a multifunctional nanomaterial exhibiting both photocatalytical and NLO properties in line with an important new direction for nanomedicine - theranostics - which combines therapeutic and diagnostic functionalities. CdSe NPLs of three different thicknesses were synthesised and their optical properties were investigated, leading to determination of thickness-dependent exciton binding energy with a new method that combines optical absorption spectroscopy and photoacoustic spectroscopy. 5.5 ML CdSe NPLs with the TPA cross section of  $8.0 \times 10^4$  GM were chosen as a model material for functionalisation towards biological application, especially in bioimaging. Encapsulation in polymeric NCs was selected as a hydrophilization method, which also provided cell viability after incubation without any significant change in optical spectra and preserving nonlinear absorption and two-photon excited emission (TPEE) properties as well as being visible through a two-photon microscope. The TPA cross section of polymeric NCs filled with 5.5 ML CdSe NPLs was estimated as  $2.0 \times 10^8$  GM. 4.5 ML CdSe NPLs were chosen for studies on the relation between noble metal doping and NLO properties. Doping with silver and copper ions led to the TPA cross sections of up to  $5.44 \times 10^6$  GM and  $1.33 \times 10^7$  GM, respectively, and thus appears to be a method for enhancement of NLO properties of semiconductor NPLs without increasing their volume.

The above-mentioned examples highlight functionalisation as a promising method to improve desired parameters of semiconductor nanoparticles. In particular, the accent was put on NLO properties and, indeed, exceptionally high TPA cross sections and intensive following emission was achieved which opens a range of currently essential applications possibilities including multiphoton microscopy for biology or encryption. Moreover, more than one function may be introduced to a nanomaterial to aim at such specialized applications as theranostics, complex anti-counterfeiting and future advanced photovoltaic systems.

## **Abstract in Polish (Streszczenie pracy)**

### **Wprowadzenie**

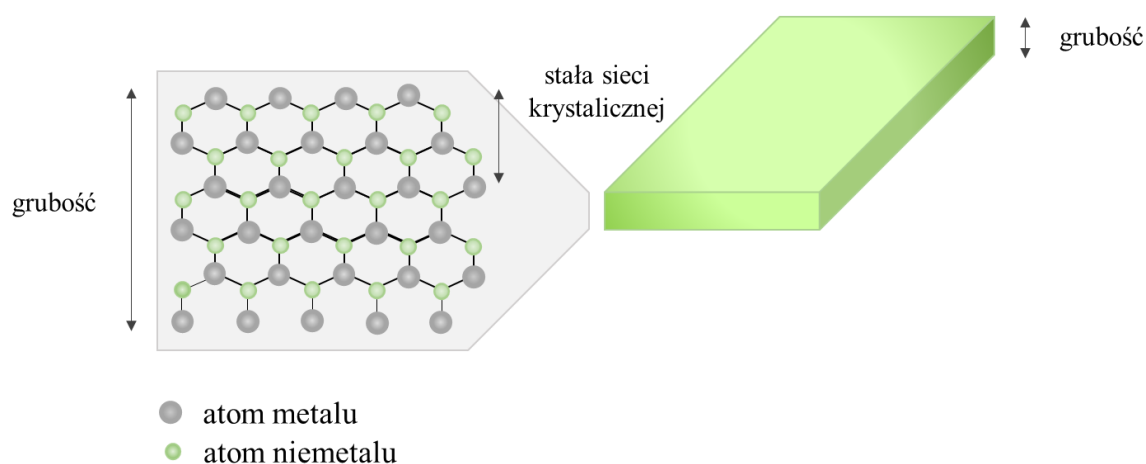
Niniejsza rozprawa odnosi się do koloidalnych nanomateriałów półprzewodnikowych i wpływie ich struktury na oddziaływania ze światłem, w szczególności na optyczne nieliniowe procesy trzeciorzędowe. Przedstawia możliwości intencjonalnej zmiany rozmiaru, w tym selektywnie poszczególnymi wymiarami nanocząstki, by w konsekwencji kontrolować spektrum absorbowanego oraz emitowanego przez nie światła, zarówno o niskiej intensywności, co prowadzi do liniowych zjawisk optycznych, gdy jeden foton absorbowany odpowiada jednemu fotonowi emitowanemu, jak i intensywności wysokiej, która jest odpowiedzialna za przewagę występowanie zjawisk nieliniowo optycznych. W tym przypadku możliwa jest konwersja energii w górę poprzez mechanizm jednoczesnej absorpcji kilku fotonów o relatywnie niskiej energii i następującej po niej emisji jednego fotonu o wyższej energii. Właściwości optyczne nanocząstek półprzewodnikowych mogą być również modyfikowane poprzez odpowiednie techniki funkcjonalizacji, które pozwalają na zachowanie, wzmocnienie lub wprowadzenie pożądanych cech wraz z jednoczesnym zniwelowaniem tych szkodliwych. Funkcjonalizacja może obejmować ingerencję w strukturę nanocząstki poprzez wprowadzenie defektów lub mieć charakter zewnętrzny, co może oznaczać osadzenie na ich powierzchni innych struktur zapewniając powstanie nowych interakcji, manipulację ligandami otaczającymi koloidalne nanocząstki czy enkapsulację materiału w wybranych

nośnikach. Kierunek manipulacji właściwościami zależy od pożądaných efektów, a w praktyce, od planowanych zastosowań.

W pracy opisane zostały dwa rodzaje materiałów koloidalnych: nanocząstki zerowymiarowe z siarczku kadmu, zwane dalej kropkami kwantowymi CdS oraz kwasi-dwuwymiarowe nanocząstki z selenku kadmu, inaczej nanopłytki CdSe. Przedstawiono syntezę hydrofilowych chiralnych kropek kwantowych CdS i wzmocnienie efektu separacji ładunku pod wpływem ekspozycji na światło występującego w półprzewodnikach poprzez osadzenie na ich powierzchni nanostruktur złota będącego odbiorcą wzbudzonych elektronów. Taki transfer ładunku utrudnia rekombinację, co objawia się w postaci wygaszania emisji, lecz również pozwala na wykorzystanie elektronów i dziur w procesach wymagających przepływu ładunku, czy też w chemicznych reakcjach redukcji i utleniania prowadzonych przy ekspozycji na światło. Ponadto, ilość osadzanego złota jest dobrana w taki sposób, aby wprowadzić właściwości fotokatalizujące reakcje redox przy jednoczesnym zachowaniu możliwości wzbudzania dwufotonowego i następującej po nim emisji światła. Hydrofilowe chiralne hybrydowe nanocząstki CdS-Au są zatem nanomateriałem o rozszerzonych funkcjonalnościach i mogą służyć jako model do zastosowań w teranostyce medycznej, gdzie część diagnostyczna związana jest z możliwością wzbudzenia nanocząstek poprzez mechanizm absorpcji dwufotonowej za pomocą fal elektromagnetycznych w zakresie podczerwieni w tzw. biologicznym oknie transmisji, obejmującym długości fal słabo oddziałujących z tkankami biologicznymi, i obrazowania dzięki dwufotonowo wzbudzonej emisji, natomiast za część terapeutyczną odpowiadają właściwości fotokatalityczne, które umożliwiają generację reaktywnych form tlenu stosowanych w terapii fotodynamicznej.

Typowe nanomateriały półprzewodnikowe mają kształt zbliżony do sferycznego i średnicę mniejszą od lub zbliżoną do ekscytonowego promienia Bohra, czego konsekwencją jest ograniczenie przestrzenne dla elektronów, zwane ograniczeniem kwantowym, które z kolei skutkuje zmianą struktury elektronowej objawiającej się, m.in. zwiększeniem przerwy wzbronionej i pojawieniem się emisji w zakresie światła widzialnego. Takie ograniczenie w każdym z kierunków wykazują wspomniane wyżej kropki kwantowe CdS. Jednakże obecny stopień zaawansowanie metod inżynierii materiałowej pozwala na projektowanie i wytwarzanie koloidalnych nanostruktur ograniczonych kwantowo tylko w wybranych kierunkach, tj. nanoprętów i nanodrutów ograniczonych w dwóch kierunkach i zwanych nanomateriałami jednowymiarowymi lub

nanopłytek ograniczonych tylko w jednym kierunku, inaczej nanomateriałów dwuwymiarowych (Rysunek 1). Te ostatnie, szczególnie w przypadku nanopłytek z selenku kadmu, w porównaniu z zerowymiarowymi kropkami kwantowymi, charakteryzują się silniejszą fotoluminescencją ze ściśle określonym położeniem maksimum i wąskim pikiem emisji, krótszymi czasami życia fotoluminescencji, większymi wartościami energii wiązania ekscytonowego, silniejszą absorpcją nieliniową i następującą po niej intensywną emisją, bardziej podatnymi na zmiany objętości nanocząstki. Z tego względu kolejne badania nad funkcjonalizacją nanomateriałów do zastosowań wymagających wysokich wartości przekroju czynnego na dwufotonową absorpcję oraz intensywnej dwufotonowo wzbudzonej emisji prowadzone były z wykorzystaniem koloidalnych nanopłytek CdSe.



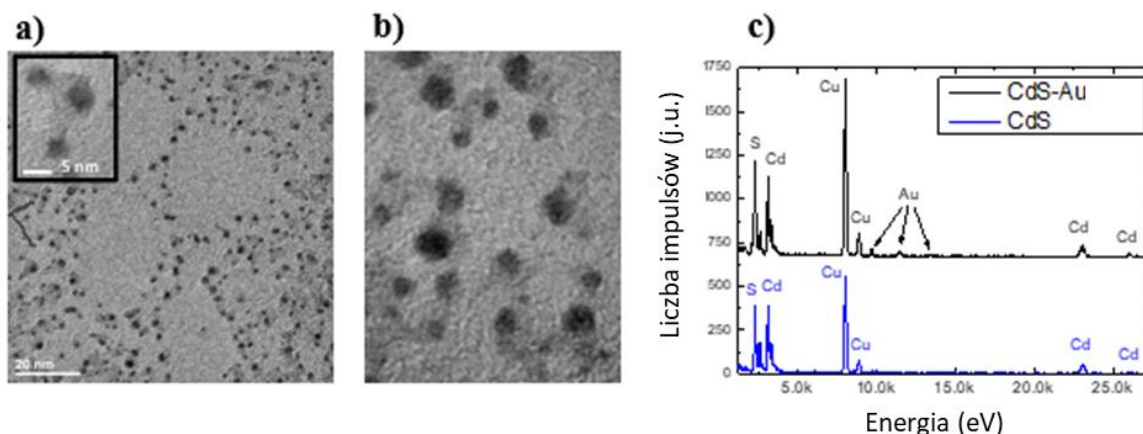
*Rysunek 1 Schemat półprzewodnikowej nanopłytki oraz jej struktury krystalicznej na przykładzie nanopłytki o grubości 5,5 warstw atomowych.*

Nanopłytki CdSe o trzech różnych grubościach zostały zsyntezowane i scharakteryzowane pod względem właściwości optycznych metodami spektroskopii absorpcyjnej, fotoluminescencyjnej i czasowo-rozdzielczej emisyjnej oraz fotoakustycznej, a także obliczone zostały wartości energii wiązania ekscytonowego zależnej od grubości nanopłytki nową metodą z wykorzystaniem widm absorpcyjnych i fotoakustycznych. Nanopłytki o grubości 5,5 warstw atomowych zamknięto w nanonośnikach polimerowych w celu hydrofilizacji oraz obniżenia toksyczności przy jednoczesnym zachowaniu silnej dwufotonowej absorpcji i dwufotonowo wzbudzonej

emisji do zastosowania jako modelowy materiał do bioobrazowania. Nanopłytki o grubości 4,5 warstw atomowych zostały wzbogacone jonami srebra i miedzi w różnych stężeniach w celu wzmocnienia efektu dwufotonowej absorpcji oraz zwiększenia wydajności kwantowej, by dodatkowo wpłynąć na wydajność dwufotonowo wzbudzonej emisji. Taki zabieg pozwolił na poprawę nieliniowych właściwości optycznych, również pięciorzędowych, bez manipulacji rozmiarem nanostruktur, dzięki czemu koloidalne nanopłytki CdSe domieszkowane jonami metali szlachetnych mogą potencjalnie zostać zastosowane w zaawansowanych systemach optycznego szyfrowania informacji czy też, po odpowiedniej dalszej funkcjonalizacji, w skomplikowanych układach do bioobrazowania.

## **Wyniki eksperymentalne i dyskusja**

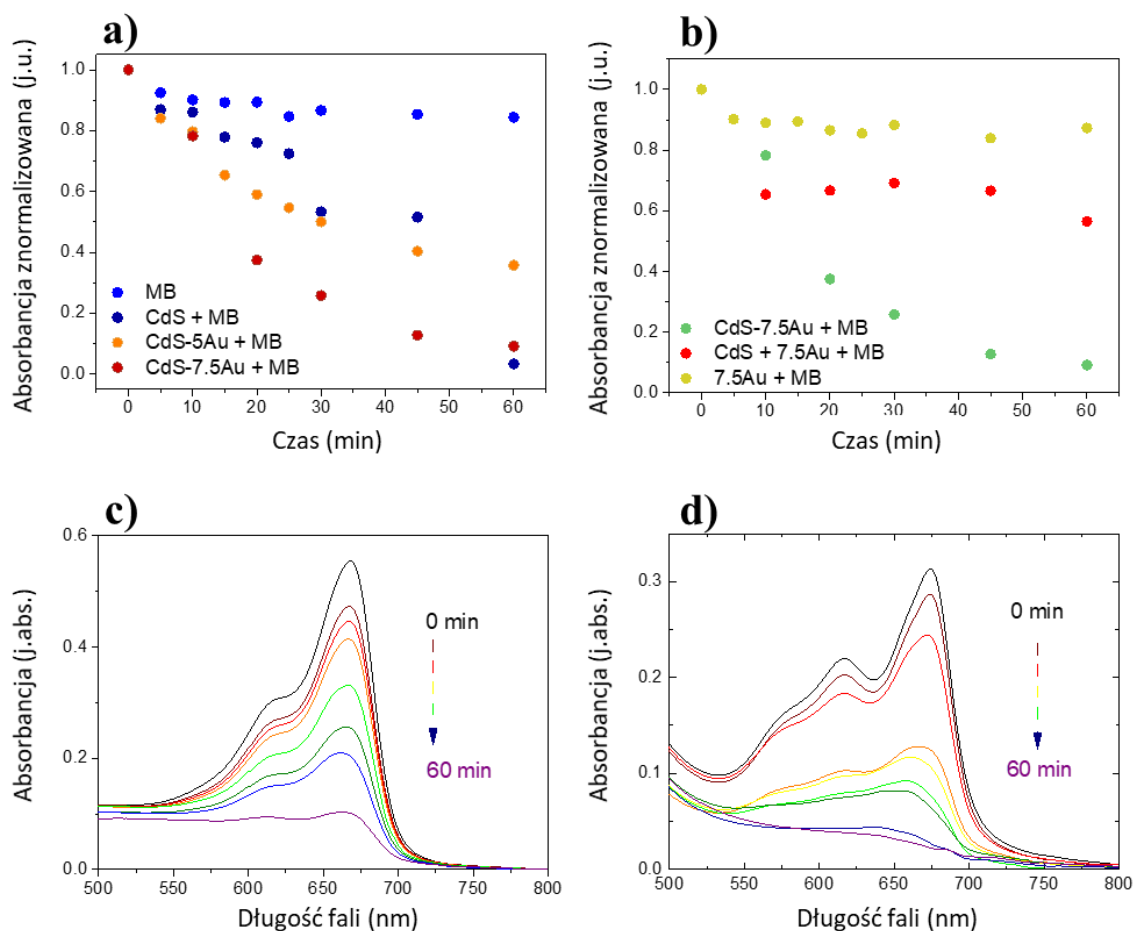
Analiza wyników obrazowania kropek kwantowych CdS poddanych procesowi osadzania nanostruktur złota obrazowanych metodą transmisyjnej mikroskopii elektronowej (Rysunek 2a-b) wskazuje na obecność nanocząstek o kształcie zbliżonym do trójkątnego, lub tetrapodowego zgodnie z referencją, która była bazą do ich syntezy,[1] dających słabszy kontrast na podłożach miedzianych sugerujący, że są to struktury półprzewodnikowe CdS oraz sferopodobnych nanocząstek wykazujących silniejszy kontrast, charakterystyczny dla metali. Widmo dyspersji energii (Rysunek 2c) wskazuje na obecność atomów kadmu, siarki i złota).



Rysunek 2 Nanocząstki hybrydowe CdS-Au obrazowane metodami TEM i HRTEM (a-b) oraz widma dyspersji energii (EDX) (c) kropek kwantowych CdS i nanohybryd CdS-Au.

Rysunek pochodzi z Nawrot i in.[2]

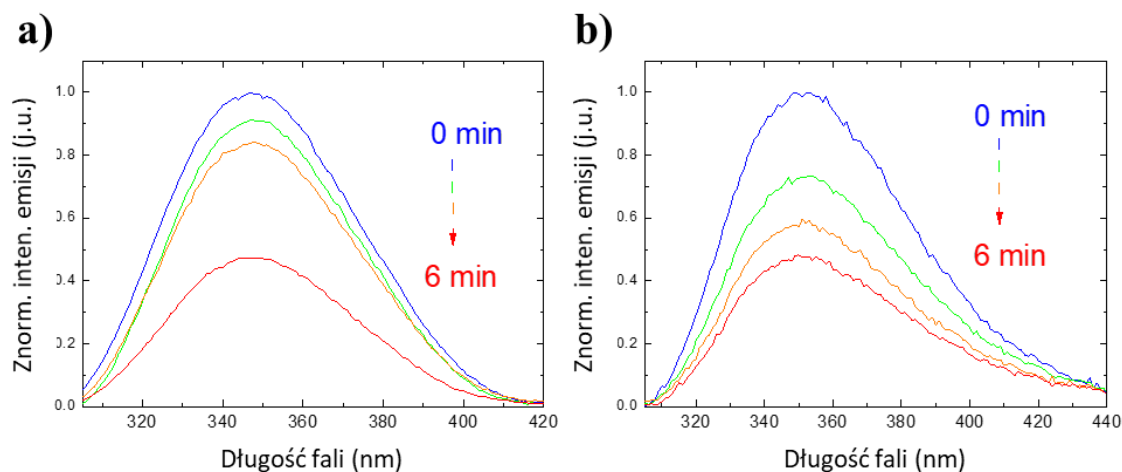
Nanohybrydy CdS-Au pełnią funkcję fotokatalizatorów reakcji redukcji, co przedstawiono na przykładzie degradacji błękitu metylenowego (MB) mierzonej poprzez zanik absorpcji (Rysunek 3), przyspieszając proces w porównaniu do prowadzenia go bez nanocząstek, w obecności samych nanostruktur złota, kropek kwantowych bez osadzonego metalu, a także mieszaniny kropek kwantowych i nanocząstek złota. Ponieważ proces redukcji wymaga obecności ładunku ujemnego, wyniki wskazują na to, że nanocząstki hybrydowe zapewniają większą dostępność elektronów, ze względu na efektywniejszy rozdział ładunku po fotowzbudzeniu półprzewodnika. Liczba w zapisie poprzedzająca symbol złota oznacza stężenie prekursora metalu użyte w procesie osadzania.



Rysunek 3 Zmiany w wartości maksimum absorpcji błękitu metylenowego w czasie ekspozycji na światło w obecności nanocząstek hybrydowych CdS-Au i referencyjnych.

Obecność nanostruktur CdS-Au powoduje również degradację surowiczej albuminy wołowej (Rysunek 4), której właściwości luminescencyjne są wrażliwe na działanie reaktywnych form tlenu, co pośrednio wskazuje na udział nanocząstek hybrydowych w ich generacji z wody wymagającej, w zależności od konkretnej reakcji, obecności elektronów

lub ładunku dodatniego. Fakt zachodzenia reakcji sugeruje, że pod wpływem światła w nanocząstkach hybrydowych nastąpił efektywny rozdział ładunku.



Rysunek 4 Zmiany w intensywności fotoluminescencji wykazywanej przez surowiczą albuminę wołową w czasie w obecności nanocząstek hybrydowych CdS-2.5Au (a) i CdS-5Au (b).

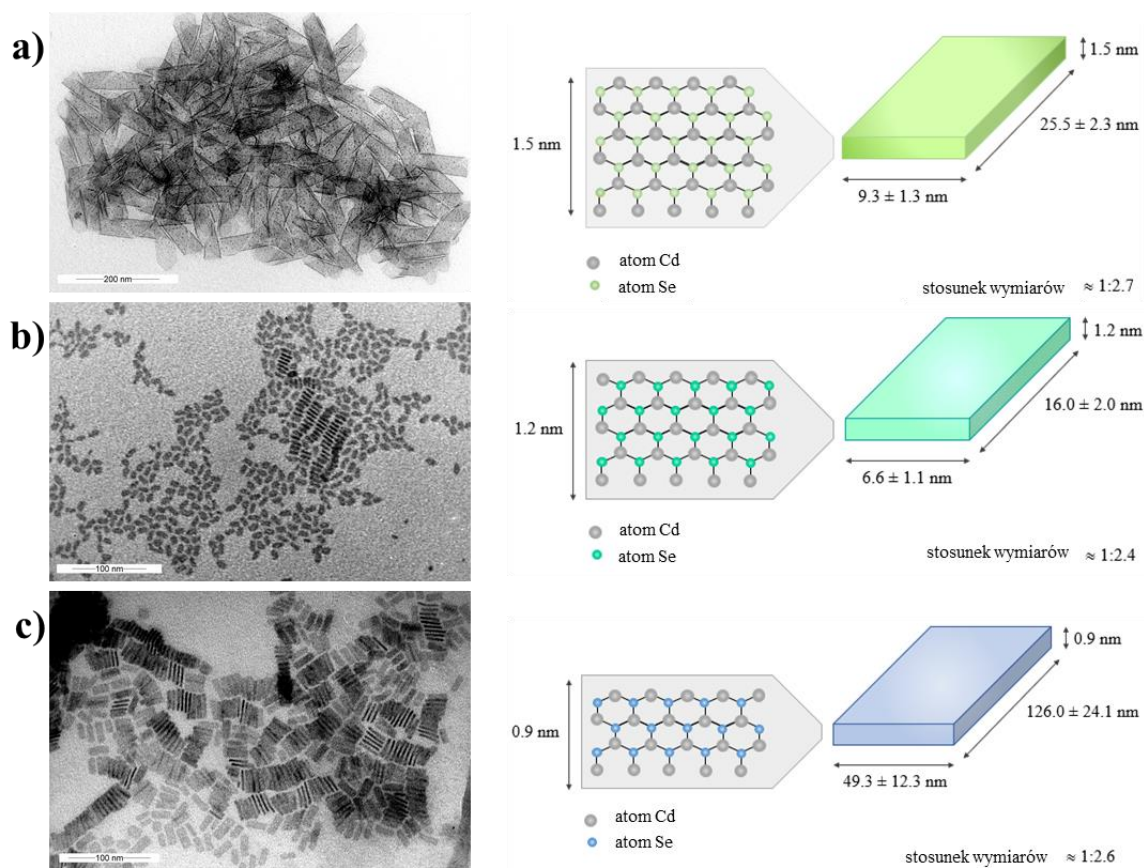
Rekombinacja ładunku prowadzi do emisji energii, która w materiałach luminescencyjnych przybiera formę emisji światła. Efektywny rozdział ładunku, blokujący rekombinację, prowadzi zatem do wygaszenia emisji, bez względu na rząd procesu absorpcji, tj. czy nastąpiła absorpcja liniowa czy nieliniowa. Aby wprowadzenie do nanomateriału jednej funkcji bez utraty innej pożądanej, dobrano stężenie prekursora złota przy funkcjonalizacji nanocząstek CdS pozwalające na fotokatalizę przy jednoczesnym zachowaniu pierwotnych właściwości emisyjnych, mając na uwadze dwufotonowo wzbudzaną luminescencję (Tabela 2). Nanohybrydy CdS-5Au okazały się być nieco silniejszym absorberem i emiterym niż kropki kwantowe CdS. Zjawisko wygaszania emisji w obecności osadzonych struktur metalicznych zostało przypuszczalnie zrekompensovane wzmocnieniem absorpcji poprzez rezonans plazmonowy.

Tabela 1 Przekrój czynny na dwufotonową absorpcję  $\sigma_2$  i intensywność następującej po niej emisji  $\sigma_2 \times QY$  wyznaczona dla nanocząstek hybrydowych CdS-5Au w porównaniu do kropek kwantowych CdS charakteryzowanych uprzednio.[2] Wzbr.  $\lambda$  – długość fali wzbudzenia. Tabela na podstawie Nawrot i in.[3]

Próbka	$\lambda$ wzb. (nm)	$\sigma_2$ (GM)	$\sigma_2 \times QY$ (GM)	$\sigma_2/MW$ (GM)	Referencja
CdS	700	$6.0 \times 10^2$	$3.66 \times 10^2$	$1.0 \times 10^{-3}$	[2]
	725	$5.7 \times 10^2$	$3.42 \times 10^2$	$0.6 \times 10^{-3}$	
	750	$2.3 \times 10^2$	$1.38 \times 10^2$	$0.2 \times 10^{-3}$	
CdS-5Au	700	$7.0 \times 10^3$	$7.00 \times 10^2$	$9 \times 10^{-3}$	[3]
	725	$15.8 \times 10^3$	$1.58 \times 10^2$	$20 \times 10^{-3}$	
	750	$6.9 \times 10^3$	$6.90 \times 10^2$	$9 \times 10^{-3}$	

Hydrofilowe nanocząstki CdS-Au wykazujące jednocześnie właściwości fotokatalizujące oraz nieliniowo-optyczne mogą służyć jako modelowy wielofunkcyjny materiał hybrydowy do zastosowań teranostycznych. Za część diagnostyczną odpowiadać może możliwość wzbudzenia nanocząstek w zakresie fal podczerwonych w obszarze biologicznego okna transmisji; znacznie redukujące absorpcję i rozpraszanie światła na tkankach, co umożliwi wyższy kontrast bioobrazowania. Część teranostyczna może być zrealizowana dzięki funkcji fotokatalitycznej, w szczególności zdolności do generacji reaktywnych form tlenu stosowanych do niszczenia komórek nowotworowych w terapii fotodynamicznej.

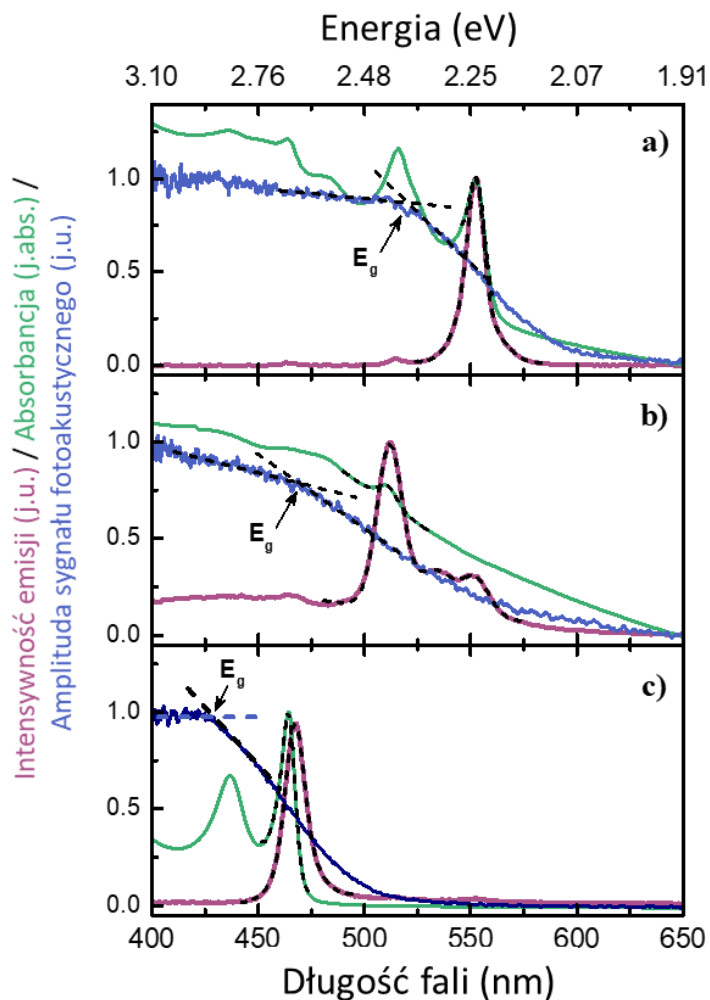
Kolejnym materiałem zsyntezowanym i poddanym charakteryzacji były kwazi-dwuwymiarowe nanopłytki CdSe. Rysunek 5 przedstawia ich morfologię i strukturę obrazowaną metodą TEM, która posłużyła do oszacowania ich średnich wymiarów.



Rysunek 5 Analiza morfologii i struktury (a) 5,5-warstwowych, (b) 4,5-warstwowych oraz (c) 3,5-warstwowych nanopłytek CdSe wraz ze schematycznym przedstawieniem ich struktury krystalicznej.

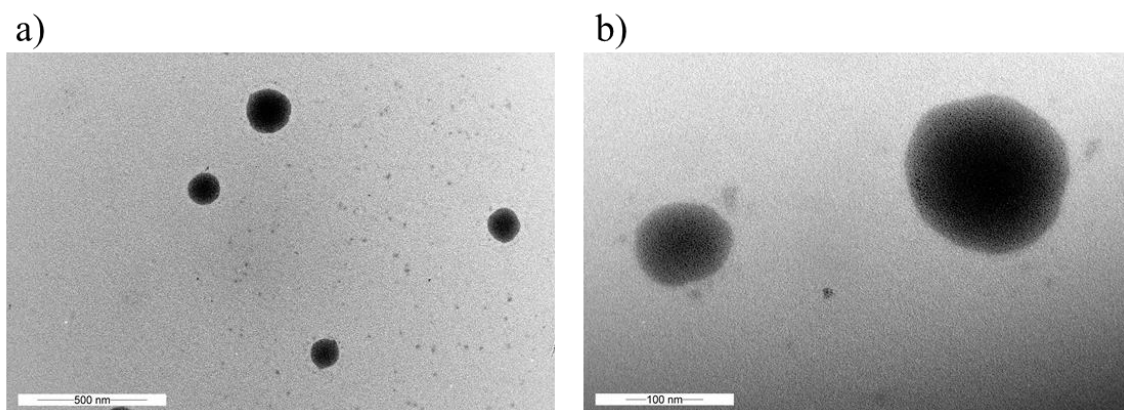
Materiały poddano charakteryzacji optycznej przy pomocy spektroskopii absorpcyjnej, oraz fotoluminescencyjnej (Rysunek 6), otrzymując charakterystycznie rozdzielone piki ekscytonowe oraz wąskie widma emisji z maksimum intensywności przy ściśle określonych długościach fali zależnych od grubości nanopłytki: 467 nm pochodzące od nanopłytek CdSe o grubości 3,5 warstw atomowych, 512 nm związane z aktywnością optyczną nanopłytek 4,5 warstwowych oraz 554 nm wynikające z obecności nanopłytek 5,5 warstwowych. Spektroskopia fotoakustyczna pozwoliła na wyznaczenie przerwy wzbronionej dla każdej grubości nanopłytek CdSe poprzez dopasowanie liniowe części widma reprezentującego krawędź pasma przewodnictwa oraz części związanej z wysyceniem sygnału i wyznaczając punkt przecięcia się linii trendu. Porównanie widma fotoakustycznego i absorpcyjnego stanowią propozycję nowej metody wyznaczania energii wiązania ekscytonowego jak różnicy pomiędzy wartością wyznaczonej w wyżej opisany sposób przerwy wzbronionej a energią, przy której pojawiły się pierwsze piki ekscytonowe widm absorpcji. Wartości tej energii wynoszą 230 meV, 210 meV i 130 meV dla

nanopłytek o grubości, odpowiednio, 3,5, 4,5 i 5,5, sugerując zastosowanie półprzewodnikowych nanomateriałów dwuwymiarowych w przestrajalnym laserowaniu i zaawansowanych urządzeniach optycznych.



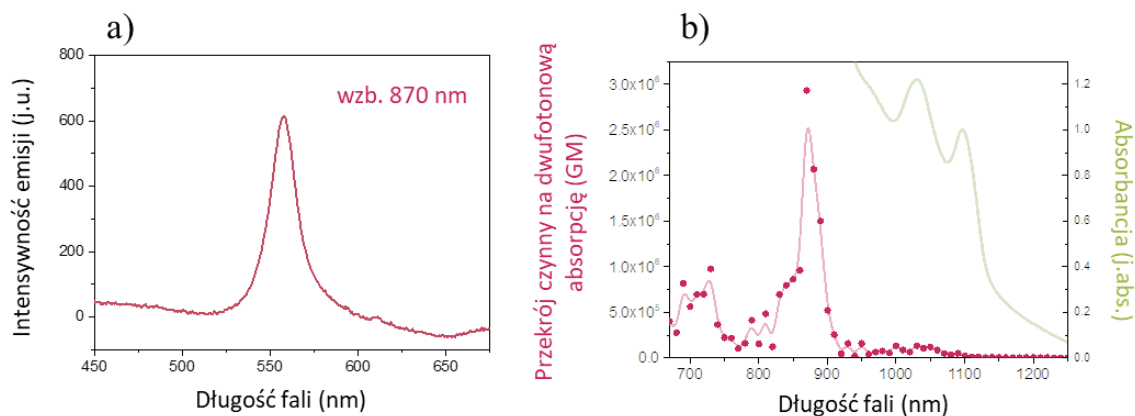
Rysunek 6 Zestawienie widm absorpcji, fotoluminescencji i fotoakustycznego nanopłytek CdSe o grubości a) 5,5 warstw, b) 4,5 warstw i c) 3,5 warstw. Wartości przerw wzbronionych zostały wyznaczone na podstawie widm fotoakustycznych. Wykres wykonany na podstawie Zelewski, Nawrot i in. [4]

5,5-warstwowe nanopłytki CdSe poddano procesowi enkapsulacji w nośnikach zbudowanych z amfifilowego polimeru w celu hydrofilizacji oraz redukcji toksyczności wynikającej z obecności jonów kadmu (Rysunek 7).



Rysunek 7 5,5-warstwowe nanopłytki CdSe zamknięte w nanośnikach polimerowych obrazowane metodą TEM.

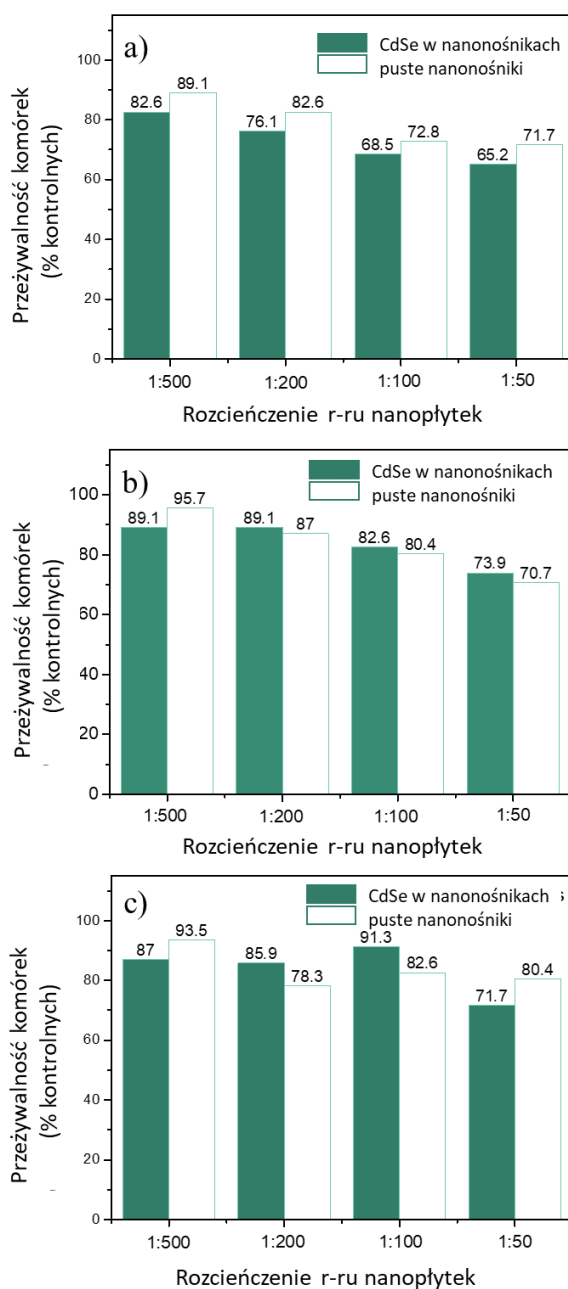
Zarówno wyniki badania liniowej absorpcji i następującej po niej emisji (Rysunek 8a) jak i spektralnie-rozdzielony przekrój czynny na dwufotonową absorpcję wyznaczony metodą dwufotonowo wzbudzonej luminescencji (Rysunek 8b) wskazują na brak niekorzystnego wpływu enkapsulacji na pierwotne właściwości optyczne nanopłytek CdSe.



Rysunek 8 (a) Widmo fotoluminescencji 5,5-warstwowych nanopłytek CdSe po wzbudzeniu wiązką laserową o dł. fali 870 nm oraz (b) spektrum absorpcji dwufotonowej (czerwony) wyznaczone metodą dwufotonowo wzbudzonej emisji wraz z porównaniem do widma absorpcji jednofotonowej (zielony) przedstawione przy podwojonej długości fali.

Funkcjonalizowany materiał poddano również testowi cytotoksyczności metodą MTT (Rysunek 9) zarówno na zdrowych (24 h), jak i na rakowych (24 h i 48 h) komórkach, uzyskując przeżywalność nie niższą niż 65% przy najwyższym stężeniu nanocząstek, przy

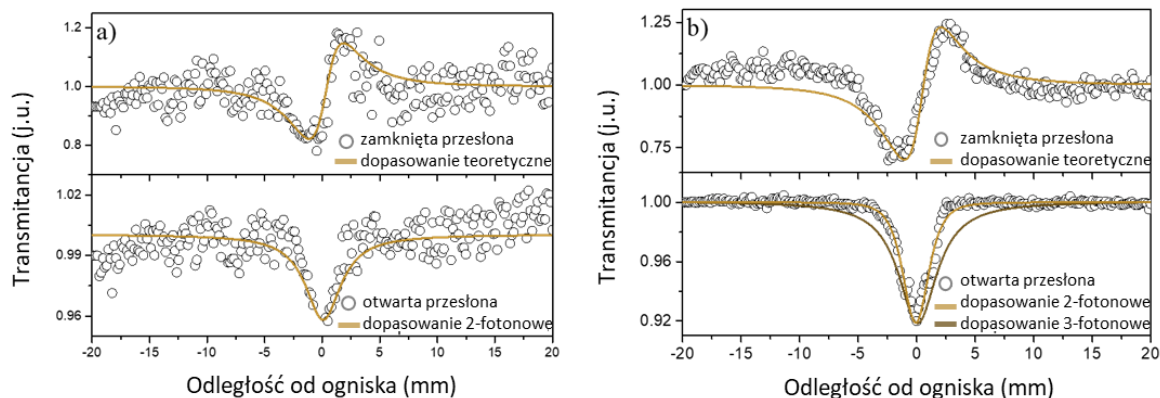
niższych dochodzącą do 90%, przy czym w odniesieniu do komórek inkubowanych w obecności pustych nanonośników, procent przeżywalności komórek w obecności enkapsulowanych nanopłytek przekroczył 90 % we wszystkich przypadkach. Enkapsulacja pozwoliła zatem na wprowadzenie pożądanej cechy (hydrofilowość), zahamowanie niechcianych procesów (toksycznego wpływu na komórki żywe) oraz zachowanie korzystnych właściwości optycznych (wąski pik emisji o zdefiniowanym spektralnym maksimum, wysoką wartość dwufotonowej absorpcji i następującą po niej intensywną emisją). Taki zestaw cech czyni nanopłytki CdSe enkapsulowane w nanonośnikach polimerowych potencjalnym modelowym biokompatybilnym materiałem umożliwiającym bioobrazowanie poprzez absorpcję w zakresie biologicznego okna transmisji i następującą po niej wyindukowaną dwufotonowo emisję.



Rysunek 9 Cytotoksyczność badana metodą MTT na (a) zdrowych fibroblastach dziąsłowych w czasie 24 h oraz komórkach raka jajnika w czasie (b) 24 h i (c) 48 h.

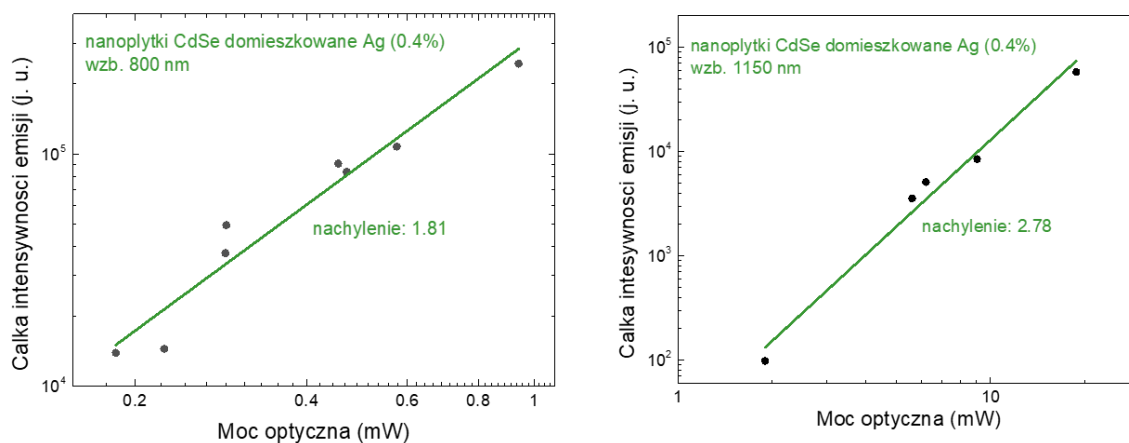
Kolejny pomysł funkcjonalizacji został zrealizowany z wykorzystaniem 4,5-warstwowych nanopłytek CdSe. Półprzewodnikowe nanostruktury zostały poddane domieszkowaniu jonami srebra oraz miedzi w stężeniach 0.4% Ag, 1.2% Ag, 0.5% Cu i 1.1% Cu, a następnie scharakteryzowano ich właściwości nieliniowo optyczne z wykorzystaniem metody Z-skan. Zaobserwowano dwa zakresy długości fal wzmożonej

absorpcji nieliniowej, przy czym dopasowanie teoretycznych przebiegów wartości transmitancji w funkcji odległości od ogniska (Rysunek 10) wskazuje na różne rzędy procesów w poszczególnych zakresach spektralnych.



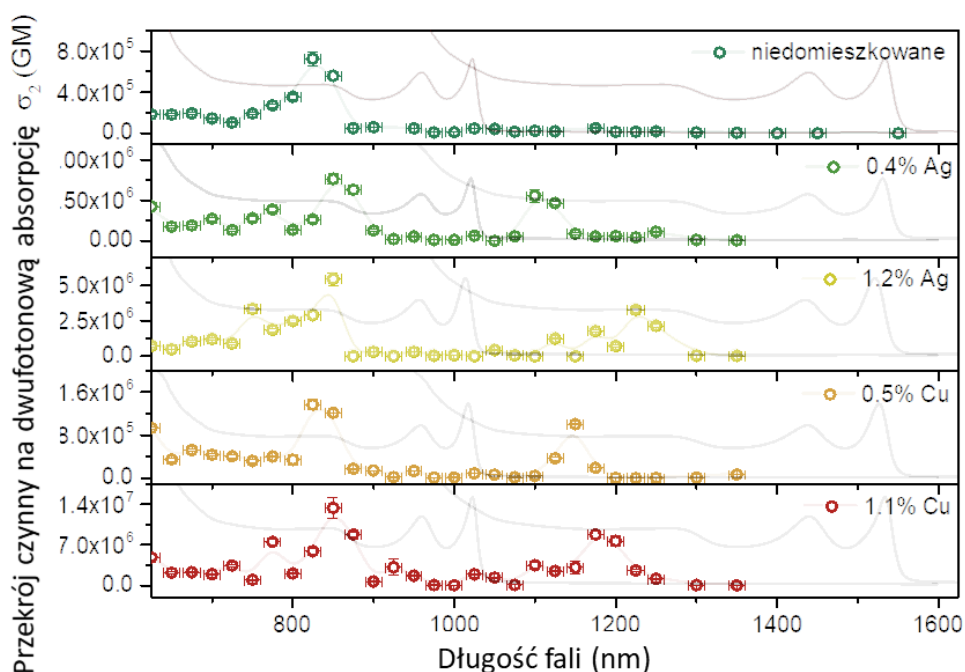
Rysunek 10 Reprezentacyjne wyniki pomiarów Z-skan w układzie z zamkniętą i otwartą aperturą wraz z dopasowaniem teoretycznym na przykładzie nanopłytek CdSe domieszkowanych jonami miedzi w stężeniu 0.5% po wzbudzeniu wiązką lasera o długości fali (a) 850 nm i (b) 1225 nm.

Dwufotonowy charakter absorpcji w zakresie krótszych długości fal i trójfotonowy przy dłuższych potwierdzają również zależności intensywności fotoluminescencji od zastosowanej mocy wiązki lasera wzbudzającego (Rysunek 11).



Rysunek 11 Zależność intensywności fotoluminescencji od mocy optycznej lasera wzbudzającego w skali logarytmicznej na przykładzie nanopłytek domieszkowanych jonami srebra w stężeniu 1.2% po wzbudzeniu wiązką lasera o długości fali (po lewej) 800 nm i (po prawej) 1150 nm.

Rysunek 12 przedstawia widma nieliniowej absorpcji nanopłytek z najwyższą wartością maksimum przekroju czynnego na dwufotonową absorpcję w przypadku materiału domieszkowanego miedzią w stężeniu 1,1% i wynoszącą  $1,33 \times 10^7$  GM przy długości fali 850 nm. Bez względu na rodzaj i stężenie domieszki, każda pozwoliła na wzmocnienie absorpcji w porównaniu do wartości wyznaczonej dla nanopłytek niedomieszkowanych, również w przypadku jej znormalizowania tj. podzielenia przekroju czynnego przez objętość nanocząstki w celu zminimalizowania wpływu wielkości na wynik (Tabela 2). Drugie lokalne maksimum, przypisywane procesom trójfotonowym, osiąga najwyższą wartość  $4,11 \times 10^{-74}$  dla tej samej próbki przy długości fali 1175 nm, a najniższą dla nanopłytek niedomieszkowanych.



Rysunek 12 Przekrój czynny na dwufotonową absorpcję nanopłytek niedomieszkowanych, domieszkowanych jonami srebra w stężeniu 0.4% i 1.2% oraz miedzi w stężeniu 0.5% i 1.1%. Jasne linie dodano dla ułatwienia obserwacji widma. Dla porównania wykreślono również spectra liniowej absorpcji przy podwojonej i potrojonej długości fali. Na podstawie Nawrot i in. [120]

Tabela 2 Maksymalny przekrój czynny na dwufotonową absorpcję, znormalizowane parametry absorpcji oraz intensywność dwufotonowo wzbudzonej emisji nanopłytek o różnych rodzajach i zawartościach domieszki oraz różnych wymiarach.

Nanopłytki CdSe	Powierzchnia (nm <sup>2</sup> )	Dł. fali (nm)	$\sigma_2$ (GM)	$\sigma_2/M$ (GM · mol·g <sup>-1</sup> )	$\sigma_2/V$ (GM · nm <sup>-3</sup> )	$\sigma_2 \cdot QY$ (GM)	Ref.
Nie-domieszkowane	132	825	$7.25 \times 10^5$ $\pm 7.01 \times 10^4$	1.31	$4.59 \times 10^3$	$1.60 \times 10^5$	[5]
Domieszkowane Ag (0.4%)	262	850	$3.82 \times 10^6$ $\pm 3.07 \times 10^5$	3.47	$1.21 \times 10^4$	$2.10 \times 10^6$	[5]
Domieszkowane Ag (1.2%)	210	850	$5.44 \times 10^6$ $\pm 4.34 \times 10^5$	6.17	$2.16 \times 10^4$	$3.26 \times 10^6$	[5]
Domieszkowane Cu (0.5%)	185	825	$1.36 \times 10^6$ $\pm 9.42 \times 10^4$	1.75	$6.12 \times 10^3$	$8.43 \times 10^5$	[5]
Domieszkowane Cu (1.1%)	213	850	$1.33 \times 10^7$ $\pm 1.79 \times 10^6$	14.8	$5.19 \times 10^4$	$9.98 \times 10^6$	[5]
Nie-domieszkowane	256	800	$4.40 \times 10^5$	0.41	$1.27 \times 10^3$	do $1.98 \times 10^5$	[6]

Domieszkowanie koloidalnych nanopłytek CdSe jonami metali szlachetnych pozwoliło na znaczne zwiększenie wartości przekrojów czynnych na dwufotonową absorpcję oraz wydajności kwantowych, a w konsekwencji poprawę parametru intensywności dwufotonowo wzbudzonej luminescencji bez manipulacji objętością nanocząstek. Taki zestaw cech mógłby być wykorzystany w optycznych ogranicznikach mocy, zaawansowanych systemach szyfrowania lub, po odpowiedniej funkcjonalizacji, jako modelowy materiał do wielofotonowej mikroskopii fluorescencyjnej.

## Podsumowanie

Zmiana kształtu i wielkości koloidalnych nanocząstek półprzewodnikowych, która wpływa odpowiednio na ilość wymiarów ograniczonych kwantowo oraz na szerokość przerwy wzbronionej, jak również funkcjonalizacja poprzez domieszkowanie, osadzanie

struktur na powierzchni lub enkapsulację pozwalają na wzmacnianie, indukowanie lub wygaszanie wybranych właściwości.

Osadzenie nanostruktur złota na powierzchni kropek kwantowych CdS pozwoliło na efektywny rozdział ładunku pod wpływem światła, przy jednoczesnym zachowaniu pierwotnych właściwości nieliniowo optycznych dzięki optymalizacji stosunku metal-półprzewodnik, co czyni hydrofilowe nanohybrydy CdS-Au potencjalnym modelowym materiałem wielofunkcyjnym do jednoczesnego bioobrazowania i terapii fotodynamicznej.

Charakterystyka nanopłytek CdSe pokazuje różnice w ich właściwościach optycznych w porównaniu z zerowymiarowymi kropkami kwantowymi, w tym intensywną emisję o wąskim pikie, krótsze czasy życia fotoluminescencji, większe wartości energii wiązania ekscytonowego oraz silniejszą absorpcję nieliniową, ale także możliwość manipulacji parametrami optycznymi poprzez dobranie odpowiedniej grubości nanopłytki. Dzięki temu można otrzymywać nanomateriały do coraz bardziej zaawansowanych urządzeń o sprecyzowanych wymaganiach.

Enkapsulacja nanopłytek CdSe w nośnikach polimerowych poprawiła ich biokompatybilność, wprowadzając hydrofilowość i redukując toksyczność, przy jednoczesnym zachowaniu wysokich wartości przekroju czynnego na dwufotonową absorpcję i intensywnej emisji, co sugeruje ich zastosowanie w bioobrazowaniu metodą dwufotonowej mikroskopii fluorescencyjnej.

Domieszkowanie nanopłytek CdSe jonami srebra i miedzi pozwala na wzmocnienie nieliniowej absorpcji i następującej po niej emisji, co sugeruje ich wykorzystanie do ochrony urządzeń jako ograniczniki mocy optycznej lub do skomplikowanego optycznego szyfrowania informacji. Wysokie wartości parametrów  $\sigma_2$  oraz  $\sigma_2 \times QY$  nawet dla niewielkich rozmiarów płytek, łatwiejszych do enkapsulacji, czynią z nich potencjalny modelowy materiał, który po dalszej funkcjonalizacji służyłby do celów zaawansowanego bioobrazowania wykorzystującego jednocześnie dwu- i trójfotonową absorpcję.

Różnorodność narzędzi, jakimi można posłużyć się do manipulacji cechami, które wykazują nanocząstki półprzewodnikowe wskazuje na ogrom możliwości otrzymywania wielofunkcyjnych nanomateriałów o coraz dokładniej dobranych parametrach do poszczególnych zastosowań.

# 1. INTRODUCTION

This dissertation combines aspects of material science and nanophononics. It discusses synthesis, physicochemical characterisation, and modification of semiconducting nanomaterials as well as mechanisms and phenomena occurring within those nanoparticles when interacting with photons, which allow for their characterisation and decide on their to-be-applied optical properties.

Materials science is a fascinating field, which relates synthesis methods to composition and morphology as well as composition and morphology to properties. It provides information of mechanisms, in-structure processes and behaviour of a material in applied conditions. Yet, although such knowledge is interesting itself, the more important fact is that it may be employed for manipulation in materials synthesis and post-processing in order to achieve a desired combination of structure and composition and, in turn, desired properties for practical applications.

The previous century was an era of a new research field, born from material science, concerning study of materials on a sufficiently small scale that displayed properties much different from those of bulk materials. As such new behaviours might be observed in particles of size in nanometric range, it is referred as nanomaterials science. As a matter of fact, nanomaterials were in use long before, however the awareness of their nanometric scale appeared, and knowledge in this field developed significantly in the 20<sup>th</sup> century. Initially, Richard Zsigmondy, 1925 Nobel Prize Laureate in chemistry, was the first to observe nanoparticles in gold colloids with a microscope and was followed by Richard Feynman, who proposed his concept on manipulating with matter at the atomic level in 1959.[7] The nature of nano-effects depends strongly on the type of material. For instance, noble metal nanoparticles, such as gold, silver, platinum, palladium, and rhodium [8], display the phenomenon of surface plasmon. Oscillations of electron plasma at the surfaces of such nanostructures interfere with local electromagnetic fields, altering their properties in comparison to bulk metals. Firstly, the surface plasmon phenomenon impacts the absorption spectrum. For instance, in spite of the constant colour of bulk gold, gold nanoparticles solutions may display a palette of colours, from violet to red, depending on the size of nanostructures. Secondly, it provides light concentration that finds its application in photovoltaic devices for absorption efficiency enhancement [9] or in near-field scanning

optical microscopy.[10] Upon light absorption, metal nanoparticles are locally heated and, therefore, may find applications that require a precisely targeted temperature increase, for example, for heating-induced mutated cells annihilation in antitumour therapy.[11] Similar action may be induced in magnetic nanoparticles, structures which earn superparamagnetic properties when their size is sufficiently decreased, for instance ferrites.[12] Another class of nanoparticles are built of semiconducting compounds displaying nano-effects based on space confinement of electrons caused by decreased size which is termed quantum confinement.[13] Such limitation for electrons movement has critical impact on band gap, i.e. increasing the difference in conduction band and valence band energy with decreasing nanoparticle size. It allows for precise control of absorbed and emitted light wavelengths which found their application in light-emitting diodes, for instance, LED displays.[14] The possibility of properties modulation makes semiconductor nanoparticles, called quantum dots (QDs), advantageous for modulating and detecting devices.[15] As upon light excitation they go through charge separation, they may be employed for light-to-electricity transformations, for example solar energy collection, or for any other light-induced charge-involving processes.[16] Some nanoparticles, including variety of QDs, go through nonlinear absorption which means that they are capable of absorbing several photons at once if exposed to high-intensity light. Nonlinear absorbers may find application in a broad range of fields, including optical limiting [17], multiphoton microscopy [18] and photodynamic therapy.[19]

The fundamental property of semiconductor nanoparticles as well as semiconductors in general, is the fact that the separation of electrons and holes is possible only when a sufficient energy is applied. As this dissertation discusses optical properties of semiconductor nanomaterials, therefore, it describes processes involved in photon-induced charge separation. Exposed to light of sufficient energy, a QD absorbs it in the process of excitement, causing transfer of electrons from the valence band to the conduction band, leaving unpaired holes on the valence band. The process is followed by relaxation including charge recombination and emission of photons. The amount of energy necessary for excitation to occur is called band gap and this value is also mainly responsible for the energy released through photon emission and thus for the wavelength of emitted light seen as a particular colour. The size of band gap depends mostly on the composition and size of a nanoparticle.[20] The case of composition encompasses not only the compound building the semiconductor structure but also any doping that may change

relaxation pathways.[21] However, many properties including energy-density of states relations, electron-hole coupling strength, volume to nonlinear absorption cross section relation are influenced by the shape of nanostructures, in particular the number of dimensions sufficiently small to undergo nano-phenomena.[6,22] Moreover, light-induced behaviour of nanoparticles is dependent on presence of any accompanying structures which may interfere with energy relaxation processes.[16] The knowledge of the above-mentioned relations is crucial in materials science for introduction or enhancement of desired functions, minimization of any drawback behaviours and, in spite of such manipulations, preservation of advantageous properties.

Various ideas have been reported for addition of new functionalities to semiconductor nanoparticles and improvement of existing ones, among which effective charge separation and enhancement of nonlinear absorption are brought up in this dissertation. Extraction of free electrons from the remaining part of the material allows for their employment in reduction reactions, for instance, hydrogen generation, whereas entrapment of electrons leads to release of positively-charged holes which may serve for oxidation reactions.[23,24] As initial charge separation or, in other words, excitation may be achieved upon light exposure, the whole process may be light-driven if a suitable functionalisation is performed. Further, NLO emitters absorb several photons of lower energy and emit one of higher energy, opening a number of possibilities, including absorption of light in desired range of wavelengths, for instance, for the field of biological and medical diagnosis [25,26] and complication of luminescence signal detection, for example, for security and encryption applications.[27] Moreover, NLO absorption is light intensity-dependent, which means it sharply changes through the radius of a laser beam providing a precision tool for 3D photopolymerization employing a two-photon active photoinitiator. This property of nonlinear absorbers also suggests their application as optical power limiters for control of laser noise or protection, for instance, of sensors or in protective gloves.[28] The broadness of the range of current world issues which are to be solved with nonlinearly active materials, encourages for studies on this subject. In this dissertation, in particular, investigation into enhancement of such properties by functionalisation is brought up.

Depending on the target field, several properties of semiconductor nanoparticles may be necessary to change. In particular, the position of emission peak, impact on living cells for biological applications, chemical affinity for the possibility to employ in particular

medium, size for passing or not passing certain boundaries are discussed in this work. Manipulation of the luminescence wavelength may be achieved by playing with composition and structure. The three latter properties, collectively or individually, may be modified through several approaches, including binding with appropriate molecules [1] or encapsulation individually or as a group into carriers.[26]

All of the manipulations aimed for introduction, enhancement, or inhibition of certain behaviours are to be performed carefully, taking into account preservation of desired properties present simultaneously. First of all, upon contact with additional substance, QDs may suffer luminescence quenching effect, including collisional quenching when after excitation the charge is transported to another molecule or particle, preventing from relaxation in the form of light emission [29] or post-quenching when, although luminescence occurs, its detection is hindered as the emitted light is absorbed or dispersed through passing boundaries introduced through functionalisation process. For this reason, addition, embedment or binding of any substance requires qualitative and quantitative selection. Examples of both types of optimizations are described in this dissertation.

The phenomena mentioned above involving light and nanometre-scale objects are a concern of nanophotonics. Studies on interactions between light and nanoparticles mostly base on methods that are also applicable to either molecules or bulk materials. Fundamental characterisation includes absorption and emission spectroscopies which, except for obvious information such as range of light wavelengths which are absorbed and emitted by the specimen, provide data on exciton transition energies, emission intensity and partially on the size-composition combination of nanoparticles, their shape and dimensionality, mono- or polydispersity, defects, and doping. Along with supplementary characterisation, which may include morphological microscopy studies, strictly composition-focused analysis such as energy dispersive X-ray (EDX), deeper emission insights, for instance, time-resolved photoluminescence spectroscopy, and additional complementary spectroscopies, for example, employing photoacoustic effect, it gives the image of linear optical properties of the material. If a material of interest is intended for applications involving NLO processes, high intensity light sources, mostly femtosecond-pulse lasers, are used to induce excitation of the specimen followed by absorption, refraction, and/or emission detection depending on the method. Further characterisation may include simulation of real processes which the materials are designed for.

## 2. PURPOSE AND SCOPE OF THE WORK

This dissertation presents studies on semiconductor nanoparticles concentrating on enhancement of their functionalities, especially NLO properties as well as manipulation of radiative and non-radiative recombination pathways. The purpose of the work described herein is to create nanosystems based on semiconductor nanoparticles that manipulate their structure by embedment, doping, and encapsulation in order to enhance advantageous, inhibit disadvantageous, and add desired properties for currently awaiting applications. In particular, I am inviting the reader to take a closer look at the mechanisms of excitation and relaxation in order to investigate the impact of the altered structure on optical pathways.

The experimental work encompasses synthesis, characterisation, and functionalisation of two types of semiconductor nanoparticles: CdS QDs and CdSe NPLs (Figure 1). The research is open with synthesis of zero-dimensional chiral hydrophilic penicillamine-capped CdS QDs and their functionalisation with gold domains for effective charge separation, resulting in introduction of photocatalytic properties preserving nonlinear absorption and TPEE abilities. Furthermore, following previous reports on dimensionality-related properties of two-dimensional semiconductor NPLs, the focus is shifted to CdSe NPLs of different thicknesses. Synthesis, morphology and properties of such material are presented, including optical behaviour as well as determination of exciton binding energy with a new method combining absorption spectrum and photoacoustic spectrum. Properties of CdSe NPLs, subjected to encapsulation, are investigated focusing on their photostability, biocompatibility and NLO properties for the material to serve as a model in bioimaging applications. Finally, the structure of CdSe NPLs is altered by doping with silver and copper ions to influence their emission spectrum, quantum yield (QY), and NLO properties.

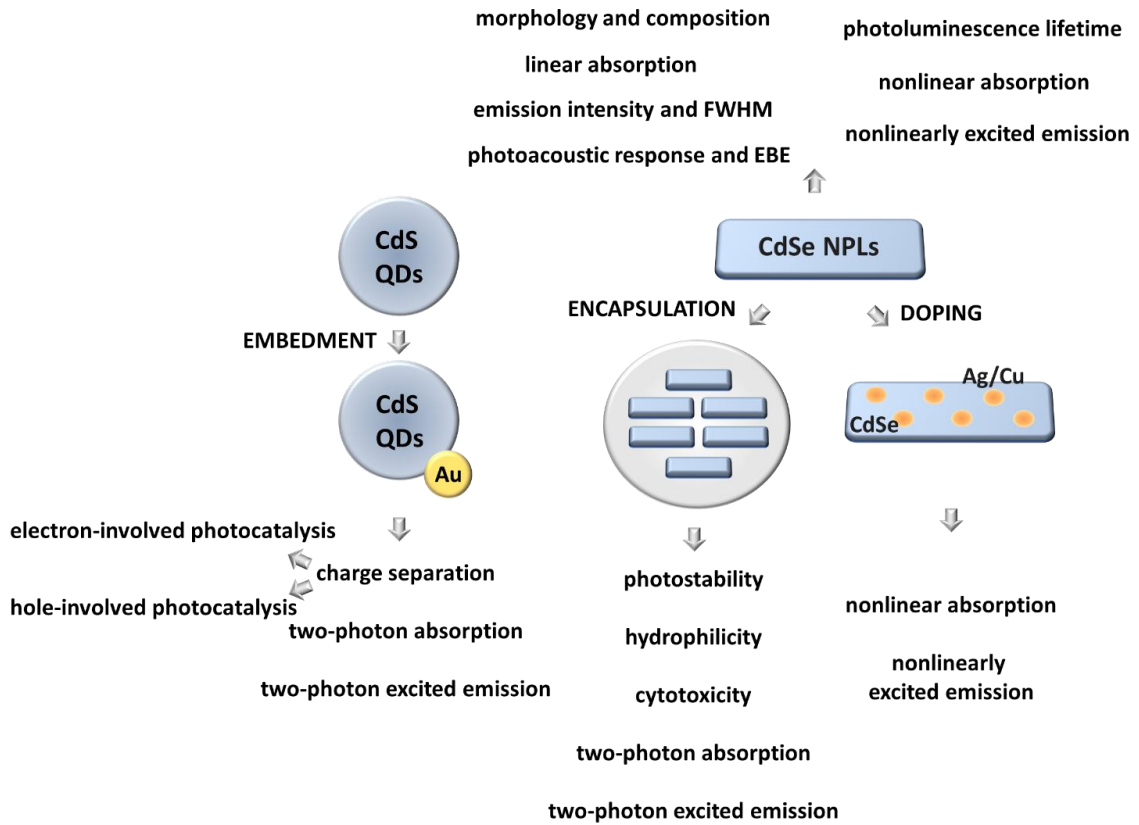


Figure 1 Scope of the experimental studies.

### 3. THEORY

Materials employed for studies described in this thesis, serving as a base modified further to obtain desired functionalities, are semiconductor nanoparticles made of CdS and CdSe. Playing with their structure influences their optical behaviour, therefore the description of materials, their properties and functionalisation possibilities along with the consequences is preceded by a short discussion on absorption and emission mechanisms.

### 3.1. Excitation and following processes

Upon excitation by light, several processes may take place depending on the composition and structure of an excited subject, on the light wavelength, and on its intensity. General phenomena may be presented on a Jabłoński diagram, named after physicist Aleksander Jabłoński. Figure 2 is a modified version of such diagram explaining main processes described in this dissertation.

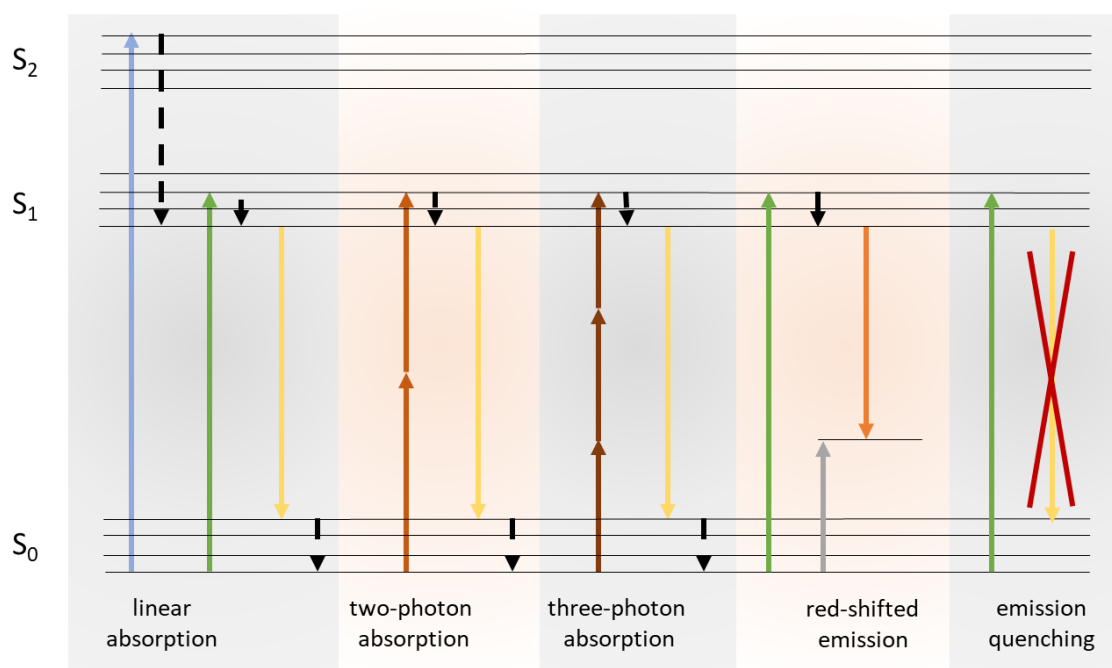


Figure 2 Modified Jabłoński diagram encompassing processes of linear and nonlinear absorption along with emission in its basic form, with a modified pathway and quenched.

The diagram presents processes occurring within and between the following electronic levels: singlet ground  $S_0$ , first electronic state  $S_1$  and second electronic state  $S_2$  whereas each of them is divided into vibrational energy levels, each depicted as a black line.

In fluorophores, exposure to light of sufficient energy leads to absorption of photons and, in turn, to excitation to the first (green arrow) or second (blue arrow) electronic state, particularly to one of the higher vibrational states. Usually, an internal conversion, which is the relaxation from the lowest energy vibrational state of  $S_1$ , occurs within ca.  $10^{-12}$  s.[29]

Subsequently, a return to the ground state is observed in the form of light emission called fluorescence (yellow arrow). Typically, fluorescence terminates at a higher excited vibrational ground state level, and the lowest state is achieved through thermal energy release.

As a side note, here is an explanation how it corresponds to a semiconductor (Figure 3). Indeed, in bulk semiconductors, electronic energy level bands are nearly continuous as the electrons may move freely in all directions of the material. On the other hand, a decrease of the size of a semiconductor particle to a certain level confines the movement of electrons so that both excited electrons on the conduction band and holes remaining on the valence band may have only discrete energy levels. Therefore, the energy level diagram is similar to that of an atom. Similarly to molecular systems, emission may occur in various ways. If it follows absorption from the highest energy level of the valence band to the lowest one of the conduction band, it is distinguished as band edge emission. However, it may also encompass other energy levels, and in this case, radiative emission is accompanied with nonradiative transitions within bands.

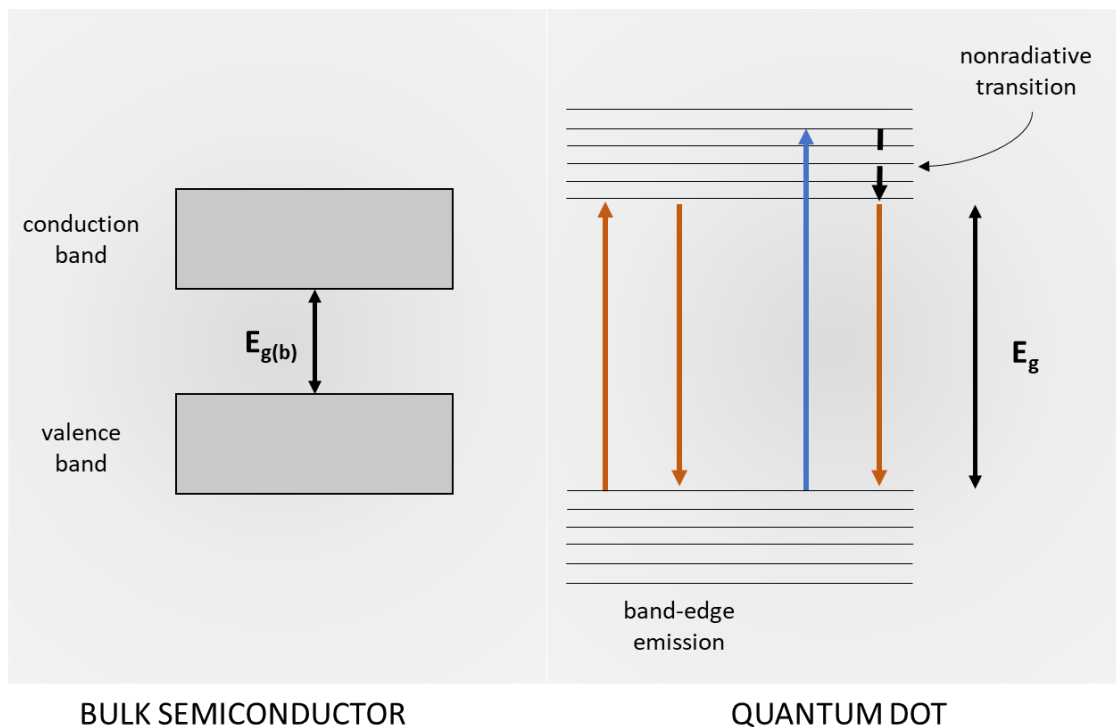


Figure 3 Energy bands in bulk semiconductor versus a quantum dot.

Such an absorption-emission process is a base. In case of nonlinearly active materials, absorption may also occur with lower energy light of high intensity (see *Third-order nonlinear optical processes* subsection below). In such cases, two (orange

arrows), three (brown arrows), or more photons of total energy sufficient for excitation are absorbed simultaneously. Such multiple absorption is then followed by the same processes, meaning that the resulting fluorescence spectrum does not differ excited either linearly or non-linearly.

The relaxation pathway may be altered through manipulation of a material composition or structure, causing changes in fluorescence spectrum or its quenching as the energy is released nonradiatively. Quenching may be observed when an excited electron is transferred to another particle or molecule (dark blue arrow). Such a transfer causes charge separation, which is relatively long and durable for employing electrons and holes in desired processes, for instance, redox reactions. Particularly, in the case of semiconductor nanoparticles, light-induced excitation leads to transport of the electrons to the conduction band, leaving unpaired holes in the valence band but the process is followed by quick recombination, resulting in photoluminescence of a spectrum characteristic for the composition and size of the QD. Strengthening the separation may be achieved by embedment of electron-accepting structures on the semiconductor surface, for example, metal domains, while holes may be trapped by positive-charge-accepting agents, called hole scavengers (Figure 4). Fluorescence of such semiconductor-metal hybrid nanoparticles, or broadly speaking, fluorophore-electron acceptor pairs, is observed to be decreased due to inhibition of trapped charge recombination.

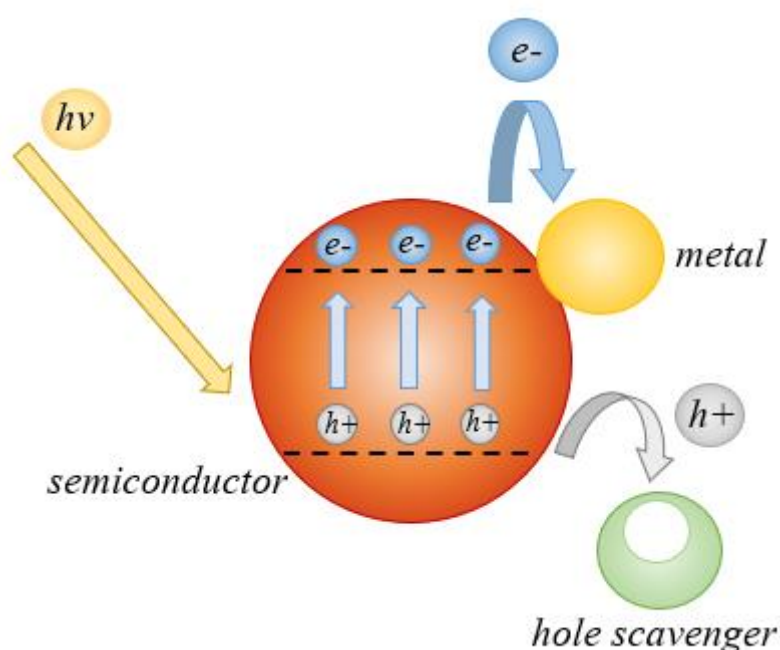


Figure 4 Charge separation on a semiconductor-metal hybrid nanoparticle upon light excitation.

An interesting fact is that metals may also alter photoluminescence spectrum of semiconductor nanoparticles without quenching. On the contrary, such a combination may even lead to improvement of QY. The secret is hidden in the character of the metal part and the way its linked to the semiconductor. If the metal is in the form of an individual nanostructure and it is placed on the surface of the QD, then after excitation, electrons are willingly transported to the metal nanoparticle, preventing from charge recombination and, in turn, decreasing emission. However, if metal is employed as a dopant, its ions are built into the structure of the semiconductor and do not serve as traps of electrons. They create defects and participate in the recombination process, changing its pathway and thus influencing the final emission spectrum. The defects serve as holes traps artificially increasing the valence band energy resulting in shortening of such metal ion-influenced band gap. In turn, the pathway of recombining electrons is reduced, finally leading to a red-shift of the emission spectrum.

### 3.2. Third-order nonlinear optical processes

One of the basic purposes of optics is the study of interaction of the electromagnetic wave with matter. The response of a material to an applied electric field is described by the polarisation density vector field  $\mathbf{P}$ . In particular under conditions of relatively low light intensity, induced polarisation is proportionally (linearly) related to the electric field strength (eq. 1).

$$P = \epsilon_0 \chi^{(1)} E(t) \text{ (eq. 1)}$$

Increasing light intensity results in appearance of nonlinear respond which requires to be presented as a more general equation 2:

$$P = \epsilon_0 (\chi^{(1)} E(t) + \chi^{(2)} E^2(t) + \chi^{(3)} E^3(t) + \chi^{(4)} E^4(t) + \dots) \text{ (eq. 2)}$$

This dissertation focuses mostly on third-order processes represented by  $\chi^{(3)}E^3(t)$  part of the above equation, mostly TPA and resulting from it TPEE with a little tribute to nonlinear refraction.

$\chi^{(3)}$  is a complex parameter comprising of real part represented by nonlinear refractive index  $n_2$  and imaginary part represented by nonlinear absorption coefficient  $\alpha_2$ . In turn, the relation of  $n_2$  and  $\alpha_2$  to the total refractive index and total absorption coefficient, respectively, may be presented as follows (eq. 3 and eq. 4):

$$n(I) = n_0 + n_2 I \text{ (eq. 3)}$$

$$\alpha(I) = \alpha_1 + \alpha_2 I \text{ (eq. 4),}$$

with its contribution dependent on light intensity  $I$ . In the above equations,  $n_0$  is the linear refractive index, whereas  $\alpha_n$  is the n-photon absorption coefficient. In fact, the nonlinear refractive index may also be considered as a complex factor (eq. 5) with its real part representing nonlinear refraction and imaginary part responsible for nonlinear absorption, in analogy to the complex linear refractive index.

$$\hat{n}_2 = n_2 + i\kappa \text{ (eq. 5)}$$

where  $\kappa$  is an extinction coefficient.

From a microscopic point of view, the response to a high amplitude optical field is described by complex cubic hyperpolarizability  $\gamma$  with its real part corresponding to nonlinear refraction and imaginary part describing nonlinear absorption of a molecule. The latter is more common presented in the form of TPA cross section  $\sigma_2$  (eq. 6).

$$\sigma_2 = \frac{\alpha_2}{N\hbar\omega} \text{ (eq. 6)}$$

where  $N$  is molecules concentration.

### 3.2.1. Determining $\sigma_2$ via two-photon excited emission method

Several approaches may be chosen for experimental determination of TPA cross section, however, none of them is a direct measurement of the parameter. The TPEE method is based on the comparison of a characterized sample with a reference fluorophore of known TPA cross section value  $\sigma_{2,r}$ . [30]

To serve as a reference, a chosen fluorophore is required to exhibit emission spectrum overlapping with a to-be-characterized sample. In fact, comparison is also possible to be performed with a non-overlapping reference, however, in such case, detectors spectral sensitivity should be known [30], which is usually unavailable when using data from literature. As the experimental part bases on measuring two-photon induced photoluminescence spectrum of a given sample and a reference (see also the *Methods* section), the comparison should be done with respect to **QY**s of the subjects as it connects photoluminescence and absorption processes (eq. 7):

$$QY = \frac{N_{emitted}}{N_{absorbed}} (\times 100\%) \text{ (eq. 7)}$$

where  $N_{absorbed}$  is the number of photons absorbed by a given sample and  $N_{emitted}$  is the number of photon emitted by the sample as a consequence of absorption. **QY** is rarely equal to 100% as part of the absorbed energy is usually released in form of non-radiative relaxation processes, for instance, internal conversion or energy transfers, causing photoluminescence quenching. Moreover, if the sample and the reference are dissolved in solvent of different refractive indexes ( $n$  and  $n_r$ ) or in different concentrations ( $c$  and  $c_r$ ), respective correction should be included, producing following equation (eq. 8):

$$\sigma_2 = \frac{F n_r c_r}{F_r n c} \times \sigma_{2,r} \text{ (eq. 8)}$$

with  $F$  and  $F_r$  referring to emission intensity (integral of the area under the emission spectrum curve) of the sample and the reference, respectively.

### 3.2.2. Determining $\sigma_2$ via Z-scan method

The TPEE method, although very convenient and quite fast, is affected by several drawbacks, including application limited to samples exhibiting photoluminescence and relatively poor susceptibility compared, for instance, to the Z-scan method.[2] The latter, based on detection of transmittance changes in respect to distance to focal point (see also the *Methods* section), is able to identify even small disturbances. In contrast to the TPEE method, it provides information not only on NLO absorption but also on nonlinear refraction, collected through one measurement. In principle, both techniques should provide comparable results and can be interchangeably used for estimation of the maximal values of the TPA cross-sections. Differences between the TPA cross-sections values measured by the two techniques were attributed to the presence of non-radiative paths of absorption or relaxation, making the z-scan technique the more accurate one. On the other hand, it should be admitted that both the experiment and data processing is far more time consuming.

As a matter of fact, Z-scan method is a comparing one as well. For reference purposes, Z-scan traces are recorded for a sample displaying no nonlinear absorption, typically a fused silica plate of known thickness. Under such requirement, the following eq. 9:

$$\Delta\hat{\Phi} = \Delta\Phi_{re} + i\Delta\Phi_{im} \text{ (eq. 9)}$$

where  $\Delta\Phi_{re}$  is the real and  $\Delta\Phi_{im}$  is the imaginary part of phase shift, the value of phase shift  $\Delta\hat{\Phi}_{ref}$  of the reference consist only of the real part.  $\Delta\hat{\Phi}_{ref}$  which is proportional to peak-to-valley amplitude of closed-aperture Z-scan traces, along with beam

waist  $w_0$ , which determines the beam waist for the measurements of investigated samples (and their solvents), may be determined from the reference traces fitted with theoretical curved. Further Z-scan measurements of characterized samples of known concentrations fitted with similar curves, although with respect to the presence of absorption, lead to determining phase shifts and  $\mathbf{T}$  factor defined as:

$$T = \frac{4\pi\Delta\Phi_{im}}{\Delta\Phi_{re}} \text{ (eq. 10)}$$

The values are then used for the calculation of the macroscopic parameters of  $\chi^{(3)}$ ,  $n_2$ ,  $\alpha_2$  and absorption coefficient  $\beta$  or microscopic  $\gamma$  and  $\sigma_2$ . Detailed description and equations derivation sequence is given in Sheik-Bahae et al. [31]. Briefly, the complex nonlinear refraction index may be calculated from real and imaginary parts of  $\hat{n}_2$  (eq. 5) given as follows (eq. 11, eq. 12):

$$Re(\hat{n}_2) = \frac{\Delta\hat{\Phi}_{re}}{\Delta\hat{\Phi}_{re,ref}} \times \frac{l_{ref}}{l} \times n_{2,ref} \text{ (eq. 11)}$$

$$Im(\hat{n}_2) = \frac{T}{4\pi} \times \frac{\Delta\hat{\Phi}_{re}}{\Delta\hat{\Phi}_{re,ref}} \times \frac{l_{ref}}{l} \times n_{2,ref} \text{ (eq. 12)}$$

Third-order susceptibility is proportional to nonlinear refractive index:

$$\chi^{(3)} = \frac{n_2 \times n^2}{c_1} \text{ (eq. 13)}$$

where  $c_1$  is a constant value dependent on the system of units. Very often a wavelength ( $\lambda$ )-dependent nonlinear absorption coefficient is presented in literature as a basic characteristic of nonlinearly-active materials:

$$\beta = \frac{4\pi \times \text{Im}(\hat{n}_2)}{\lambda} \text{ (eq. 14)}$$

Moving to microscopic characteristics, cubic hyperpolarizability is related to macroscopic parameters (eq. 15) with respect to local field factor  $\mathbf{L}$  which may be derived from Lorenz equation (eq. 16).

$$\gamma = \frac{\chi^{(3)}}{NL^4} \text{ (eq. 15)}$$

$$L = \frac{n_2+2}{3} \text{ (eq. 16)}$$

TPA cross section, which will be mentioned very often in this dissertation, along with its volume and molar mass-dependent derivatives of  $\sigma_2/\mathbf{M}$  and  $\sigma_2/\mathbf{V}$ , as a convenient nonlinear absorption characterising parameter, may be then calculated as:

$$\sigma_2 = \frac{\hbar\omega \times \beta}{N} \text{ (eq. 17)}$$

### 3.3. Materials

Optically active materials are those that interact with electromagnetic waves through refraction or absorption, which may then be followed by light emission. Such properties are displayed by organic fluorophores, among which both proteins and non-protein molecules may be found, and by inorganic optically active agents, including metal nanoparticles, perovskites and QDs.

### ***3.3.1. Colloidal semiconductor quantum dots (QDs)***

The history of QDs began in 1981, when Alexey Ekimov discovered crystalline nanostructures in a glass matrix, and a few years later Louis Brus detected their colloidal form. The term came along with Mark Arthur Reed's article [32] to name three-dimensionally confined quantum wells displaying discrete density of states. Since then, the knowledge of QDs has grown enormously as a result of numerous theoretical and experimental research. Nevertheless, much is still to be discovered and this thesis is intended to be a tiny contribution to the science of colloidal semiconductor nanomaterials, their characterisation, and functionalisation.

The term “quantum dots” may refer to all semiconductor nanomaterials or, specifically, to the spherical, zero-dimensional ones, to differ them from one-dimensional semiconductor nanorods (quantum rods, QRs) and two-dimensional semiconductor nanoplatelets (NPLs) and in this thesis the second nomenclature is used. Nanomaterials used to be defined as structures with at least one dimension smaller than 100 nm: all dimensions smaller than 100 nm for 0D QDs, two dimensions smaller than 100 nm for 1D QRs and one – for 2D NPLs. However, less artificial and more practical classification differs nanomaterials from bulk materials taking into account quantum confinement. Therefore, the discussion in this thesis is based on the assumption that nanomaterials are such structures whose respective dimensions are smaller than the exciton Bohr radius [33].

#### ***3.3.1.1. Relation between the structure of a QD and its optical properties***

Properties of any material are clearly dependent on its composition. The type of compound building a QD has its reflection in its optical behaviour, for instance, roughly determines the range of absorbed wavelengths of light and, in turn, of emitted photons. Also, depending on the elements making up a QD, the nanomaterial exhibits different affinities to ligands or any to-be-deposited structures dictating the choice of post-processing and functionalisation methods. In this dissertation, however, more accent is put on how

optical properties are influenced by the structure of nanoparticles, including their size and, especially, their dimensionality.

#### 3.3.1.1.1. *Size effect*

The exciton Bohr radius is the distance between an electron on the conduction band and a respective hole on the valence band after excitation. Its value depends on the composition of the semiconductor (Table 1).

*Table 1 Exciton Bohr radius of several semiconductors.[34]*

<b>Semiconductor composition</b>	<b>Exciton Bohr radius (nm)</b>
<b>ZnSe</b>	4.5
<b>CdSe</b>	5.3
<b>CdS</b>	5.3
<b>CdTe</b>	7.3
<b>InP</b>	15
<b>InAs</b>	34

The movement of electrons and holes is also always confined to the size of a semiconductor structure. Therefore, if the radius of a semiconductor structure is smaller than its exciton Bohr radius, the band gap becomes larger, increasing the excitonic transition energy. The smaller the QD (of a given composition), the larger the bandgap, which has its consequences in their optical properties, especially in blue-shifted luminescence (Figure 55).

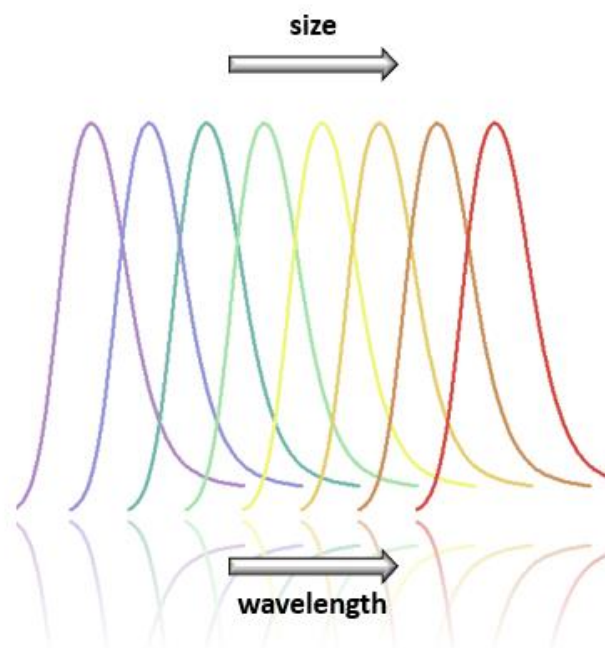


*Figure 5 Decrease of bandgap with increasing size of semiconductor nanoparticles manifesting itself in a red-shift of their emission spectrum.*

#### 3.3.1.1.2. Dimensionality

As mentioned above, semiconductor nanomaterials may be divided into three groups, 0D QDs, 1D QRs, and 2D NPLs, depending on the number of dimensions which quantum confinement occurs within. For QDs, this phenomenon refers to all directions. As emission properties are a significant part of this thesis, let me first focus on the width of emission spectrum. Considering the size effect, one may conclude that for a narrow spectrum of emission, QDs have to be not only monodisperse but also as similar to a sphere as possible, so that in all directions a QD has the same size and display the same value of energy band gap and therefore emit light of possibly narrow range of wavelength.

The requirements are, however, decreased in case of QRs. Until year 2000, QRs of II-IV and III-V semiconductors were only obtained as a co-product with QDs in difficult to separate reaction mixtures and, nonetheless, they should not be called QRs as their cross sections were usually too high to observe the confinement effect. Optically active QRs were for the first time synthesised intentionally and separately from QDs by the group of Paul

Alivisatos [35]. This contribution provided new possibilities for nanomaterials science and applications and one of them is the fact that in order to obtain QRs of narrow emission, in comparison to QDs, only the cross-sections of the nanocrystals have to be round with constant radius. Currently available synthesis methods allow to obtain QDs of typical full width at half maximum (FWHM) in the range of 25-40 nm.[36] To compare, the FWHM of blue-emitting ZnSe/ZnS QRs has been reported as in the range of 10 nm to 20 nm [37],[38].

Let me consider how narrow the emission peak may be if only one dimension would be required to be monosized. The answer came shortly after the first description of 2D NPLs in 2008 by Sandrine Ithurria and Benoit Dubertret.[39] NPLs are thick of several nanometers, which corresponds to a few atomic monolayers and this dimension is responsible for the confinement effect. In contrast, their lateral dimensions are, respectively, larger enabling free movement of electrons in the length-width plane. The case of narrow emission appears to be the most facile for NPLs which only needs to have the same thickness, practically independently on their lateral dimensions. The thickness of NPLs depend on reaction conditions, especially temperature and reagents ratio, and is relatively more facile to control in comparison to all dimensions in QDs or two dimensions in QRs. Therefore, 2D NPLs exhibit narrow luminescence peaks with strictly defined wavelengths of the maximum, depending on the number of atomic layers in a NPL.

The significance of narrow emission is related to the currently intensively developed applications in wide range of domains including displaying devices in information technologies [40], bioimaging in medical diagnosis[41] and military field.[42] Narrow spectra of photoluminescence provide saturated colours for high-colour-quality display and result in higher efficiency of devices.[43] In case of diagnosis, narrow, defined and constant wavelength range of emitted light is crucial for reliable imaging, especially for simultaneous imaging of multiple targets or processes.[44] Finally, narrow emission materials may be used for highly sensitive military sensors in object targeting. [45]

Nevertheless, dimensionality has an impact not only on the shape of the emission peak width. It strongly influences electronic spectrum and decides how the density of states changes with energy (Figure 66). In 0D QDs, electron and hole states levels display discrete character whereas with one elongated dimension in QRs change to a saw-like quasi continuum. For 2D NPLs, the levels may be presented as a step-like quasi continuous.

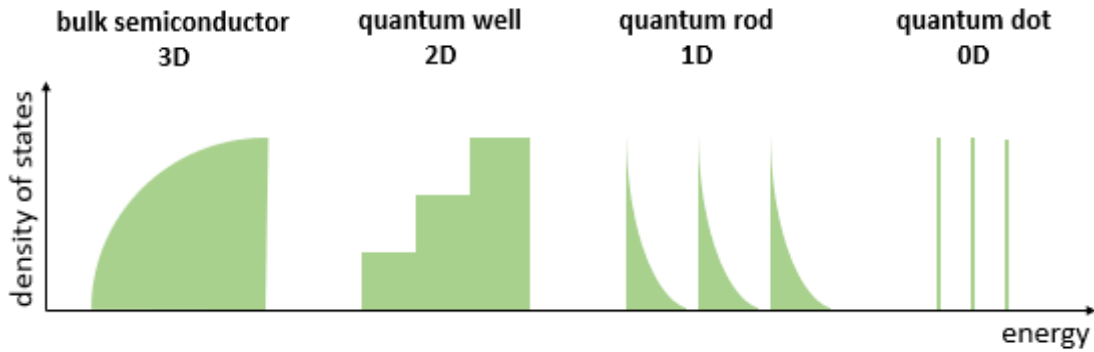


Figure 6 Dimensionality-dependent semiconductor electronic spectrum. Drawn basing on.[46]

The change in dimensionality involves changes in the strength of interactions within the structure.[22] It influences electron-hole Coulomb coupling and, as a result, exciton binding energy (EBE) which describe the strength of electron-hole interactions after excitation. EBEs of both QRs [47] and NPLs [48] exceed not only that of the bulk semiconductor but also those of 0D QDs. Moreover, when a photon penetrates a 1D or 2D structure, the tangential component of its electric field is constant. It has its consequence in the strength of exciton coupling with emitted photons and leads to shorter fluorescence decay in QRs and NPLs in comparison to QDs.

The elongated structure of QRs leads to interesting properties such as linearly polarized emission [49], [50] highly desirable in displaying devices as it improves their efficiency [43], in the emission of lasers to increase the efficiency and lower the pumping threshold as well as in conformational change and energy transfer studies in biological systems.[49] The rod-like shape also improves charge separation simply because it naturally guides electrons along their structure [51]; the phenomenon may be especially seen in semiconductor-metal heterostructures, where metal domains may be grown on the tips of quantum rods, providing better separation between electrons transported to the metal part and holes left at the semiconductor core.[52] Such properties may then find application in photocatalysis of both reduction [52] and oxidation [53] reactions. Moreover, elongated semiconductor nanostructures display an interesting property of higher TPA cross sections.[18] This may simply be the result of their larger areas [6] as the length of QRs is not restricted to be smaller than the exciton Bohr radius as it is in the case for QDs but also from their lower degree of symmetry. It causes splitting of degenerate energy states in

non-spherical nanomaterials increasing the density of energy states and, thus, increasing the probability of electron transitions.[18] An interesting phenomenon is observed in semiconductor QRs: their TPA cross section increases super linearly with their volume (is nearly proportional to their volume to the second power) whereas for 0D QDs this relation is linear. This discrepancy has been attributed to the strong confinement effect in rod-like structures.[6]

The super linear volume-TPA cross section dependence has also been observed in 2D colloidal NPLs and has been connected to the ultra-strong and anisotropic character of their confinement.[6] Thus, TPA cross sections of colloidal CdSe NPLs have been detected to reach the values up to  $10^7$  GM. In comparison to QRs, two dimensions are to be manipulated which opens a wider range of possibilities to obtain materials with high TPA cross section but, for example, short enough to be encapsulated as cargo in desired carriers. For example, to reach a volume of about  $170 \text{ nm}^3$ , the length of 3 nm-diameter QRs has to be 25 nm, while even more that two times thinner NPLs (4.5 ML which corresponds to 1.2 nm) may be still shorter having the lateral dimensions of 16 nm x 8 nm. Such materials have been compared and their TPA cross sections are very similar:  $1.45 \times 10^5$  GM and  $9.22 \times 10^4$  GM, respectively.[6]

### ***3.3.2. Two-dimensional semiconductor nanomaterials – colloidal nanoplatelets***

The analysis of the relation between dimensionality and properties encouraged me to focus on the 2D NPLs as they display enhancement of many advantageous properties in comparison to 0D and 1D semiconductor structures.

Colloidal semiconductor NPLs can be defined as nanostructures thick of several atomic monolayers (typically in the range of 2-6, however thicker structures are also presented in literature [54] and lateral dimensions larger than, or comparable to, the exciton Bohr radius of the material so that the strong confinement effect appears only in the thickness direction. Typically, NPLs are made of CdSe, CdS or CdTe compounds [22], however, recently other materials, for example red and near-infrared emitting PbS

[55] and PbSe [56], have been employed to form NPLs. This thesis focuses on CdSe NPLs as the best defined and widest characterized ones so far, which allows them serving as a model example for interesting characteristics comparisons, different functionalisation approaches, and attempts for practical applications. The thickness-based nomenclature refers to the number of atomic monolayers in which one monolayer corresponds to one pair of chemical elements in a crystal. As the thickness of NPLs starts and ends with a metal compound (Figure 77) [57], Cd or Pb in the examples mentioned above, then the number of monolayers is never an integer. Therefore, in this thesis, as in many scientific publications, NPLs of respective numbers of monolayers (ML) will be termed 2,5 ML, 3,5 ML, 4,5 ML etc., however an alternative nomenclature omitting one metal atom layer (2 ML, 3 ML and 4 ML) may also be faced in the literature. In this thesis, NPLs of zinc-blende structure are studied, however, wurtzite structure is also possible to obtain depending on the synthesis method.[58]

As the distances between atoms in a crystal are constant and depend on the composition and the type of crystal structure, the number of monolayers in a NPL automatically defines its thickness and the other way around. For instance, the crystal lattice constant of zinc-blende CdSe NPLs is equal to 0.608 nm.[59] Following the structure of zinc-blende (Figure 7), one can notice that this constant describes the distance between two Cd atoms and encompasses one additional Cd and two Se atoms. It means that the thickness of 2.5 ML CdSe NPLs is about 0.6 nm, 3.5 ML – 0.9 nm, 4.5 ML – 1.2 nm etc. The thickness of the obtained NPLs depends on the reaction conditions. Most protocols report an increase in the number of monolayers with temperature during the reaction and an impact on the quantity ratio between the respective precursors.[22] For thicker NPLs (more than 6.5 ML) different approaches have been proposed such as atomic layer deposition or the addition of chloride anions to induce thickening.[54]

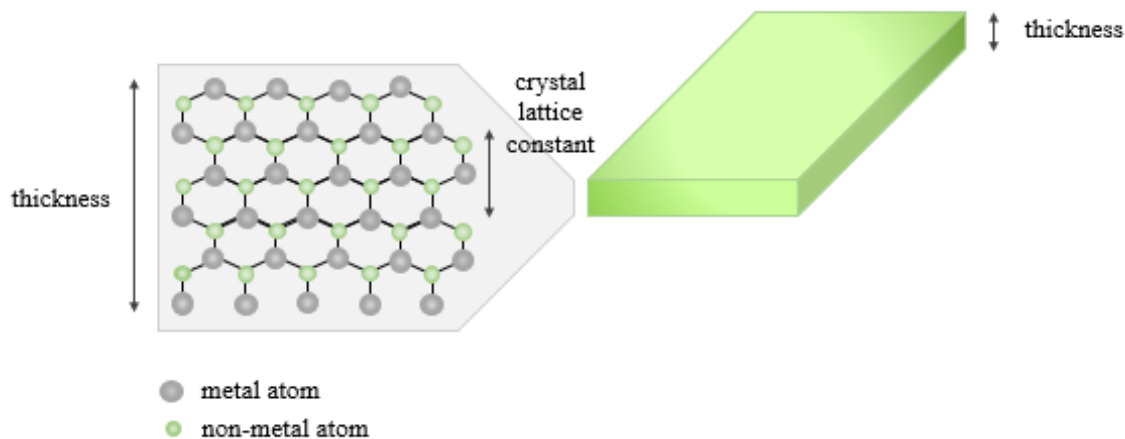


Figure 7 Schematic representation of a NPL and its crystal structure.

### 3.3.2.1. Synthesis mechanism

QDs may be prepared via either top-down or bottom-up route. The first approach is based on fragmenting bulk material into nanometric parts and includes photolithography and nanoscale inkjet printing. Bottom-up techniques start with atoms or molecules assembling them into nanoparticles and they are mostly based on wet chemical synthesis. In order to obtain colloidal QDs, the second approach is more commonly harnessed, as ligands, which are crucial to provide dispersity of QDs in a medium creating a colloid, may be simply added to the reaction mixture or are already a part of nanoparticles precursors. Ligands control particle growth and are responsible for colloidal stability during synthesis; therefore, they are integral materials for most syntheses of nanoparticles.

The mechanism of the synthesis of colloidal semiconductor NPLs has aroused controversy, and different explanations have been proposed in the literature. One of the hypotheses, called oriented attachment, assumes formation of small nanoparticles in the first stage which then assemble into NPLs. Growth in two directions is energetically preferred as opposed to isotropic growth due to the presence of ligands. The attachment of small nanoparticles to each other results in densification of the ligand layer on two opposite sides of the to-be NPL defining its thickness (Figure 8). Such a mechanism was presented as an explanation for the growth of PbS nanosheets [60] and then proposed for CdSe NPLs.[61]

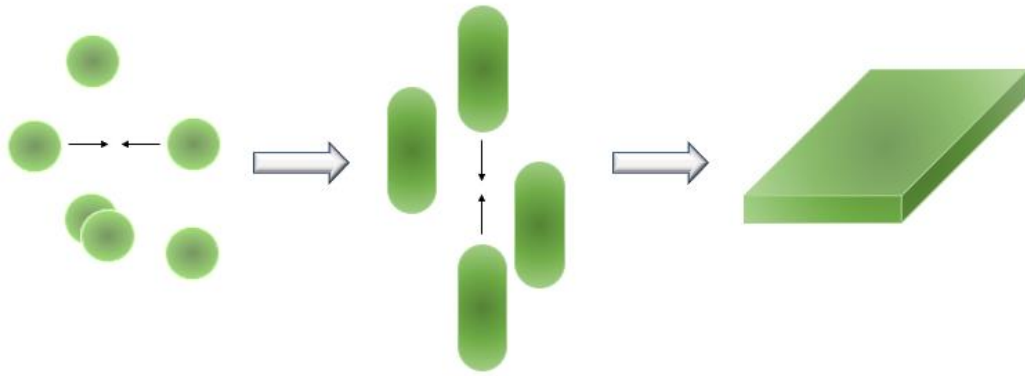


Figure 8 Scheme of oriented attachment mechanism.

However, Son et al. [62] developed an interesting method for the synthesis of CdSe NPLs that requires the presence of an organic molecular template that defines the space in which a 2D structure can grow. This suggested that general mechanism of NPLs synthesis bases on presence of respective organic mesophase (Figure 99).

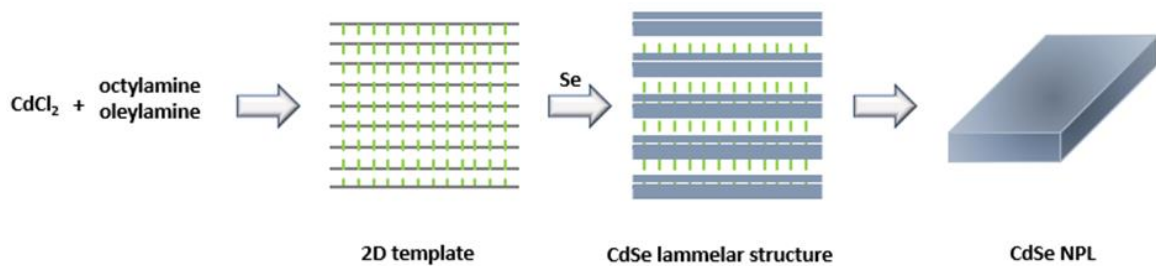
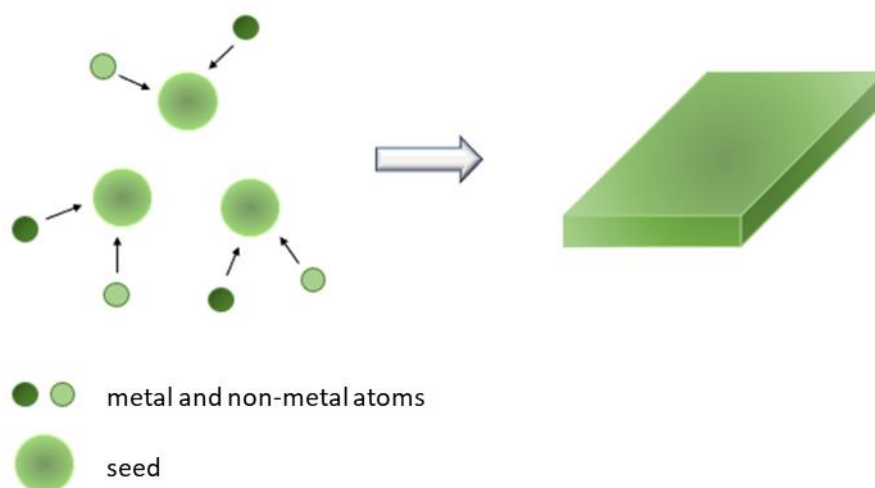


Figure 9 Mesophase-mediated mechanism (based on [62]).

Another scenario assumes the formation of nuclei at the beginning of the reaction which then does not attach to each other like in the hypothesis of orientation attachment but growth in the 2D direction as ‘monomers’ (respective atoms) are continuously attached to their structure (Figure 10). Growth at the edges of NPLs is much faster than at the plane surface resulting in creation of 2D structures rather than isotropic QDs.[63]



*Figure 10 Continuous transition mechanism.*

The first [39] and still most widely used methods to synthesise NPLs require addition of short-chain ligands, acetates, or sometimes propionates, along with a long-chain carboxylate following the assumption that such mixture induces growth in two directions. However, this hypothesis has been denied when CdSe NPLs were obtained in melt of either cadmium propionate or cadmium myristate [64] and then in a more typical solvent synthesis but with the use of cadmium octanoate without the addition of shorter ligands.[65] Riedinger et al. explain that the presence of short-chain ligands decreases the solubility of the metal precursor inducing phase separation. According to their work, NPLs are created when the precursor is insoluble whereas if it is dissolved, QDs form.

Therefore, the hypothesis of oriented attachment, which was based on the presence of ligands, was called into question. The measurements of small-angle X-ray scattering (SAXS) and wide-angle X-ray scattering (WAXS) also showed gradual lateral extension of NPLs suggesting a continuous transition from seeds to 2D nanostructures by the addition of monomers.[66] The above-mentioned measurements also rule out the scenario of molecular template mechanism as no evenly-spaced diffraction peaks which indicates the presence of lamellar structures are visible. No mesophase was also detected by differential scanning calorimetry (DSC) or observed via a polarized scanning microscope.[64]

While these two mechanisms are questioned, currently the third one assuming a continuous transition of nuclei into NPLs via the addition of ‘monomers’ seems to be the most probable. It has been confirmed by the above-mentioned SAXS measurements, as well as in agreement with calculations made on the basis of density-functional theory and kinetic Monte Carlo simulations.[64]

### 3.3.2.2. Properties

While the case of synthesis mechanism is still discussed, the outstanding properties of 2D semiconductor nanomaterials, compared to low dimensional structures, are unquestionable. The already explained size effect which connects decrease of a QD size with increase of its bandgap resulting in a blue-shift of its absorption and photoluminescence peaks works also in the case of 2D nanostructures. The only difference is that in the case of NPLs only their thickness influences the position of the absorption/emission peak while the lateral dimensions may stay constant. The wavelengths corresponding to the maximum absorption/emission are strictly defined for each thickness of the NPLs (Figure 11).

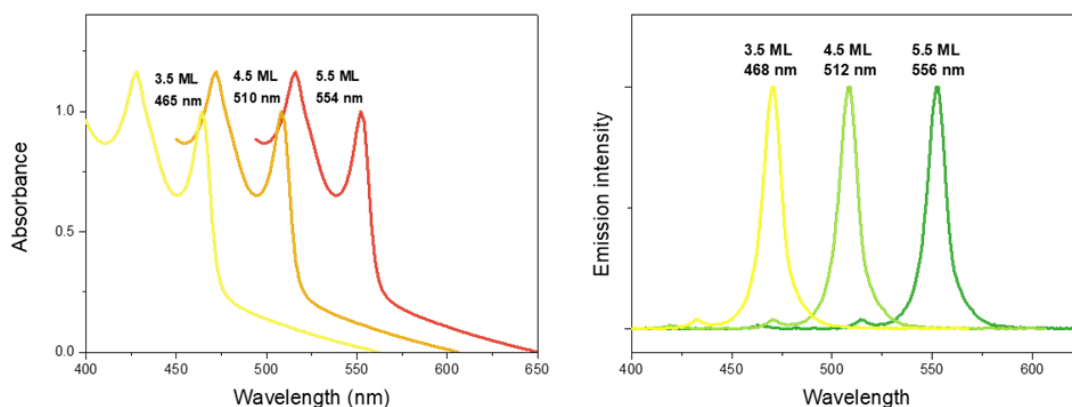


Figure 11 Strictly defined excitonic transitions and emission maxima wavelengths of 2D CdSe NPLs.

The anisotropy of NPLs causes splitting of the heavy hole (HH) and light hole (LH) valence band states resulting in characteristic narrow peaks observed in the absorption

spectrum of NPLs. Splitting between LH and HH takes place in QDs as well, however, with a value of about 40 meV, it is too small to be visible in an inhomogeneously broadened absorption spectrum.[67] Therefore, in case of 0D QDs, the LL and HH bands are completely overlapped.

The wavelengths at which NPLs display maximum intensity of emission are strictly defined for each thickness (Figure 11) and varies only with a few nanometers between batches, which may be due to differences between measuring sets and their inaccuracies. [6,54] The Stokes shift is very small, typically few nanometers.[68] For such atomically flat nanoparticles with extended lateral dimensions, very narrow spectra are typical. Full width at half maximum does not exceed 40 meV (31 nm) for different Cd-compound NPLs and for CdSe NPLs it reaches 38 meV (10 nm). The photoluminescence intensity of NPLs is enhanced with QYs reaching up to 50% ([68], [6],[39]) while 0D QDs exhibit QYs in the range of 5-30%. Also, the 2D shape influences the strength of exciton coupling decreasing emission decay times.[22]

The strength of Coulomb interactions between an electron and a hole after excitation increases with dimensionality. For example, bulk CdSe exhibits an EBE of 10-15 meV [69,70], for 0D CdSe QDs this parameter was determined experimentally and theoretically as up to 100 meV for 12.5 nm diameter particles whereas for 2D NPLs of corresponding thickness (4.5 ML) was reported to be in the range of 58-335 meV, depending on the conditions and dielectric constant [71,72]. Interestingly, the exciton recombination rate scales with the area of NPLs. [22]

The values presented above confirm that the lateral dimensions are not to be neglected. The length and width of NPLs are responsible for the quality of their self-assembly and, therefore, on the interparticle processes, such as charge and energy transfer.[73] Moreover, they have crucial impact on TPA cross sections; Scott et al. reported differences in  $\sigma_2$  of CdSe NPLs measured by the z-scan method of nearly 3.5 orders of magnitude depending on their area. Due to the superlinear volume-TPA cross section dependence attributed to the ultra-strong confinement in NPLs and described earlier, it is possible to reach TPA cross section of magnitudes up to  $10^7$  GM [6], the highest result reported in the literature confirmed by two independent methods. For practical applications requiring TPEE, the crucial parameter is two photon action cross section (alias two-photon brightness), which is dependent not only on TPA cross section but also

increases linearly with QY of the material. Therefore, even if high TPA has also been observed in other materials, for example, gold clusters which display the TPA cross sections up to  $17 \times 10^3$  GM per atom [74], their low QYs decrease their worth for emission-related applications. With QYs  $10^{-5} - 10^{-6}$  %, their two-photon action cross section is only up to  $17 \times 10^3$  GM/atom. To compare, this parameter reaches about 1.1 GM/atom and 2.5 GM/atom for CdSe QDs and QRs, respectively, while for the largest NPLs it was observed to reach 45 GM/atom.

### 3.3.2.3. *Application*

In terms of broadly understood semiconductor nanoparticles, they exhibit crucial advantages over other optically active nanomaterials. Their high stability [75], in all colloidal, optical, thermal and chemical senses, in many examples orders of magnitude larger than those of organic dyes, makes them easy to handle simplifying not only their storage and many experiments, but also their usage in potential applications. Broad absorption spectra provide flexibility of excitation wavelengths. Due to bright emission, often 10-100 times brighter than organic dyes [76] of symmetrical, narrow bands with a position tuneable with their size, which simplifies the difference of their signals from noises, they found application in quantum light-emitting diodes (QLED) displays.[14] With high QYs in the NIR region [75] and high TPA cross sections [77], [78] they become promising candidates for medical staining and bioimaging applications. This is because if the signal is to be detected, in spite of the presence of variety of substances that absorb, scatter and disturb it in any other way, it is crucial to excite the nanomaterial with photons of a wavelength which is as optically neutral for biological tissues as possible. Living organisms and, along with them, their tissues are visible, meaning they highly absorb visible light. Therefore, a suitable wavelength should be searched outside of the visible range. Looking among near IR wavelengths, harmless for biological tissues, seems to be the clue and, indeed, absorption and scattering from blood, skin and fat are low within the following ranges: 650-950 nm and 1000-1350 nm, which are called the first and the second biological transmission windows, respectively [79]. The literature mentions more such windows [25], however, for materials emitting in the visible range, exciting with deeper IR would mostly involve four and more photon processes which are rarely effective.

High TPA cross sections, which means red-shifted absorption, usually appearing in the IR region, if resulting in TPEE, are thus desired for biological applications. Most of these properties are enhanced with increasing dimensionality, as was previously described, making 2D NPLs the most promising type of semiconductor nanoparticles for such applications.

Despite promising properties and commercial adaptation in some domains, for some applications semiconductor nanoparticles are in the phase of studies and proof-of-concept reports. Mostly, they could be applied for medical diagnosis applications due to their advantageous and tuneable emission and NLO properties, unless following drawbacks. Raw semiconductor nanoparticles are hydrophobic, which means that in water-based bioliquids they tend to aggregate and precipitate, which in turn blocks their transport through tissues.[76] Also, probably the most serious problem is that nanoparticles with the most promising optical properties including narrow emission spectra, high TPA cross sections and QYs and action in “biological transmission windows”, are based on cadmium or lead, questioning their safety.[80] Moreover, typically long emission lifetimes (10-100 ns, [75]) are not ideal for real-time tracking of imaging processes.

High stability, broad absorption spectrum and charge separation possibility in semiconductor nanoparticles suggest their application as catalysts in electrons- and holes-involved processes such as photoinduced redox reactions. Photons, which may simply originate from sunlight, excite semiconductor nanoparticles transporting electrons to the conduction band and leaving holes at the valence band, thus providing both negative and positive charge for reduction and oxidation reactions, respectively. However, electrons and holes recombine very quickly, decreasing the possibility of harnessing the charges to catalyse a desired reaction.

#### *3.3.2.4. Functionalisation*

In spite of the disadvantages, the previously mentioned unquestionable superiorities over other materials are too tempting to abort studies on semiconductor nanoparticles, in particular on 2D NPLs, in various application fields including information technology, security, biology, and photocatalysis. Therefore, numerous approaches on modification and functionalisation have been reported in a very wide spectrum of directions in order to

overcome the problems arising from the nature of semiconductor nanomaterials with no negative impact on their key properties.

Starting from the hydrophobicity, which is undesirable for biological and very often for the photocatalytic applications, several methods have been employed to prevent aggregation in water-based liquids. The most popular method tells to exchange or add particular hydrophilic ligands, mainly thiols.[81] This approach provides a similar size of hydrophilized material comparing to the raw hydrophobic nanoparticles. On the other hand, more and more research is focused on ligand exchange toward polymers or preparation of polymer coating without getting rid of original hydrophobic ligands.[82] On the side note, if the hydrophilic ligands are chiral, eg. cysteine [83], penicillamine [84,85] or glutathione [86], then not only hydrophilicity but also chirality is introduced into the system. This opens more possibilities for the treated material, as combined with its water-solubility, it may be applied in chiral drug recognition.[83] Moreover, symmetry breaking in semiconductor nanoparticles leading to increase of the density of states enlarges their TPA cross sections.[87]

Further hydrophilization methods base on encapsulation of the nanoparticles in different kinds of carriers, such as polymeric nano- or microbeads [88], oil-core/polymer-coat carriers [26], micelles [89]. Among various materials, polyethylene glycol (PEG) is willingly used in such encapsulation, especially for biological applications, as along with stability improvement provides minimalization of any nonspecific interactions with cell membranes.[82] In those strategies, one carrier typically contains a number of nanoparticles and, in natural consequence, the resulting particle is respectively larger. That may be either a drawback or an advantage depending on the final size and the planned application. For example, the bigger the particles, the more probable precipitation of the material. However, the size may be quite a selective factor for cancer cells-targeting application as quickly developing tumour blood vessels tend to be leaky and let larger particles into the mutated cells compared to normal vessels and healthy cells.[90] Targeting abilities may also be achieved through attachment of folic acid to the surface of QDs in polymer-coated [91] or encapsulated [92] form due to bolder take-up of folates by tumour cells in comparison to healthy cells.

The encapsulation strategies for hydrophilization are at the same time approaches for toxicity reduction simply based on creation of a physical barrier between living cells

and toxic ions, mainly  $\text{Cd}^{2+}$ . For instance, the percentage of viable HeLa cells after exposure to CdSe QDs encapsulated in self-assembling micelles reached 91.6% or 87.9% depending on the concentration of the nanomaterial in contrast to 22.7% and 16.1%, respectively, for non-encapsulated QDs.[89] Similarly, encapsulation of CdSe QDs in silicone oil-core/polymer-coat nanocarriers (NCs) vastly reduced their toxicity to normal human umbilical vein endothelial cells (HUVEC).[26]

Moving on to applications requiring charge separation, functionalisation strategies focus on lengthening the separation and delaying recombination processes. This may be very successfully achieved by deposition of metal nanostructures onto semiconductor nanoparticles. On such nanocomposites exposed to light, first electrons and holes are separated between the valence band and the conduction band of the semiconductor and then the electrons are willingly transported onto the metal.[24] Such approaches were already applied on 0D QDs [16], 1D QRs [52] and even first attempts were tried on 2D NPLs [93] as it is expected that on elongated QRs and extended in space NPLs with metal domains on their tips or corners, the charge separation may be much enhanced. On a side note, such modification results in diametrical decrease of emission capabilities, which may be a drawback depending on desired application. However, longer charge separation on semiconductor-metal nanocomposites makes them promising candidates for redox reaction photocatalysis. Some reactions are performed in organic media and in these cases hydrophobic heteronanoparticles may be used without much post-synthesis modification. However, for such important applications as water splitting for hydrogen generation in power engineering or reactive oxygen species generation in the field of medical therapy, aqueous medium is essential. Here, the above-mentioned hydrophilization techniques should be used. It is an example of a need for multifunctional nanoparticles.

Functionalisation may not only overcome existing drawbacks but also enhance already promising properties. Semiconductor nanoparticles, especially 2D NPLs, exhibit exceptionally high QYs and intensive photoluminescence, making them potential candidates for any emission applications. It has been proposed to further increase QY of CdSe nanoparticles by doping with copper ions [21], [94] basing on the reports that Cu ions work as deep electron traps and are responsible for the presence of a wide low energetic emission peak.[95] As a side note, doping should not be confused with deposition, as in the latter case whole metal nanostructures are being placed onto the surface of a semiconductor nanoparticle. On the other hand, during doping, individual ions are

being built into the structure of a semiconductor crystal lattice, creating defects. Dopant-induced defects may exist in a substitutional or an interstitial form (Figure 12). The first type appears when a native atom of a semiconductor is replaced with a heteroatom, occupying its original place. If a heteroatom takes an in-between place in the semiconductor crystal, where no native atom was originally supposed to settle, then the defect is called interstitial.

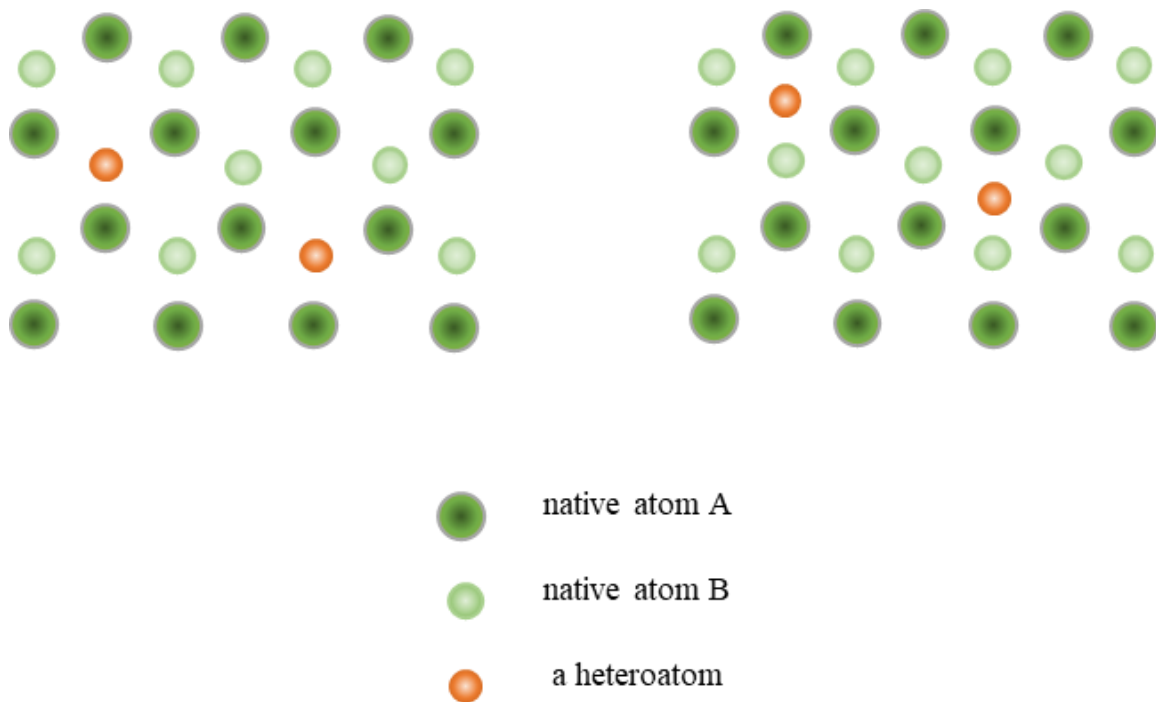


Figure 12 Types of defects as results of heteroions introduction: substitutional (left) and interstitial (right).

Depending on its electronic structure, a dopant may be isovalent with the original atom or be donor- or acceptor-like, if has more or less valence electrons, respectively.[96] The defects which introduce charge imbalance are mostly isolated point defects whereas charge may be compensated either by introduction of originally isovalent substitute or by formation of higher-order defects (defect pairs). The type and the charge of a heteroion incorporated as a dopant depends on chemical potential which determines the energy necessary for formation of defects either isolated or in pairs.

Doping influences emission without any significant change in the absorption spectrum. In particular, this phenomenon is beneficial in the case of CdSe NPLs with already very high QYs, typically about 40% [22], increasing the factor nearly unity.[94] It

is important to emphasise that this doping does not result in enhancing the characteristic of the narrow emission peak of NPLs but in the appearance of an additional wide band, meaning that such functionalisation is beneficial in application where the high overall QY is desired but not a very intense and simultaneously narrow emission peak.

## **4. EXPERIMENTAL**

The experimental part of the dissertation encompasses description of chosen materials and their synthesis, presentation of functionalisation processes, report of physicochemical characterisation methods and discussion of the results. The nanoparticles selected for the experiments should be treated as a model representative of materials which enables performing further modification, functionalisation, and characterisation of such advanced and complex systems. For that reason, CdS and CdSe nanoparticles were chosen as one of the most broadly studied and described and, consequently, characterized by the best understood mechanisms. Nevertheless, for many destined applications, including medical diagnosis and other biological purposes, but also in any field to minimize negative impact on the environment, more research should be done in synthesis of nanoparticles constructed of less toxic compounds.

### **4.1. Methods**

All semiconductor colloidal nanomaterials characterized in this dissertation were synthesised via bottom-up wet chemical synthesis, and this section provides a general description of such methods, while details for individual NPs types are given further. Moreover, here, all characterisation methods are presented while explanations of which particular experiment was performed on which material may be found in *Results and discussion* sections.

### 4.1.1. Synthesis

The chemical synthesis was performed under the Schlenk line (Figure 13). Substrates including medium substance along with magnetic stirring dipole are put in a three-neck flask. The side necks serve for a thermocouple sensor and for any injections during synthesis. The central neck is connected to a reflux condenser which is linked to the Schlenk line, either transporting nitrogen or removing gases to provide vacuum through a vacuum pump. Such an apparatus enables one not only to perform processes under vacuum or a chosen gas but also to change atmosphere conditions during synthesis. The flask is put in a heating mantle on a magnetic stirrer.

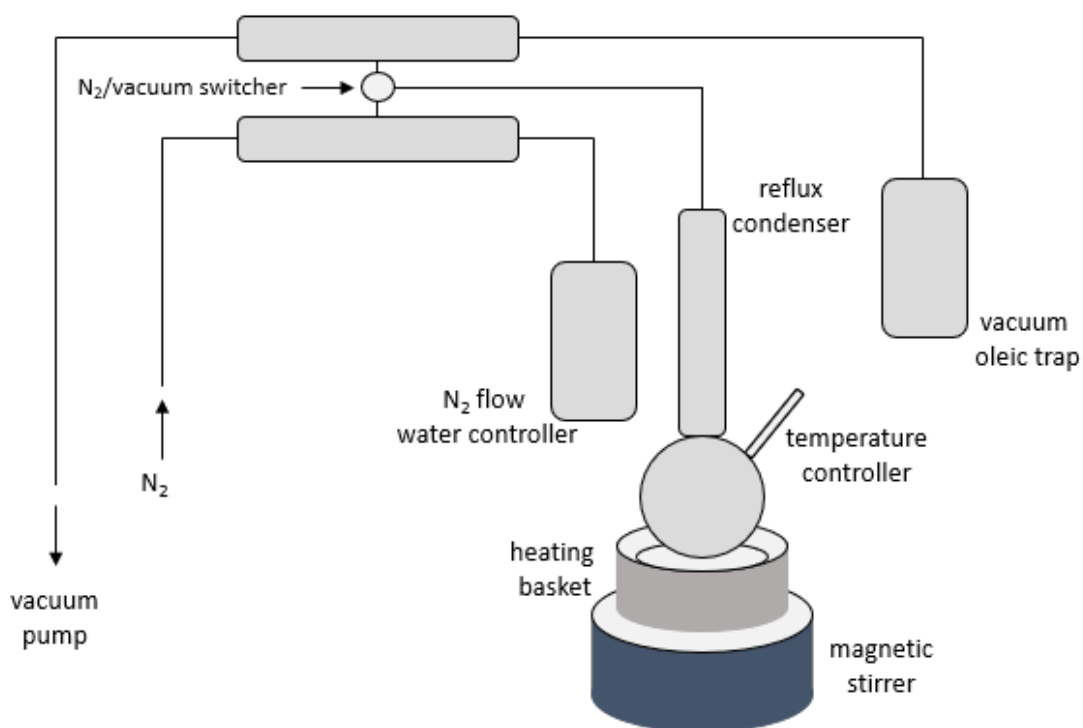


Figure 13 Schematic representation of a Schlenk line.

### 4.1.2. Characterisation

The structure of the nanoparticles presented in this dissertation was analysed using transmission electron microscopes (TEMs), details of which may be found in the descriptions of specific materials and their characterisation. The composition of the nanoparticles was studied using the energy-dispersive X-ray spectroscopy method (EDX) and performed either on a FEI Tecnai G<sup>2</sup> 20 X-TWIN microscope with EDX analyser or on a JEOL JSM-6610LVnx scanning electron microscope with attached EDX probe. The analyses were performed in cooperation with PhD Andrzej Żak (Faculty of Mechanical Engineering, Wrocław University of Science and Technology) and prof. Leszek Kępiński (Institute of Low Temperature and Structural Research, Polish Academy of Sciences).

UV-VIS absorption was measured on a JASCO V-670 spectrophotometer or, for dried probes (in cooperation with PhD Szymon Zelewski, (Department of Semiconductor Materials Engineering, Wrocław University of Science and Technology)), on a thermoelectrically cooled CCD spectrophotometer (Avantes AvaSpec-HSC1024x58TEC-EVO).

Photoluminescence spectra were obtained on a Hitachi-4500 spectrofluorimeter or, for dried probes (in cooperation with PhD Szymon Zelewski, (Department of Semiconductor Materials Engineering, Wrocław University of Science and Technology)), on a thermoelectrically cooled CCD spectrophotometer (Avantes AvaSpec-HSC1024x58TEC-EVO) with a 405 nm diode-pumped solid-state laser for excitation.

Time-resolved photoluminescence was measured with a custom-made Time Correlated Single Photon Counting (TCSPC) Becker & Hickl system on a TCSPC Module (SPC-130-EM), detected on a hybrid PTM detector (HPM-100-06) with a detector control card (DCC 100) on a Princeton Instruments spectrograph (ActonSpectraPro-2300i). Samples were excited using a picosecond 375 nm laser diode (BDL-375-SMC). Dedicated Becker & Hickl SPCImage software was used for the calculations.

Second method for emission lifetimes investigation based on a Hamamatsu C5677 (time resolution: 14 ps) streak camera measurements. The samples were excited either in single-photon (400 nm) or two-photon (800 nm) regime with a Coherent Libra-S ultrafast

oscillator and regenerative amplifier system (pulse duration:  $< 100$  fs and repetition rate: 1 kHz) equipped with a Coherent OperA-Solo optical parametric amplifier. The analysis was performed in cooperation with PhD Bartłomiej Cichy, (Institute of Low Temperature and Structural Research, Polish Academy of Sciences).

Photoacoustic spectra were obtained in cooperation with PhD Szymon Zelewski, (Department of Semiconductor Materials Engineering, Wrocław University of Science and Technology) as follows. The dried samples were set between glass plates and mounted in a non-resonant, airtight measurement cell. A 250 W halogen lamp coupled with a 320 nm focal length grating monochromator (Horiba iHR320) was used as an excitation source. In order to detect acoustic waves generated inside the cell, an electret condenser microphone was used. A lock-in amplifier (SR830) further demodulated the voltage signal obtained from the transducer.

Exciton binding energy was determined in cooperation with PhD Szymon Zelewski, (Department of Semiconductor Materials Engineering, Wrocław University of Science and Technology) from a combination of absorption spectroscopy described above and photoacoustic spectroscopy following a new method. The energy of the lowest exciton transition (hh1-ee1) appeared as a local maximum in the absorption spectrum was found. Next, the band gap energy was determined from the photoacoustic spectrum using the so-called knee method. Briefly, the band edge region line and the signal saturation region line were fitted with a bimodal linear regression model and lengthened to meet each other, and the energy at the intersection of these two lines was taken as the band gap energy. The difference between as determined the lowest exciton transition and the band gap energy was defined as the exciton binding energy.

Nonlinear optical properties of semiconductor nanomaterials and their functionalised analogues were characterised via TPEE and Z-scan techniques. The TPEE method is based on the excitation of a sample with a high-power source in the range of its TPA and detection of emission excited in such a way. The resulting photoluminescence spectra are then analysed for the calculation of desired NLO parameters. A reliable characterisation is possible only if the sample is excited by a range of wavelengths which enables finding the nonlinear absorption maximum and the shape of the absorption spectrum. Therefore, a femtosecond laser system should not only generate and amplify a beam but also be spectrally tunable. In our case, colloidal samples in quartz cuvettes in

a holder were set in the optical path of a laser beam generated from a femtosecond laser (~130 fs) system: an Integra-C Ti:sapphire regenerative amplifier (Quantronix Corp., East Setauket, NY, USA) and Palitra-FS optical parametric amplifier (Quantronix Corp., East Setauket, NY, USA) for wavelength tuning. The system operated at the repetition rate of 1 kHz. Such excited samples emitted light collected through an optical fiber by an Ocean Optics QE Pro-FL fiber optic spectrograph or an OceanOptics FLAME-T-VIS/NIR, depending on the experiment. Such procedure was repeated for a range of excitation wavelengths, again, depending on the studied material and its emission spectrum. The method enables us to calculate TPA cross section ( $\sigma_2$ ) of investigated samples compared to the reference two-photon active substances with known  $\sigma_2$ . In this case, the organic dyes listed by Makarov et al. [30] were used, specific compounds were chosen with respect to the requirement of overlap of the emission spectra of nanoparticles and dyes. Both samples and references were appropriately diluted in order to minimize errors arising from uneven colloidal distribution and avoid any internal filter effects.

The Z-scan technique was first proposed by Sheik-Bahae et al. [31] for characterisation of third-order NLO properties and become very popular due to its simplicity as it uses only a single beam and is quite uncomplicated to set up. It requires a high power excitation source for nonlinear effects to appear. The laser beam is then directed through a set of optical mirrors and a lens to reach the colloidal sample in a quartz cuvette. Transmitted through the sample, the focused Gaussian beam is directed to two detectors, one preceded by an aperture. The cuvette with the sample is set on a transporting table that moves the sample in parallel (z axis) to the beam during the measurement. The cuvette with the sample behaves like an additional optical lens that focuses or defocus the laser beam while being moved. As one of the detectors is preceded with an aperture, the intensity of the signal it detects changes with the move of the sample – increases with focusing, decreases with defocusing. It is therefore sensitive for both nonlinear absorption and nonlinear refraction. However, the second detector catches the whole intensity of the beam after it is transmitted through the sample, either it is focused or not, therefore the signal is only sensitive to nonlinear absorption and not to nonlinear refraction. Combination of both – so called closed aperture and open aperture – signals allows us to calculate both parameters. An additional detector is set before the beam is transmitted through the sample enabling detection of any laser inconsistencies. Similarly to the TPEE experiment, a 1 kHz-repetition rate system of an Integra-C Ti:sapphire regenerative

amplifier (Quantronix Corp., East Setauket, NY, USA) and a tunable Palitra-FS optical parametric amplifier (Quantronix Corp., East Setauket, NY, USA) were used. The emission signal was collected through an optical fiber by either an Ocean Optics QE Pro-FL fiber optic spectrograph or an OceanOptics FLAME-T-VIS/NIR, depending on experiment. Scanning along the propagation direction was repeated using a range of wavelengths.

Photocatalytic activity measurements were performed with a focus on both reduction and oxidation reactions. Reduction abilities were investigated by measuring the progress in time of nanoparticles-driven reduction of methylene blue (MB). This dye absorbs visible light in its oxidated form, while its reduced form is colourless. Specifically, 1 mL of an investigated nanoparticles solution, 1 mL of the solvent and 1 mL of ethanol was mixed. The alcohol was introduced as a so-called hole scavenger which traps positively-charged holes making electrons and holes recombination even harder. The MB aqueous solution was prepared with concentration corresponding to absorbance low enough to minimize errors. 1 mL of such MB solution was added to the nanoparticles and stirred. The mixture probe was taken as the "0" time point and measured using a JASCO V670 spectrophotometer. The mixture was exposed to light generated from a solar simulator (OPTEL Fiber illuminator, Opole, Poland) and samples were taken after defined time for absorbance measurements.

Oxidation abilities were examined indirectly through measurement of bovine serum albumin (BSA) concentration oxidized by reactive oxygen species (ROS) generated from aqueous medium with the support of characterized nanoparticles. 4 mg of BSA dissolved in 3.5 mL was mixed with 500  $\mu$ L of nanoparticles aqueous solution and a sample of the mixture was taken as the "0" time point. The photoluminescence spectrum was measured using FluoroMax-4 spectrofluorometer. The remaining mixture was continuously stirred and exposed to light from a solar simulator (OPTEL Fiber illuminator, Opole, Poland) and samples were taken after defined time for photoluminescence measurements.

Photochemical photostability was examined as the sensitivity of photoluminescence intensity to changes of pH and temperature. The pH of the characterized samples was adjusted between 6 and 9.5 to encompass possible extremes present in a human body (pH about 6 for tumour cells, pH about 8.8 of pancreatic fluid) using HCl and NaOH. For

an investigation of the stability at different temperatures, characterized samples were incubated in ThermoMixer C (Eppendorf) at 25°C, 30°C, 33°C, 37°C and 40°C.

The biocompatibility of the characterized samples was investigated in vitro in cooperation with PhD Julita Kulbacka (Department of Molecular and Cellular Biology, Wrocław Medical University) using a MTT reduction assay on normal human gingival fibroblast from primary culture (HGF, normal cell line) and on human ovarian endometrioid adenocarcinoma cell line (MDAH-2774). Characterized nanoparticles were prepared in four dilutions (1:50, 1:100, 1:200 and 1:500) and incubated with above-described cells for 24 h and 48 h. The cytotoxicity was evaluated using a GloMax® Discover multimode microplate reader (Promega).

The possibility of applying characterized nanoparticles in two-photon bioimaging was tested in cooperation with PhD Grzegorz Chodaczek and PhD Monika Toporkiewicz (Łukasiewicz Research Network - PORT Polish Center for Technology Development) in murine fibroblasts (L-929 cell line, ATCC®CCL-1™) in the logarithmic growth phase. The cells at a density of  $0.5 \times 10^5$  cell per well were set for 24 h in a 24-well plate in Iscove's Modified Dulbecco's Medium (GIBCO) with 100 U/mL penicillin, 0.1 mg/mL streptomycin and 10% fetal bovine serum, GIBCO). Next, cells were treated with diluted solutions of characterized nanoparticles, washed with Phosphate Buffer Saline (PBS) for removal of free nanoparticles, and fixed with formaldehyde. Both cells and free nanoparticles were mounted in Prolong Gold anti-fade solution and excited with a femtosecond infrared (IR) laser Chameleon Vision II (Coherent). The signal was detected with spectral PMT detectors using a 63x oil objective (HC PL APO CS2 63x/1.4 OIL) and visualized on a Leica SP8 MP microscope. Both excitation and emission scans were performed in the ranges compatible with the examined nanomaterial. ImageJ (NIH) software was used for image analysis.

## **4.2. Colloidal semiconductor nanomaterials: synthesis, characterisation, and functionalisation**

The present section describes the synthesis of CdS QDs and CdSe NPLs of different thicknesses, which are further subjected to the following processes: ligand exchange,

encapsulation, metal deposition and metal ion doping. As a result, convenient and advantageous functions were added to or enhanced in these materials including hydrophilicity, chirality, non-toxicity to cells, size modification, light-induced charge transfer, high nonlinear absorption and nonlinearly excited emission intensities. Both raw and functionalised materials were characterized by the methods described above.

### **4.2.1. Cadmium Sulfide QDs**

The first historically synthesized, best defined and most widely characterized type of colloidal semiconductor nanomaterials are zero-dimensional QDs. The research is open by commonly investigated QDs made of cadmium sulphide as a representative model. Light-induced charge transfer phenomenon as well as TPA may be observed on CdS QDs and in the following sections, their synthesis, functionalisation, and characterisation description and results are presented with focus on preserving and enhancing the above-mentioned properties in order to investigate the possibility of applying the final material as multifunctional in reduction reaction photocatalysis, reactive oxygen species generation, nonlinear optics including bioimaging and chiral drug recognition.

#### *4.2.1.1. Synthesis of hydrophilic CdS QDs*

For most of the above-mentioned applications, water-dispersibility of the material is crucial. Quite a few post-synthesis hydrophilization methods are available as described in *Functionalisation* paragraph of the *Theory* chapter, however, 0D QDs may be synthesised at lower temperature which opens the possibility to prepare them right away in water-based solution. Such an approach is based on the addition of hydrophilic ligands to the reaction mixture, and the resulting material may be compared to the one synthesised traditionally and subsequently subjected to ligand exchange process. The chosen ligand was penicillamine which is not only hydrophilic but also chiral, thus, depending on the chosen enantiomer, may serve for chiral drug recognition. An interesting fact is that the resulting material was in the shape of tetrapods which may be connected with

the presence of organic molecules inducing growth of the nanomaterial anisotropically. However, the tetrapods are small enough in all dimensions not to exceed exciton Bohr radius, and therefore are treated as 0D nanomaterials and are called QDs.

The synthesis method described below is based on literature protocols.[1,2] Briefly, 40 ml of distilled water, 8 ml of 0.01 M CdCl<sub>2</sub> as the source of cadmium, 2 ml of 0.01 M thioacetamide as the source of sulphur and 10 ml of 0.01 M penicillamine racemic mixture aqueous solutions were mixed in a three-neck flask. This ligand composition was chosen as a reference sample but, further manipulation with the L- to D-enantiomer ratio should not have a significant impact on morphology, absorption and emission spectra, QY or lifetime.[97] The pH of the penicillamine solution was previously adjusted to 11 with NaOH solution. The mixture was then stirred under reflux at the temperature of 100°C for 2 h and left overnight in the dark at room temperature. CdS QDs solution was then concentrated in a rotary evaporator, centrifuged (2min, 1800 rpm) and filtered to separate any possible aggregates.

#### 4.2.1.2. *Further functionalisation*

The synthesis described above already introduces two functionalities to the CdS QDs: hydrophilicity and chirality for potential application of the material in chiral drug recognition. However, my intent was to benefit from charge separation phenomenon occurring on semiconductor nanoparticles, such as CdS QDs, as well as from NLO activity of the material creating a multifunctional nanomaterial. Indeed, hydrophilic penicillamine-capped 5 × 14 nm CdS QDs exhibit the TPA of  $7.9 \times 10^3$  GM measured with the Z-scan method (or  $6.0 \times 10^2$  GM measured with the TPEE method) [2] which is comparable or slightly lower to analogues hydrophobic nanomaterials nonlinear properties. [96, 97, 98] Nevertheless, as described in the *Theory* chapter, although light-induced charge separation occurs on semiconductor nanoparticles, it is followed by quick recombination. For more effective electrons and holes separation, metal domains were deposited on the penicillamine-capped CdS QD to form CdS-Au nanocomposites. Specifically, Au nanostructures were harnessed to play the metal part because of their affinity to sulphur atoms. However, the presence of metal domains weakens the optical properties of semiconductor nanoparticles. Therefore, the aim of this functionalisation was to

precisely select the amount of deposited gold for preservation of NLO properties and simultaneous incorporation of photocatalytic abilities. The present study was published as the article: Nawrot et al., Functional CdS-Au Nanocomposite for Efficient Photocatalytic, Photosensitizing, and Two-Photon Applications, *Nanomaterials*. 10 (2020) 715.

The CdS-Au nanocomposites were formed by the reduction  $\text{Au}^{3+}$  ions on the surface of CdS QDs. As long as no additional reducing agent is added, the efficient reduction is expected only at the non-metal-containing surface of semiconductor nanoparticles due to sulphur affinity to gold. 1 mL of CdS QDs was mixed for at least one hour with 1 mL of  $\text{HAuCl}_4$  aqueous solution of different concentrations: 1 mL, 2.5 mL, 5 mL and 7.5 mL changing the colour of the solution to form light to dark brown. For clarity, the resulting solutions are called CdS-1Au, CdS-2.5Au, CdS-5Au and CdS-7.5Au, respectively. Additionally, free Au nanostructures were prepared for reference. Four 750  $\mu\text{L}$  of penicillamine racemic mixture aqueous solution of the concentration corresponding to the one used in the CdS QDs synthesis were prepared. Each of them was stirred with 1 mL of  $\text{HAuCl}_4$  of different concentrations: 1 mM, 2.5 mM, 5 mM or 7.5 mM. Next, 1.8 mg of  $\text{NaBH}_4$  was dissolved in 250  $\mu\text{L}$  of cold water and quickly introduced into the gold ions solution as a reducing agent. The stirring was continued for at least 1 h. The resulting solutions are hereinafter called 1Au, 2.5Au, 5Au and 7.5Au.

#### *4.2.1.3. Results and discussion*

The structure of the penicillamine-capped CdS QDs functionalised with Au nanostructures was studied using two electron microscopes: a FEI Tecnai G<sup>2</sup> 20 X-TWIN microscope with EDX and a Philips CM-20 SuperTwin instrument operating at 160 kV (Figure 144). Triangle-shaped CdS QDs of sizes ca. 5-7 nm are visible with lower contrast, whereas darker spots represent the presence of Au domains due to the higher density of gold in comparison to cadmium sulphide. EDX measurements confirm expected composition: the spectrum of raw CdS QDs contains peaks characteristic for elements of cadmium and selenium (copper lines arise from TEM grids), whereas the spectrum of functionalised nanoparticles is analogous with additional peaks resulting from Au presence.

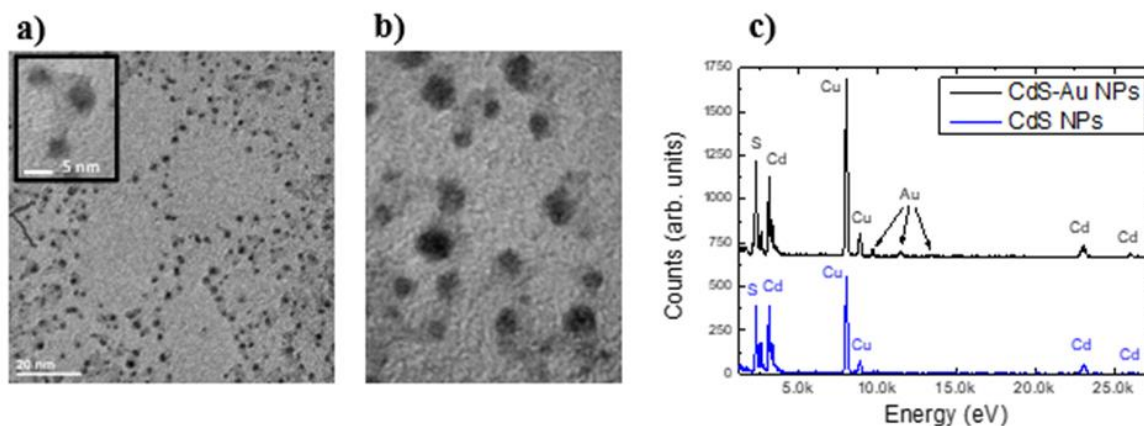


Figure 14 Representative TEM and HRTEM images of CdS-5Au hybrid structures (a-b) along with EDX spectrum (c) of both CdS NPs and CdS-Au hybrids. Reproduced from Nawrot et al. [3]

Figure 15a presents the absorption of CdS QDs and CdS-Au nanocomposites obtained by the addition of different amounts of Au precursor. The linear part of the curve corresponding to the raw CdS QDs was extrapolated to zero absorption, giving the band gap of  $E_g \approx 2.65$  eV. A similar procedure for the remaining samples shows a slight reduction of  $E_g$ . The maximum of CdS QDs photoluminescence appears at 508 nm and its intensity decreases with increasing concentration of Au (Figure 15b). Such results not only confirm direct contact between semiconductor and metal but also suggest interactions visible as photoluminescence quenching, which is attributed to prevention of efficient charge recombination. Such prevention results, in turn, from electron transfer from the CdS QDs conduction band to the Au nanostructures. A higher concentration of the Au precursor probably leads to larger metal domains that are expected to enhance the charge transfer. Dana et al. [16] suggest the presence of more electron-accepting sites in larger Au domains resulting in more effective electron entrapping.

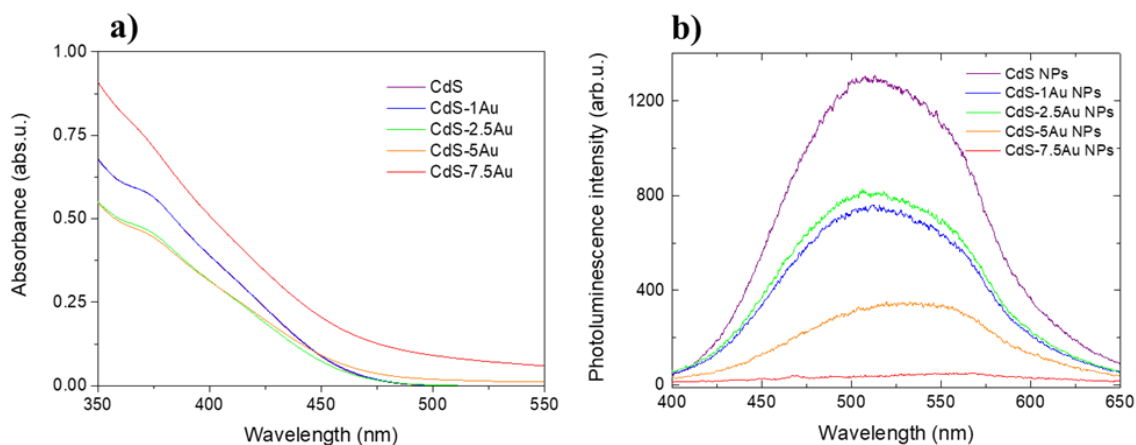


Figure 15 Absorption spectra of CdS NPs and CdS-Au hybrid nanostructures as well as photoluminescence spectra upon excitation of 375 nm decreasing in the presence of gold domains at the surface of CdS NPs. Reproduced from Nawrot et al. [3]

Such a metal domain size dependent electron transfer rate was also confirmed by time-resolved photoluminescence studies. Figure 16 presents decreasing emission lifetimes with increasing Au concentration, especially for CdS-5Au and CdS-7.5Au samples, as for the remaining systems the results and differences between them are probably too small to be effectively detected.  $\tau_1$  and  $\tau_2$  components of the raw CdS QDs calculated as 1.0 ns and 25.1 ns, respectively, were consistent with the results reported previously for similar systems. [2] For CdS-7.5Au the decay time reduction was the largest, reaching ca. 50%.

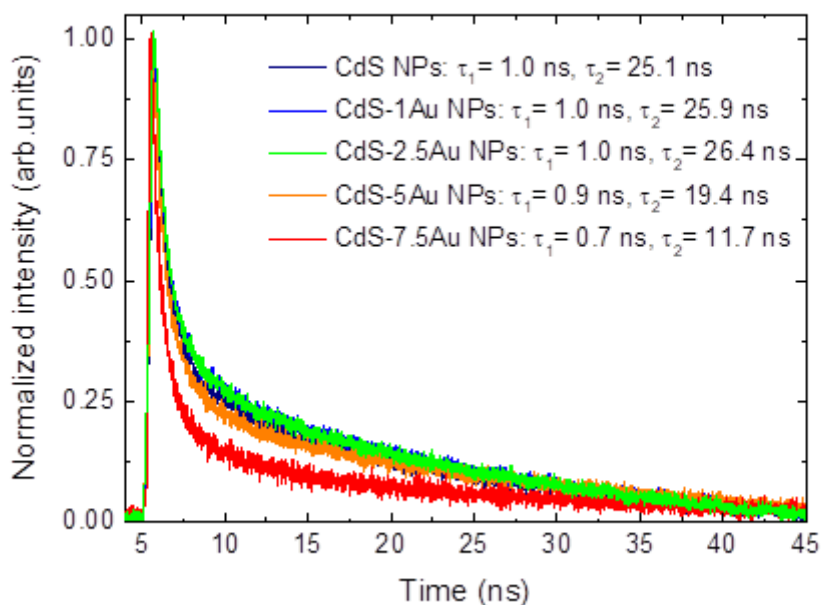


Figure 16 Time-resolved photoluminescence of CdS NPs and CdS-Au nanostructures under excitation with a picosecond 375 nm laser diode. Calculated luminescence lifetime components are attached.

The confirmation of effective charge separation suggests application of CdS-Au nanocomposites in electron- or hole-driven processes. The ability of the functionalised QDs to photocatalyse a reduction reaction was examined at ambient temperature in an aqueous environment in the presence of sunlight as was described in *Methods* chapter. Such a procedure was performed for CdS-5Au and CdS-7.5Au samples, as the above-described results suggest their most promising charge separation properties, and for references: raw CdS QDs, free 5Au nanostructures, free 7.5Au nanostructures, MB itself as well as raw CdS QDs mixed with free 5Au nanostructures and raw CdS QDs mixed with free 7.5Au nanostructures. The results are presented in Figure 17. MB itself is reduced on the light exposure only slightly at the beginning and then remains stable. Free Au nanostructures added to the dye solution showed no reduction abilities, as expected. In the case of raw CdS QDs, some photocatalytic effect was observed due to light-driven charge separation phenomenon characteristic for semiconductors which was probably enhanced by the presence of ethanol as a hole scavenger. However, the most effective reduction was observed in the presence of CdS-Au nanocomposites, which is attributed not only to holes trapped by the hole scavenger but also, most of all, to electrons accepted on gold

domains and thus separated from the positive charge. Negative charge is thus available for reduction reaction, in this case for MB degradation. As expected, a higher concentration of Au precursor used in the functionalisation resulted in a more efficient photocatalysation process: after an hour of light exposure 64 % and 91% of MB were reduced in the presence of CdS-5Au and CdS-7.5Au respectively. This significant difference is consistent with photoluminescence and time-resolved photoluminescence studies, as well as with previous work [16], suggesting faster charge transfer for larger gold domains.

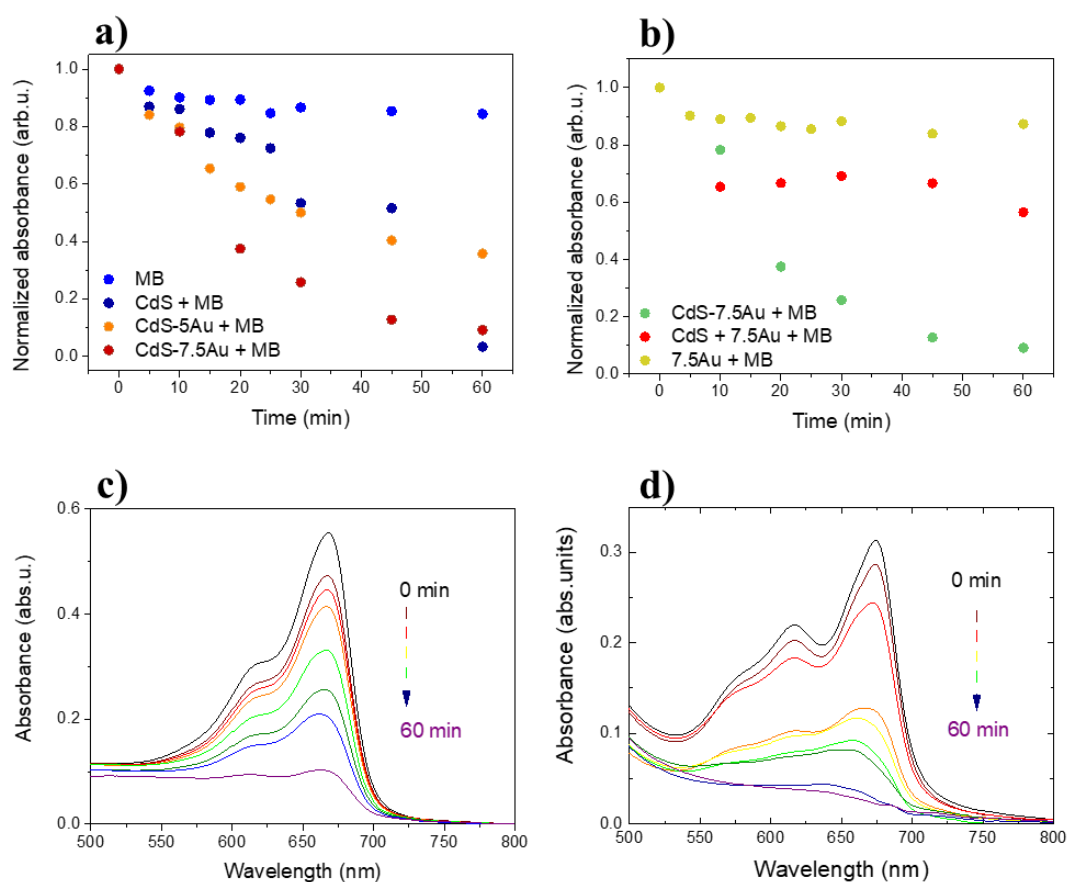
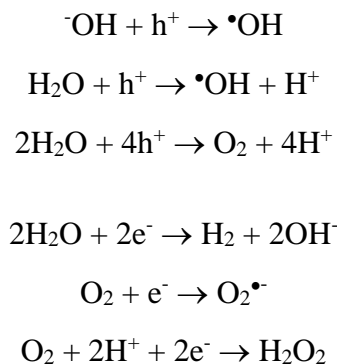


Figure 17 (a) Absorption maxima (at 668 nm) of MB changes in time upon light exposure in the presence of MB, mixture of CdS QDs and MB, mixture of CdS-5Au and MB or mixture of CdS-7.5Au and MB. (b) Reduction properties of CdS-7.5Au hybrid NPs compared to those of a mixture of CdS QDs and 7.5Au NPs as well as to 7.5Au NPs alone. Absorption spectra of MB changes in time in the presence of CdS-5Au (c) and CdS-7.5Au (d).

Further photocatalytic abilities were examined by detecting the ROS-sensitive photoluminescence intensity of BSA in the presence of CdS-Au nanocomposites and

exposed to solar simulator light. Emission spectra upon excitation at 290 nm of BSA mixed with CdS-2.5Au and CdS-5Au with maximum at 347 nm are presented in Figure 18. Both systems led to a slightly more than 50% decrease in photoluminescence intensity and similar degradation of BSA was observed for CdS-2.5Au and CdS-5Au with a pseudo first-order rate constant  $k_v$  of ca.  $1.98 \times 10^{-3} \text{ s}^{-1}$  and  $1.99 \times 10^{-3}$ , respectively. Depending on the type, ROS can be generated from water by either reduction of the molecular oxygen present in water producing, eg. hydrogen peroxide ( $\text{H}_2\text{O}_2$ ) or superoxides ( $\text{O}_2^-$ ) or oxidation of water molecules and hydroxide ions ( $\text{OH}^-$ ) creating hydroxyl radicals ( $\bullet\text{OH}$ ) (Eq. 18) and such product of water splitting photocatalysed with semiconductor-metal nanohybrids have been detected e.g. by Waiskopf et al. [101] Indeed, when measuring the BSA emission signal without a hole scavenger, we observed clear signal decreasing linearly with time of exposure on light and CdS-Au nanocomposite (Figure 18). However, performing the experiment in an ethanol-water environment, as alcohol serves as a trap for holes and prevents water oxidation, we observed not only a hardly detectable signal but, also no tendency in time-intensity correlation. The reason for such a minute and unsteady signal may be low and variable molecular oxygen concentration in water (ca.  $10 \frac{\text{mg O}_2}{\text{L}}$ ) suggesting low contribution of reduction reaction in total ROS production in comparison to oxidation reaction, which in turn means that the main ROS type generated in this process are hydroxyl radicals.



(Eq. 18)

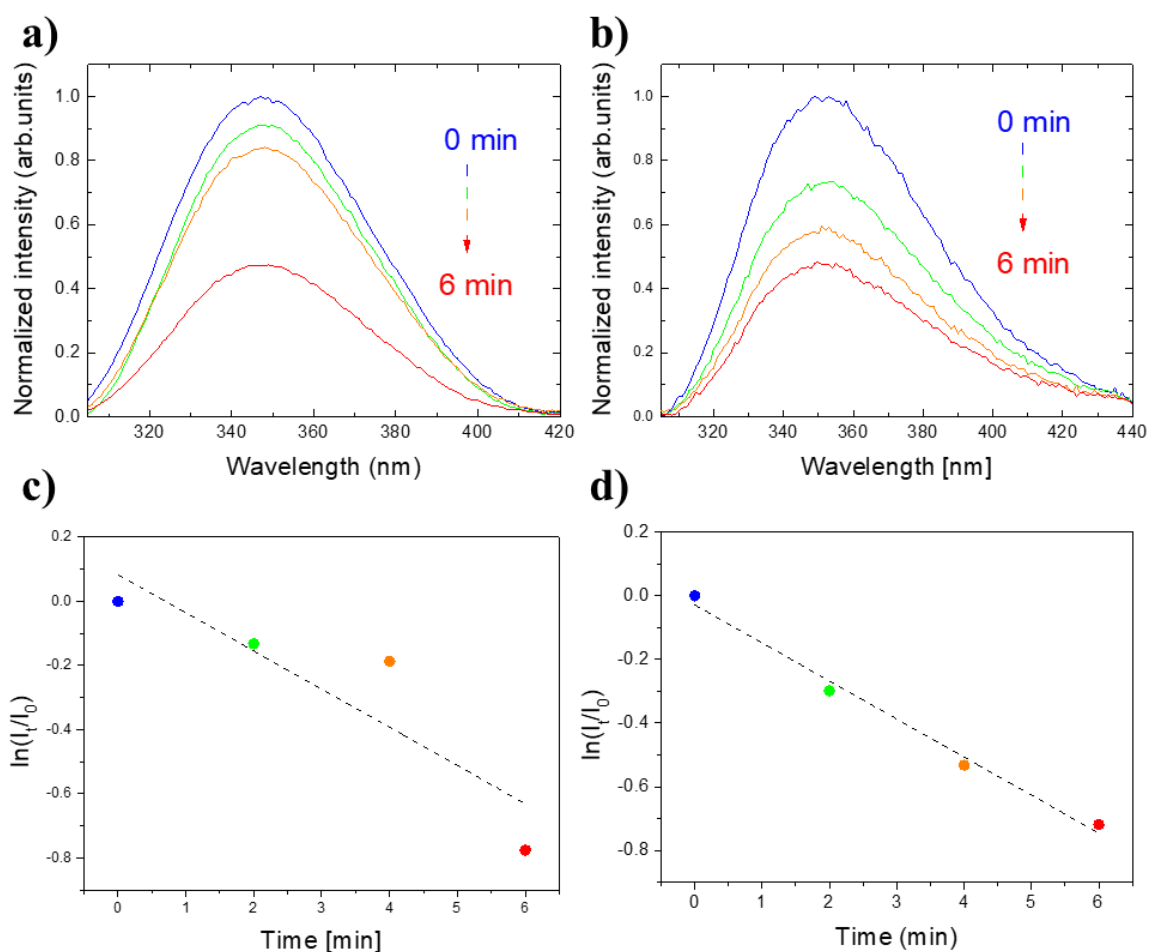


Figure 18 Changes in photoluminescence of BSA intensity in time when in contact with CdS-2.5Au (a) and CdS-5Au (b). BSA photooxidation kinetic curves in the presence of CdS-2.5Au (c) and CdS-5Au (d).

Furthermore, we desired to include promising NLO properties of semiconductor nanoparticles into the palette of CdS-Au nanocomposites functionalities, creating a model multifunctional nanomaterial for medical diagnostics. Specifically, an attractive biological application for nonlinearly active nanomaterials is two-photon bioimaging as it allows for excitation in “biological transmission windows” localized in the infrared region minimizing signal disturbances. For a bioimaging agent, however, not only nonlinear absorption but also nonlinearly induced emission is required. In spite of the fact that metal deposition on a semiconductor QDs causes photoluminescence bleaching, we still desired to benefit from nonlinear activity of the CdS part selecting a concentration of gold sufficient for efficient photocatalytic activity but low enough to preserve the ability of two-photon excited photoluminescence. With that in mind, the CdS-5Au sample was selected as it displayed

excellent reduction (Figure 17) and oxidation (Figure 18) properties, but at the same time its emission was not totally bleached (Figure 13b) and had the potential for two-photon excited photoluminescence. Indeed, we detected emission using the TPEE method and representative spectra with a maximum at ca. 520 nm, very close to the linearly excited emission, is shown in Figure 19. The maximum TPA cross section  $\sigma_2$  of  $15.8 \times 10^3$  GM was found at 725 nm which is in the range of the first biological transmission window (650-950 nm, [79]) making penicillamine-capped CdS-Au an excellent model for two-photon bioimaging. The NLO properties of the nanomaterial for few wavelengths around the maximum are presented in Table 2. The  $\sigma_2$  of CdS-Au is higher than  $\sigma_2$  of CdS reported previously [2] also when scaling with molecular weight (MW) of a single particle. This discrepancy may result from a combination of semiconductor's exciton band gap edge absorption and plasmon resonance arising from the presence of Au nanostructures [102]. But in fact, not TPA cross section but two-photon action cross section,  $\sigma_2 \times QY$ , otherwise called two-photon brightness, which describes two-photon excited photoluminescence intensity, is essential for nonlinearly excited emission-based applications. In case of metal-functionalised semiconductor nanoparticles, this parameter is particularly vulnerable to weaken due to charge separation followed by emission quenching, even if the nanocomposite displays high TPA cross section. However, interestingly, two-photon brightness values calculated for the CdS-Au nanocomposite are slightly higher than those of similar CdS QDs (Table 2). Such unexpected results suggest that resonance effect plays decisive part over the quenching effect. It means that CdS QDs functionalisation with Au nanostructures surprisingly enhanced two-photon brightness rather than weakened the parameter, which, along with hydrophilicity, chirality and excellent photocatalytic – both reducing and oxidating – properties, makes resulting hydrophilic penicillamine-capped CdS-Au nanocomposites a model example of a multifunctional nanomaterial.

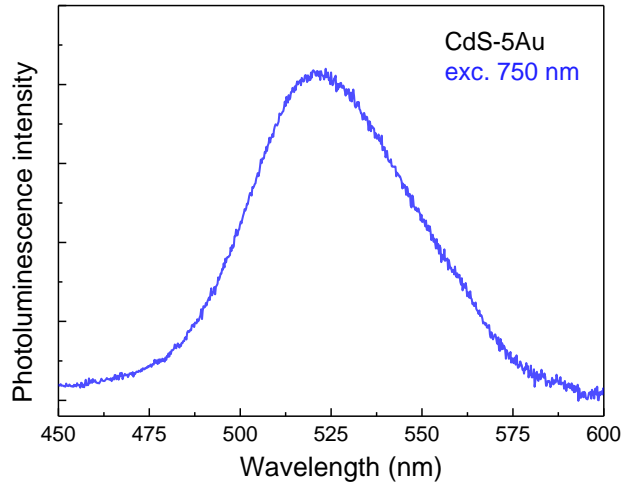


Figure 19 Representative photoluminescence spectrum of CdS-5Au hybrid nanostructure induced upon two-photon 750 nm excitation.

Table 2 TPA cross sections  $\sigma_2$  and two-photon brightness  $\sigma_2 \times QY$  of as-prepared CdS-Au hybrid nanostructures in comparison to CdS NPs characterized in a previous work [23]. Exc.  $\lambda$  – excitation wavelength.

Sample	exc. $\lambda$ (nm)	$\sigma_2$ (GM)	$\sigma_2 \times QY$ (GM)	$\sigma_2/MW$ (GM)	Ref.
CdS	700	$6 \times 10^2$	$3.66 \times 10^2$	$1 \times 10^{-3}$	[23]
	725	$5.7 \times 10^2$	$3.42 \times 10^2$	$0.6 \times 10^{-3}$	
	750	$2.3 \times 10^2$	$1.38 \times 10^2$	$0.2 \times 10^{-3}$	
CdS-5Au	700	$7.0 \times 10^3$	$7.0 \times 10^2$	$9 \times 10^{-3}$	[3]
	725	$15.8 \times 10^3$	$1.58 \times 10^3$	$20 \times 10^{-3}$	
	750	$6.9 \times 10^3$	$6.90 \times 10^2$	$9 \times 10^{-3}$	

#### 4.2.2. Cadmium selenide NPLs

Functionalisation provides a wide range of possibilities in modification, enhancement and introduction of desired properties. So far, though, the possibilities are limited and the final effect depends largely on the initial material. Indeed, several functionalities were achieved in the CdS-Au nanocomposites based on QDs, but, as described in the *Theory* chapter, QDs have their drawbacks in comparison to 2D NPLs.

Narrow photoluminescence intensity with high intensity, enhanced QY and the largest  $\sigma_2$  have been reported for 2D colloidal nanomaterials [6], thus functionalised NPLs are expected to have even more interesting properties.

The preparation of CdS NPLs, functionalisation with penicillamine, and deposition of Au nanostructures would enable direct comparison between QDs and NPLs enriched with gold domains. However, literature [103–105] indicates on very low QY values of CdS NPLs, from 0.9% up to a few percent, which makes such structures inapplicable as a model material. Therefore, cadmium selenide was chosen as a building compound for 2D NPLs for characterisation and further investigation as it was reported to exhibit QYs up to 80% at ambient temperature [104], spectrally narrow and intense emission [54] and exceptional NLO properties [6].

#### *4.2.3. Synthesis of CdSe NPLs*

According to Riedinger et al. [64] and later confirmed by Castro et al. [66], 2D nanostructures form instead of 0D QDs when the cadmium precursor is insoluble in the reaction medium. This may be achieved, for instance, by adding a short-chain Cd salt into the reaction mixture and this approach was chosen for the synthesis of CdSe NPLs with the thickness of 3.5 ML, 4.5 ML and 5.5 ML investigated in this work.

For the synthesis of 4.5 ML and 5.5 ML NPLs, short- and long-chain Cd precursors were introduced into reaction mixture. The long-chain cadmium myristate was synthesised in a methathesis reaction described by Tessier et al. [106]. 1.23 g of cadmium nitrate was dissolved in 40 mL of methanol and, in a separate flask, 3.13 of sodium myristate was completely dissolved in 250 mL of methanol. The solutions were mixed in ambient temperature resulting in precipitation of white cadmium myristate. The precipitate was filtered and washed with methanol on a Buchner vacuum kit for elimination of nitrate and sodium ions. The product was dried overnight.

5.5 ML NPLs were prepared basing on the first protocol for the synthesis of colloidal NPLs [39] with few modifications. 85 mg of cadmium myristate, 12 mg of selenium mesh and 15 mL of octadecene were put in a three-neck flask and installed in the Schlenk line. The flask was degassed under vacuum while stirring and purged with nitrogen

at 10 min intervals at ca. 100°C. Then, the mixture was heated up to 195°C and 60 mg or 40 mg of cadmium acetate as the short-chain precursor for 5.5 ML and 4.5 ML NPLs, respectively, was quickly added. The temperature was then increased to 240°C and maintain for 10 min. The flask was then cooled. Although such method allows to obtain 2D nanostructures, 0D QDs are also present after the synthesis, therefore separation was performed by addition of butanol in 3:4 ratio and centrifugation for 10 min (3,000 rpm). The desired product was expected to be the less dispersible, therefore, the supernatant was discarded, and the precipitate was suspended in chloroform. Separation was repeated several times.

3.5 ML NPLs were prepared from short-ligand Cd precursor without any long-chain Cd salt added as described by Dufour [107] with some modifications. A three-neck flask with 240 mg of cadmium acetate and 10 mL of octadecene was heated up to 100°C, purged with nitrogen and degassed under vacuum. The temperature was then increased to 190°C and a mixture of 400 µL of TOP-Se 0.1M, 200 µL of oleic acid and 3.75 mL of octadecene was introduced dropwisely with the speed of 5 mL/h. Afterwards, the reaction mixture was cooled and subjected to centrifugation with butanol for 30 min (10,000 rpm). The resulting precipitate was resuspended in chloroform.

I have also received an additional batch of 4.5 ML NPLs from Nanyang Technological University (Singapur) for further characterisation which was prepared as follows. The sample was similarly synthesised from a mixture of long- and short-chain cadmium precursors but with some modifications. 340 mg of cadmium myristate, 24 mg of selenium and 30 mL of octadecene were mixed in a three-neck flask and degassed at ca. 100°C for 1 h. The temperature was increased to 190°C, either 100 µl of TOP-ODE solution or a mixture of Ag/Cu(II) acetate and TOP in different concentrations was injected and the mixture was cooled down to 90°C to be degassed for a few minutes. The mixture was then heated up to 130°C under argon to introduce 120 mg of cadmium acetate dihydrate powder and then to 240°C to be kept at this temperature for 10 min. 1 mL of oleic acid was added and the flask was cooled down. The synthesis was followed by post-processing in order to separate any nonplatelet-shape nanoparticles and the reaction medium. The solution was centrifuged for 5 min (6,000 rpm). Next, ethanol was added, centrifugation was repeated under the same conditions and resulting precipitate was resuspended in

hexane. The sample is hereinafter called undoped 4.5 ML NPLs for the distinction between 4.5 ML NPLs synthesised in our laboratory.

#### *4.2.3.1. Characterisation*

The morphology of the separated CdSe NPLs were analysed via a Hitachi H-800 TEM. Centrifugation resulted in efficient separation, which is visible in TEM images presented in Figures 20 a-c, showing 5.5 ML, 4.5 ML and 3.5 ML NPLs, respectively, as no spherical or other nonplatelet-shaped nanoparticles may be observed. 5.5 atomic monolayers with CdSe lattice constant of 0.608 nm corresponds to the thickness of  $\sim 1.67$  nm (Figure 2020). The lateral sizes distributions of the thickest NPLs display Gauss tendency with an average length of  $25.5 \pm 2.3$  nm and an average width of  $9.3 \pm 1.3$  nm exhibiting an aspect ratio of  $\sim 1:2.7$  and volume equal to  $357 \text{ nm}^3$ . The size distributions of 3.5 ML NPLs and 4.5 ML NPLs also show Gauss tendency with average sizes of  $49.3 \text{ nm} \times 126.0 \text{ nm}$ ,  $15.7 \text{ nm} \times 6.6 \text{ nm}$ , aspect ratios of  $1:2.7$  and  $1:2.4$ , and volumes equal to  $5 \text{ 590 nm}^2$  and  $124 \text{ nm}^2$ , respectively. Undoped CdSe 4.5 ML NPLs display more square-like shape with lateral dimensions of about  $10.2 \times 12.9 \text{ nm}^2$ , the aspect ratio of  $1:1.26$  and a volume of  $158.4 \text{ nm}^3$ .

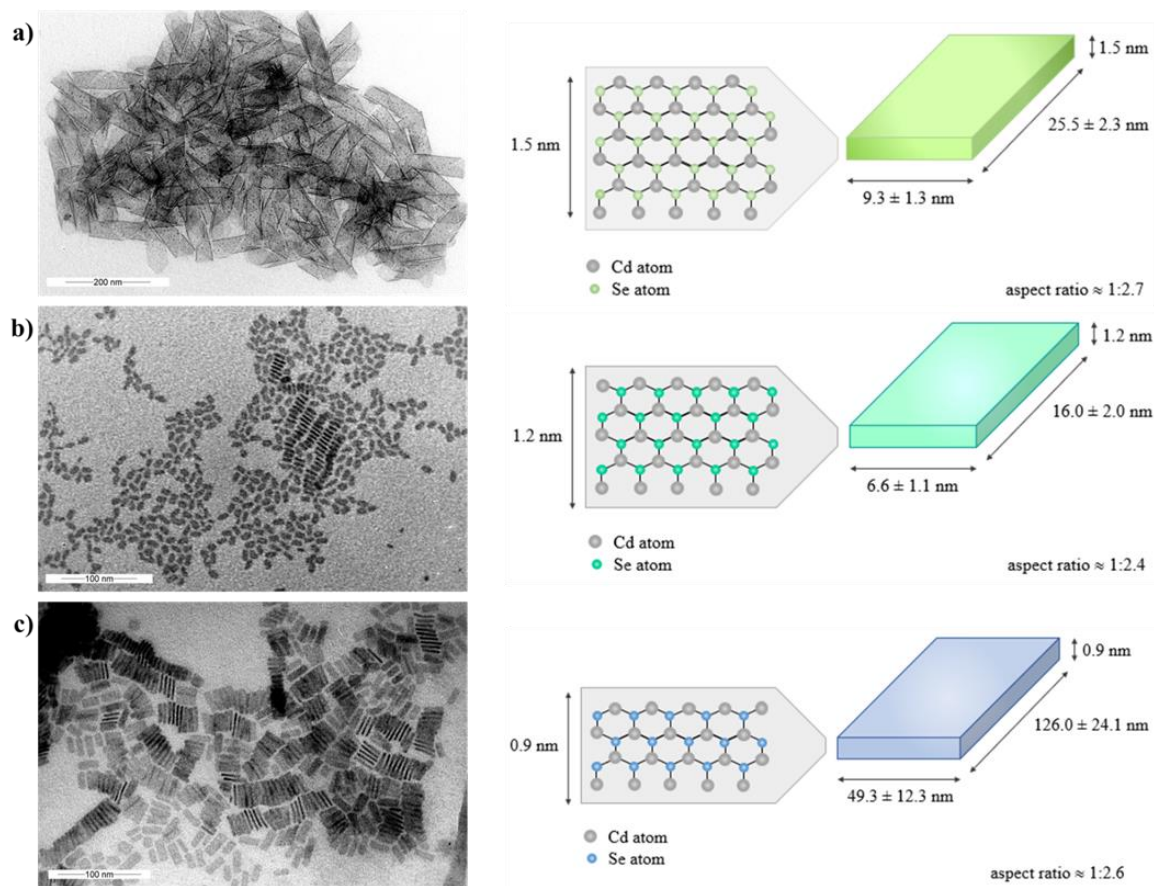


Figure 20 TEM images of (a) 3.5 ML, (b) 4.5 ML and (c) 5.5 ML CdSe NPL with schematic representations of their crystal structures.

Linear optical properties of as-synthesised NPLs were characterized with absorption and photoluminescence for colloidal and dropcasted-on-glass forms of the samples as well as with photoacoustic spectroscopy for dried NPLs as was described in *Methods* section. No significant differences between spectra of colloidal and dried NPLs are observe.

Anisotropy-connected splitting of the HH and LH valence band states is seen for all of the three samples (Figure 2121) with the lowest-energy excitonic peak, resulting from the transition involving the HH band, at 552 nm (2.245 eV), 510 nm (2.431 eV), and 465 nm (2.669 eV) for 5.5 ML, 4.5 ML and 3.5 ML NPLs, respectively. The second peak is attributed to light-hole transition.

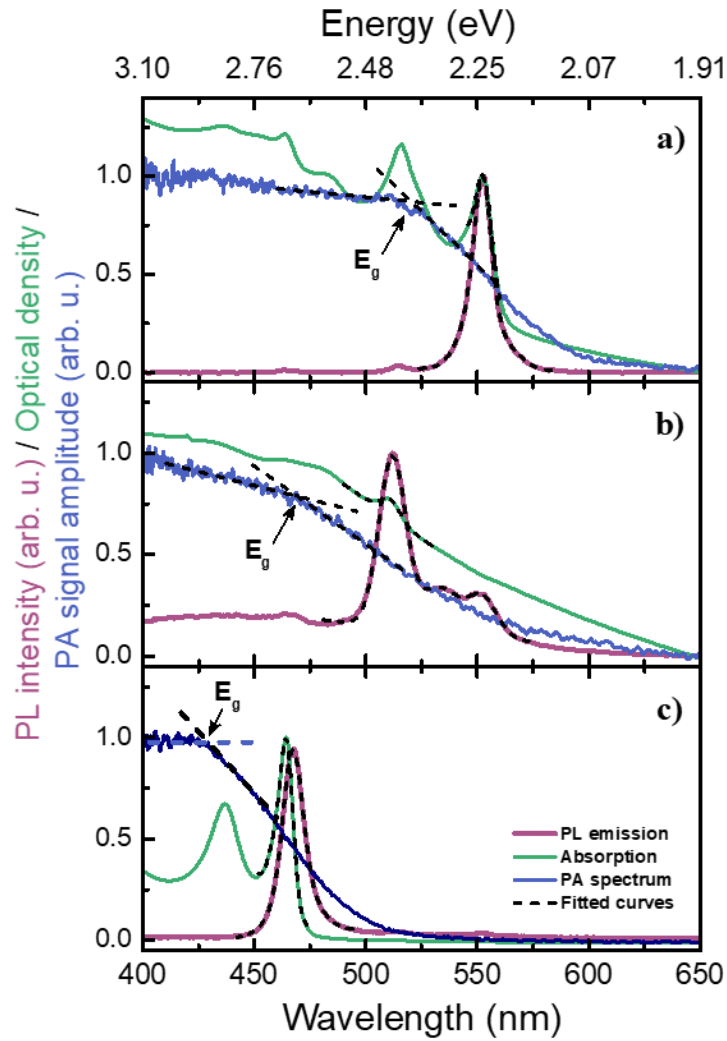


Figure 21 Juxtaposition of PL, absorption and photoacoustic spectra measured for CdSe NPLs of following thicknesses: a) 5.5 ML, b) 4.5 ML and c) 3.5 ML. The knee method was employed to determine  $E_g$ .

Based on Zelewski, Nawrot et al. [4]

Photoluminescence spectra show a very small Stokes shift ( $S_s$ ) at  $\sim 554$  nm (2.238 eV) for 5.5 ML ( $S_s = 7$ ),  $\sim 512$  nm (2.419 eV) for 4.5 ML ( $S_s = 12$ ), and  $\sim 467$  nm (2.654 eV) for 3.5 ML ( $S_s = 15$ ). Such minute shifts are consistent with literature reports [54,68]. Moreover, the narrowness of emission spectra deserves attention with FWHM of 10 nm, 13 nm and 10 nm for 5.5 ML, 4.5 ML and 3.5 ML NPLs, respectively. Such sharp peaks suggest further application of the luminescent material in fields requiring high-resolution signal differentiability from displays in information technologies to science and diagnosis for tracking several processes at the same time.

Further characterisation was performed with the use of photoacoustic spectroscopy. As presented in Figure 21, the photoacoustic spectrum of each of the three 3.5 ML, 4.5 ML and 5.5 ML CdSe NPLs samples consists of three regions, as typically for this method. Starting from the lowest energy, below the band gap, the signal is low as intrinsic material absorption is neglectable. As the excitation energy approaches the band gap, signal intensity rises due to a higher optical absorption near the band edge. The third region of lower slope of the spectrum line, represents signal saturation resulting from high optical absorption. The photoacoustic signal arises roughly from 2.0 (620 nm) to 2.5 eV (500 nm) for 5.5 ML, from 2.0 (620 nm) to 2.7 eV (460 nm) for 4.5 ML and from 2.4 (515 nm) to 2.9 eV (430 nm) for 3.5 ML CdSe NPLs. The widest range in the case of 4.5 ML sample is attributed to residual presence of thicker NPLs visible also in the photoluminescence spectrum as shorter peaks.

Photoacoustic spectroscopy complements absorption spectroscopy because upon light excitation it provides detection of acoustic signal insensitive to light scattering. Such a complementation may be applied to find EBE. Several methods for the determination of EBE have already developed, including measuring electric field-induced changes in transition energies [48], diamagnetic shifts of excitonic transitions [108,109] or combination of photoelectron, X-ray and optical spectroscopy [69]. Although applicable in some conditions, they suffer from inaccuracies, high equipment requirements or complexity, depending on the method. Therefore, EBEs of CdSe NPLs were determined using a new method proposed in our publication Zelewski, Nawrot et al., Exciton Binding Energy of Two-Dimensional Highly Luminescent Colloidal Nanostructures Determined from Combined Optical and Photoacoustic Spectroscopies, *J. Phys. Chem. Lett.* 10 (2019) 3459–3464 [4] and described in the *Methods* section as a simple alternative approach that does not require complex equipment and processing.

The fitting of a bimodal linear regression model is presented in Figure 222 as black dashed lines. Energy values at the intersection of the lines corresponding to the saturation region and the band edge region are blue-shifted from the maximum of the absorption peak corresponding to the lowest excitonic transition energy. These shifts are treated as EBE values and are calculated 130 meV for 5.5 ML, 210 meV for 4.5 ML and 230 meV for 3.5 ML CdSe NPLs, with uncertainty of 15 meV. For clarity, Figure 222 presents the relation between the thickness of NPLs versus excitonic absorption taken from optical absorption measurements and the band gap energy determined from photoacoustic spectra using

the knee method. The results were confirmed by theoretical k-p band-to-band transition calculations performed by PhD Marta Gladysiewicz-Kudrawiec (Department of Experimental Physics, Wrocław University of Science and Technology).[4] The blue arrow-ended lines indicates the value of EBE defined as the difference between the two determined energies. Such results are consistent with both theoretical [71,72] and experimental [48] reports. Therefore, the proposed method based on a simple comparison of photoacoustic and optical absorption spectrum gives results similar to those obtained with existing approaches, making it a useful alternative. Moreover, it confirms high EBE values of 2D CdSe NPLs, dependant on their thickness, suggesting the application of such structures in lasing and future optical devices.

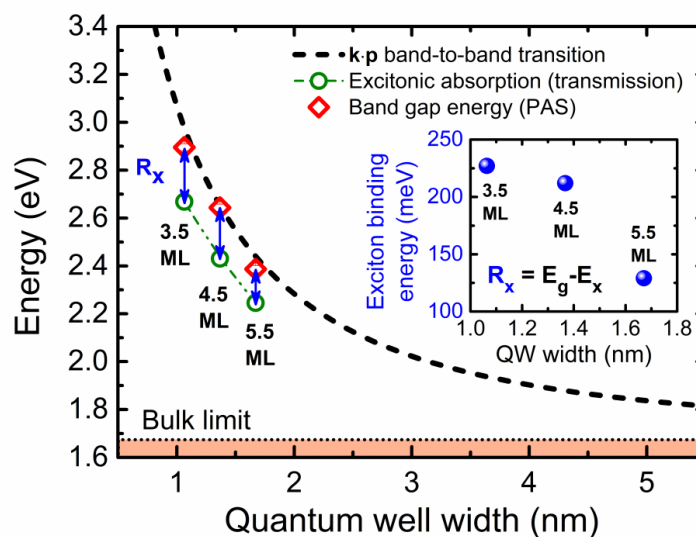


Figure 22 Relationship between potential well width and band-to-band transition energy. Dashed line represents k-p calculations results, green circles are experimental absorption maxima whereas red diamonds are band gap energies determined from photoacoustic spectra.

Reproduced from Zelewski, Nawrot et al. [4]

Strong electron-hole coupling in 2D nanostructures raises questions about exciton-emitted photon interactions directly connected to photoluminescence lifetimes. Figure 23 shows photoluminescence intensity decay of the 5.5 ML CdSe NPLs which were chosen to serve hereafter as a model material. For the fitting of the emission decay curve, a two-component model was chosen as the most consistent with the experimental data with  $\tau_1 = 0.9$  ns and  $\tau_2 = 6.5$  ns. Although the literature proposes different fittings, for example a three-component model [110] or even four-component [111] models (the latter concerned

NPLs of 4.5 ML), the orders of magnitude are consistent and all of the reports claim shorter photoluminescence lifetimes of NPLs in comparison to QDs. The long- or short-lasting emissions are beneficial, depending on the application. The latter, characteristic to flat nanostructures, are favourable for real-time tracking of processes, for instance in form of bioimaging.

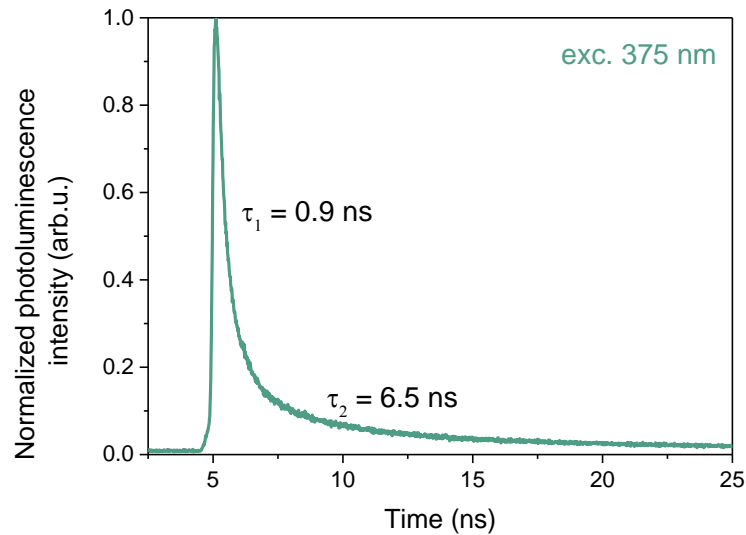
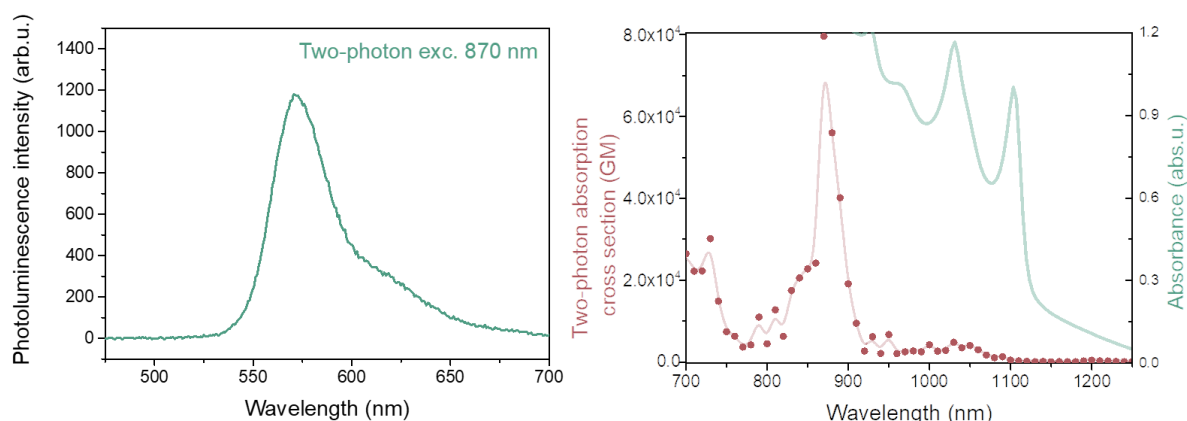


Figure 23 Time-resolved photoluminescence spectrum of 5.5 ML CdSe NPLs.

Rapid emission cease is only one of requirements for application of nanomaterials in biofields and, in fact, not even the most important. The signal must be detectable, which may be facilitated, or in some cases actually enabled, when it appears in a biological transmission window. The TPEE method for NLO properties characterisation is based on emission measurements and Figure 244 (left) shows a representative two-photon induced photoluminescence spectrum upon excitation with 870 nm corresponding to the maximum TPA (Figure 244, right), in the range of the first biological transmission window. Although  $\sigma_2$  scales super-linearly with the volume of NPLs and lateral dimensions of the characterized sample are relatively small in comparison to what is possible to achieved, high maximum TPA cross-section of  $8.0 \times 10^4$  GM was calculated, an order of magnitude higher value than that of typical 0D QDs [6,112]. Limited data is available in the literature concerning thickness-dependent NLO properties of NPLs, however, the already reported results for 3.5 ML and 4.5 ML CdSe NPLs of similar volumes are of the same order of magnitude. [6] The here reported result for 5.5 ML CdSe NPLs is also comparable to the TPA cross-section of  $3.43 \times 10^5$  GM [6] reported for 4.5 ML CdSe NPLs

of similar volume ( $307 \text{ nm}^3$ ). The results collected in Table 3 indeed confirm that TPA cross sections of NPLs are hardly influenced by thickness, whereas strongly dependent on total volume. For a more adequate comparison with other materials, an additional parameter of molar mass-normalized  $\sigma_2$  was calculated. Moreover, two-photon brightness essential for emission-connected applications, including two-photon bioimaging, was determined as  $3.6 \times 10^4 \text{ GM}$  making an even larger contrast between NPLs and QDs properties, as with lower QYs, brightness of 0D structure decreases.

Such comparisons with literature data, although important for analysis of relationships between structure and properties, and in general to both give to and draw from the available knowledge, ought to be treated carefully as many variables take into account on the final result, such as synthesis protocol and its performance in practice, characterisation method and, even if it is consistent, individual details in its execution, individual parameters of referencing samples, equipment inaccuracies etc.



*Figure 24 Left: TPEE spectrum of 5.5 ML CdSe NPLs and right: spectrally-resolved TPA cross section of 5.5 ML CdSe NPLs (rosewood dots) with light rose line added to guide eyes. Celadon line represents doubled-wavelength one-photon absorption drawn for comparison.*

Table 3 Comparison of NLO properties determined via TPEE methods for 0D and 2D CdSe colloidal nanoparticles.

CdSe NPs	Size (nm)	Volume (nm <sup>3</sup> )	$\lambda$ (nm)	$\sigma_2$ (GM)	$\sigma_2/M$ (GM · mol·g <sup>-1</sup> )	$\sigma_2/V$ (GM · nm <sup>-3</sup> )	$\sigma_2 \cdot QY$ (GM)	Reference
QDs	Diameter							
	3	14.1	900	$1.24 \times 10^4$	0.23	879	$1.12 \times 10^3$	[113]
	3.2	17.1	800	$6.88 \times 10^3$	0.11	401	$6.88 \times 10^2$ (For assumed QY = 10%)	[6]
NPLs	Width × length							
3.5 ML	11 × 17	168	800	$3.30 \times 10^5$	0.56	1960	$8.25 \times 10^5$ - $3.30 \times 10^5$	[6]
3.5 ML	20 × 77	1386	800	$1.61 \times 10^7$	3.31	11616	$4.0 \times 10^6$ - $7.25 \times 10^6$	[6]
4.5 ML	8 × 16	153	800	$1.98 \times 10^5$	0.37	1289	$4.25 \times 10^4$ - $8.90 \times 10^4$	[6]
4.5 ML	8 × 32	307	800	$3.43 \times 10^5$	0.32	1117	$8.58 \times 10^4$ - $3.30 \times 10^5$	[6]
4.5 ML	23 × 27	745	800	$1.31 \times 10^6$	0.5	1758	$3.28 \times 10^5$ - $5.90 \times 10^5$	[6]
5.5 ML	9.3 × 25.5	356	870	$8.0 \times 10^4$	$6.4 \times 10^{-2}$	$3.6 \times 10^4$	$3.6 \times 10^4$	[114]
5.5 ML	22 × 82	2706	800	$1.82 \times 10^7$	1.92	6726	$4.55 \times 10^6$ - $8.19 \times 10^6$	[6]

#### 4.2.3.2. Encapsulation in polymeric nanocarriers

Intensive and narrow emission, short photoluminescence lifetime, TPA spectrum in the range of a biological transmission window and high TPA cross-section, despite a relatively small size, of as-synthesised 5.5 ML CdSe NPLs are promising properties for

application in two-photon bioimaging. The material, however, should be functionalised to overcome drawbacks limiting its applications, including hydrophobicity that induces aggregation in biological liquids and toxicity related to the presence of  $\text{Cd}^{2+}$  ions. As was described in *Theory* chapter, several hydrophilization methods may be applied, generally based on ligand exchange, whether short or polymeric, or on encapsulation. In order to choose the most adequate one, desired properties of designed material should be taken into account. In case of CdSe NPLs for application in biofields, encapsulation might be a promising method as, along with providing hydrophilicity, it significantly decreases their toxicity to cells [26,112,115] and increase the size of final product. The latter aspect is a step for creation a tumour-targeting nanosystem because mutated cells, as opposed to healthy cells, are highly permeable [90]. However, the hereinafter described studies, published in Nawrot et al., Polymeric Nanocarriers with Luminescent Colloidal Nanoplatelets as Hydrophilic and Non-Toxic Two-Photon Bioimaging Agents, *Int. J Nanomedicine*. 16 (2021) 3649–3660, were mostly focused on introducing hydrophilicity and reducing toxicity.

The crucial aim of such functionalisation was not only to achieve the above-described advantages but also to preserve excellent optical properties of CdSe NPLs.[114] Different ligands or a polymeric carrier along with an aqueous surrounding may make a barrier weakening excitement of the loaded NPLs and further detection of the emitted signal influencing its intensity and shape. Therefore, despite predictions based on the literature, both methods were performed in order to experimentally compare emission properties of CdSe NPLs functionalised in different ways and then choose the most promising one for investigation of NLO properties.

Ligand exchange for cysteine was performed basing on the protocol provided by Wang et al. [116] 2 mL of CdSe NPLs chloroform solution and 2 mL of 0.2 M cysteine aqueous solution with pH adjusted to 12 were mixed for 24 h. Next, the stirring was turned off and the mixture was left for 1 h to achieve phase separation. The lighter aqueous phase was collected with a syringe, purified by precipitation with a mixture of ethanol and distilled water and, finally, redispersed in water. Figure 255 presents the result of the TEM analysis on as-hydrophilized NPLs.

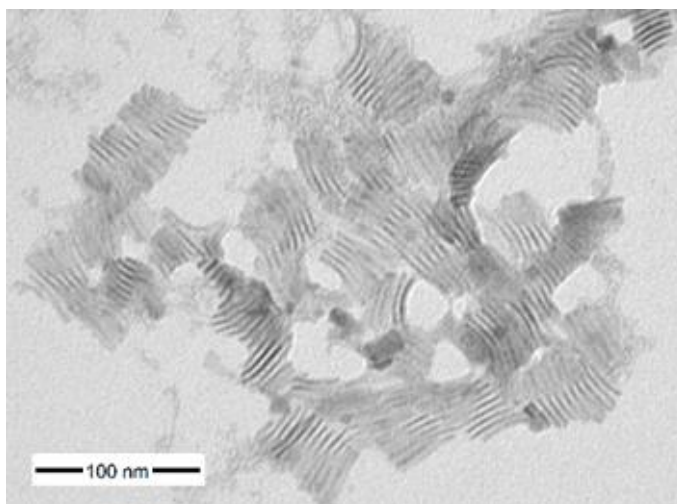


*Figure 25 TEM image of 5.5 ML CdSe NPLs after ligand exchange to cysteine.*

5.5 ML CdSe NPLs were encapsulated via solvent-evaporation method proposed by PhD Urszula Bazylińska (Department of Physical and Quantum Chemistry, Wrocław University of Science and Technology).[26] 5.5 ML CdSe NPLs chloroform solution (concentration 1.17 mg/mL) and 3% Pluronic P-123 dichloromethane solution were put in a round-bottomed flask. The excess of solvents was evaporated with the rotation speed of 150 rpm on a rotary evaporator (Hei-VAP Value Digital, Heidolph Instruments, Schwabach, Germany). Next, the temperature of the mixture was ensured as 45°C by placing the flask in a water bath 5 mL of distilled water was added and the mixture was stirred to ensure evaporation of remaining chloroform and dichloromethane. A few polymer-to-NPLs ratios were tested (Table 4) in order to achieve satisfying emission abilities and stability.

Table 4 Composition of respective mixtures for the encapsulation process. Reproduced from Nawrot et al. [114].

<b>Nr</b>	<b>CdSe NPLs chloroform solution [<math>\mu</math>l]</b>	<b>Pluronic P-123 dichloromethane solution [ml]</b>	<b>Water [ml]</b>	<b>Ratio</b>
<b>1</b>	500	5	5	1:10:10
<b>2</b>	500	10	5	1:20:10
<b>3</b>	750	5	5	1:6.7:6.7
<b>4</b>	750	10	5	1:13.3:6.7
<b>5</b>	1000	5	5	1:5:5
<b>6</b>	1000	10	5	1:10:5

Screening photoluminescence measurements (Figure 266a) suggest that the most advantageous sample is the 5<sup>th</sup> one with the most intensive photoluminescence and lowest additional emission connected with the presence of Pluronic P-123. An additional wide peak between 400 and 530 nm characteristic for Pluronic P-123 is observed confirming that the encapsulation process indeed took place, however, it is the lowest for the 5<sup>th</sup> sample, not interfering with the main signal. Such results are predictable for the lowest NPLs to polymer ratio, however though, TEM analysis indicates that the NCs prepared with such ratio are the most spherical and homogeneous (Figure 266b-f).

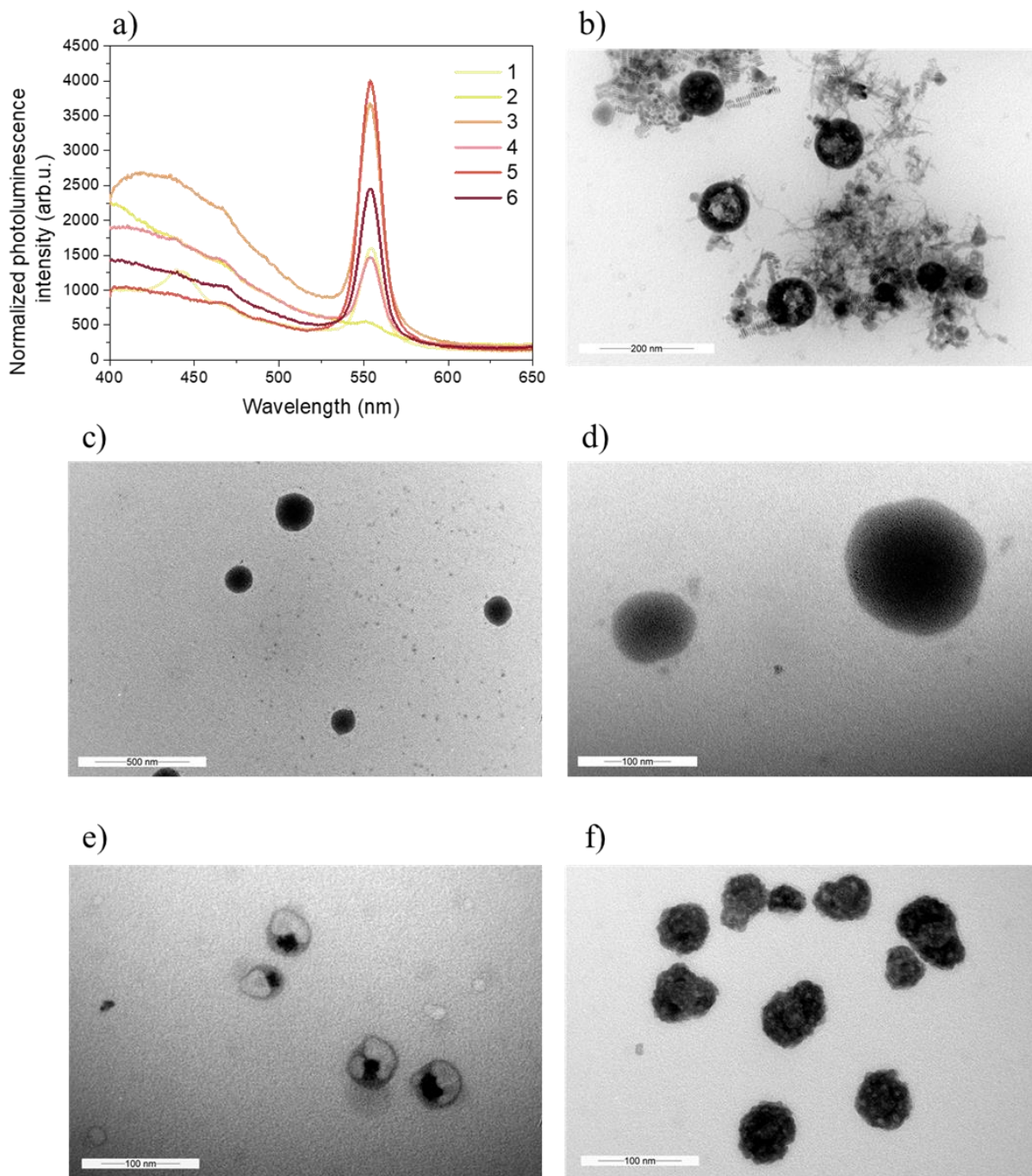


Figure 26 (a) Photoluminescence of 5.5 ML CdSe NPLs after encapsulation versus polymer-to-NPLs ratio. TEM images of NPLs encapsulated in polymeric NCs of optimized nanoparticles-to-polymer ratio (sample 5) (b) before and (c) after purification. The results of not optimized process are shown for comparison: (e) sample 4 and (f) sample 6.

Photoluminescence spectra of as chosen NPLs-loaded NCs, cysteine-capped NPLs and non-functionalised raw NPLs are presented in Figure 277. For screening

measurements, the spectra heights were normalized as determination of the concentration of capped/encapsulated is neither trivial nor essential. No emission shift is observed between the peak arisen from raw and encapsulated NPLs and only a very slight widen with FWHM of 12.2 nm. In the case of cysteine-capped NPLs, the maximum is red-shifted to 576 nm and the peak is almost 4 times wider. Similarly to the spectrum of NCs, an additional wide peak, characteristic for organic molecules, is also present here.

The experimental results were in favour of encapsulation over ligand-exchange, therefore, NPLs-loaded polymeric NCs were further characterized in order to investigate whether they may serve as a model material for the development of bioimaging agents.

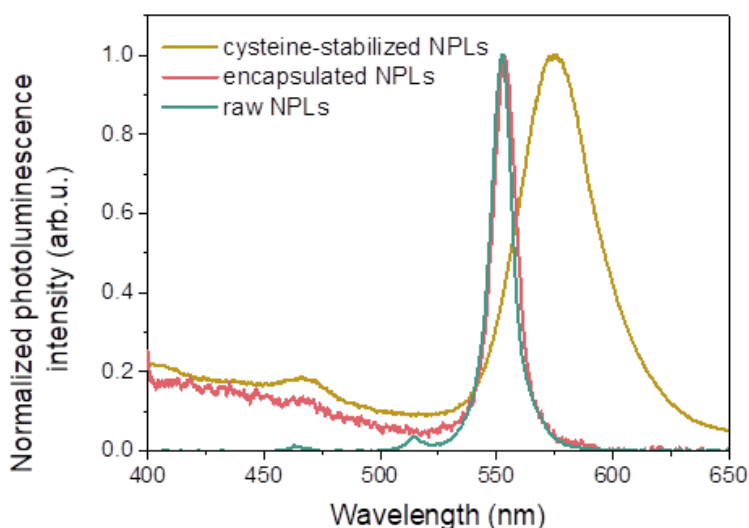


Figure 27 Photoluminescence spectrum of 5.5 ML CdSe NPLs in chloroform (celdon) and in water after ligand exchange to cysteine (gold) or encapsulation in polymeric NCs (rosewood).

Figure 288 compares further linear optical parameters of raw NPLs and NPLs-loaded NCs. The absorption spectrum of NPLs-loaded NCs displays slight smoothing of the sharp peaks, characteristic for anisotropic NPLs along with a delicate blue-shift of the lowest-energy excitonic peak from 552 nm to 549 nm. Nonetheless, the peaks arising from transitions involving the HH and LH bands peaks are still splitted and both are clearly visible.

The photoluminescence lifetime curve of the NPLs-loaded NCs exhibits the best accordance with a two-component model, similar to the sample before functionalisation

(Figure 288b). A slight delay in the initial phase of PL decay was detected for the functionalised nanoparticles, whereas a steeper slope in the second part of the spectrum is observed. However though, the respective components are of the same order of magnitude with the values of  $\tau_1 = 0.5$  ns and  $\tau_2 = 7.0$  ns making photoluminescence lifetime very short, promising for real-time tracking applications.

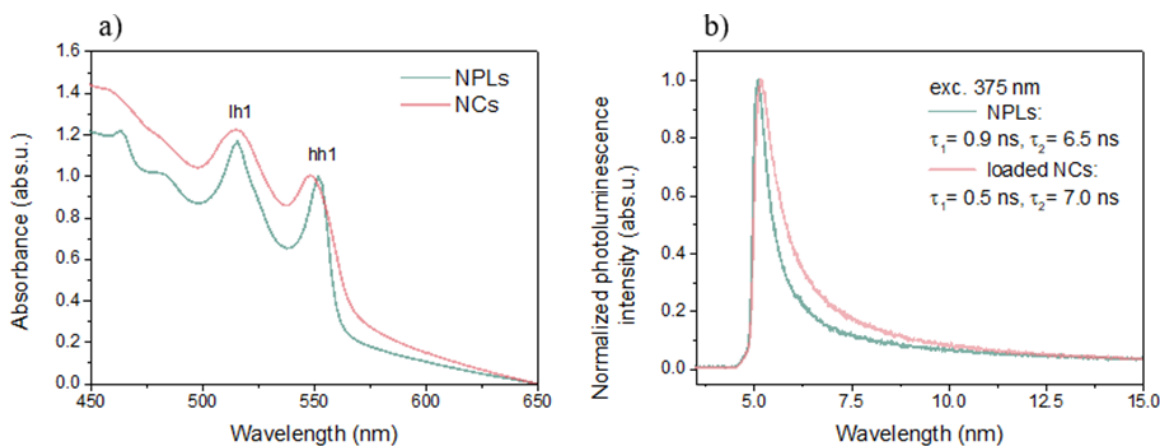


Figure 28 (a) Absorption spectrum and (b) time-resolved PL intensity of 5.5 ML CdSe NPLs encapsulated in NCs compared to NPLs in chloroform.

As no significant differences in linear absorption, photoluminescence and time-resolved luminescence spectra were detected, NPLs-loaded NCs were subjected to investigation of third-order NLO properties with the TPEE method. Figure 299a shows a representative two-photon excited spectrum of NPLs-loaded NCs upon excitation at 870 nm. At this wavelength, nonlinear absorption maximum appears (Figure 299b) as it was for the sample before functionalisation indicating no changes in peak position despite encapsulation.

In order to calculate the value of TPA of the nanosystem, an assumption of the amount of NPLs in one capsule had to be made. Taking into account an average volume of a NPL and a NC, minimal distance between nanoparticles and arrangement of the NPs in NCs from TEM analysis as well as assumptions taken previously for QDs in a NC [26], one capsule was estimated to contain ca. 2000 NPLs.

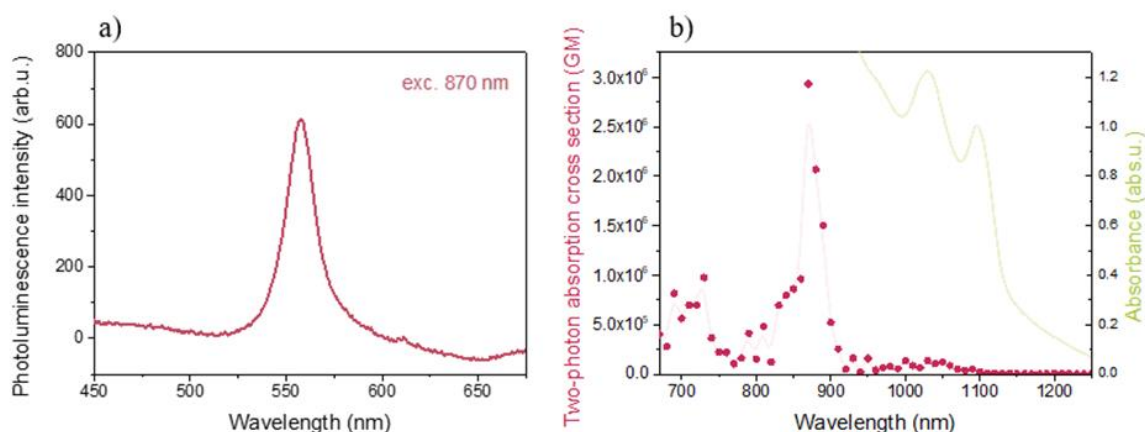


Figure 29 (a) Photoluminescence spectrum upon two-photon excitation (870 nm) and (b) spectrally-resolved TPA cross section (rosewood dots) with light rose line added to guide eyes compared to doubled one-photon absorption spectrum (green line) of 5.5 ML CdSe NPLs encapsulated in polymeric NCs.

The TPA cross section of this system was calculated as  $2.0 \times 10^8$  GM. To compare TPA abilities of a NPL in chloroform and in a carrier in water, a free from the above explained assumption molar-mass normalized  $\sigma_2$  was calculated as  $7.8 \cdot 10^{-2}$  GM which, comparing to  $6.4 \times 10^{-2}$  GM for raw NPLs, indicates that encapsulation does not weaken the TPA process. Moreover, Table 5 presents further calculation results of two-photon brightness and molar-mass normalized two-photon brightness, essential for application involving nonlinearly excited emission. The latter parameter, which omits the mass and, thus, also the amount of NPLs in a NC is lower for functionalised NPLs than for their raw counterparts, suggesting that within NCs some sub-aggregates form introducing non-radiative decay pathways. In practice, however, all the NPLs in a NC emit together achieving exceptionally high  $\sigma_2 \cdot QY$  values.

Table 5 TPA cross section upon excitation at 870 nm and TPEE of 5.5 ML CdSe NPLs encapsulated in polymeric NCs in comparison to NPLs in chloroform and to Rhodamine B which was used as a reference., Nawrot et al. [114]

	Solvent	QY [%]	$\sigma_2$ (GM) at 870 nm	$\sigma_2/M$ (GM·mol/g)	$\sigma_2 \times QY$ (GM)	$(\sigma_2/M) \times$ QY (GM·mol/g)
<b>Rhodamine B</b>	CH <sub>3</sub> OH	45[21]	74[21]	0.154	33.3	$6.9 \times 10^{-2}$
<b>CdSe NPLs</b>	CHCl <sub>3</sub>	45	$8.0 \times 10^4$	$6.4 \times 10^{-2}$	$3.6 \times 10^4$	$2.9 \times 10^{-2}$
<b>CdSe NPLs- loaded NCs</b>	H <sub>2</sub> O	11	$2.0 \times 10^8$	$7.8 \times 10^{-2}$	$2.2 \times 10^7$	$8.5 \times 10^{-3}$

The optical properties of NPLs-loaded systems suggest their application in real-time tracking in biological systems which requires additional tests of biocompatibility. Their stability in human organism conditions, encompassing pH ~ 6.5 of some tumour cells, pH ~ 7.4 of blood and pH ~ 9.0 in intestine as well as temperature up to 40°C during inflammation, was investigated by detecting their PL in the above ranges of pH and temperature. No more than 15% of the decrease in PL intensity appeared despite changing conditions (Figure 30).

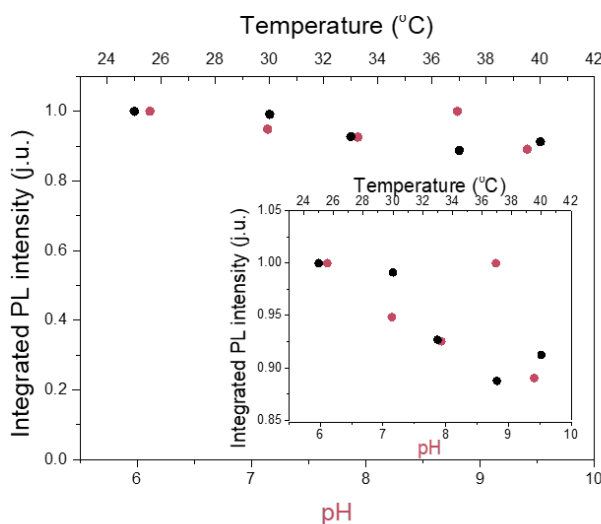


Figure 30 Photoluminescence stability of NPLs encapsulated in NCs with changing temperature and pH conditions. The inset shows that PL decreases not more than 12% comparing to the higher value (based on Nawrot et al. [114])

Next, MTT viability assay was used for evaluation of the nanosystem cytotoxicity as described in the *Methods* section. For such test, empty NCs were prepared as a reference in the same way as NPLs encapsulation was performed, but with no addition of the fluorescent nanomaterial. The impact of either loaded or empty NCs on cell viability is presented in Figure 3131. The lowest viability detected after exposition of MDAH-2774 cells and HGF cells to encapsulated CdSe NPLs was higher than 65% but, if compared to empty NCs, the value never decreased below 90%, even when the incubation time was prolonged. Such results confirm the preserving effect of the polymer shell, previously reported for analogous systems [26,112,115].

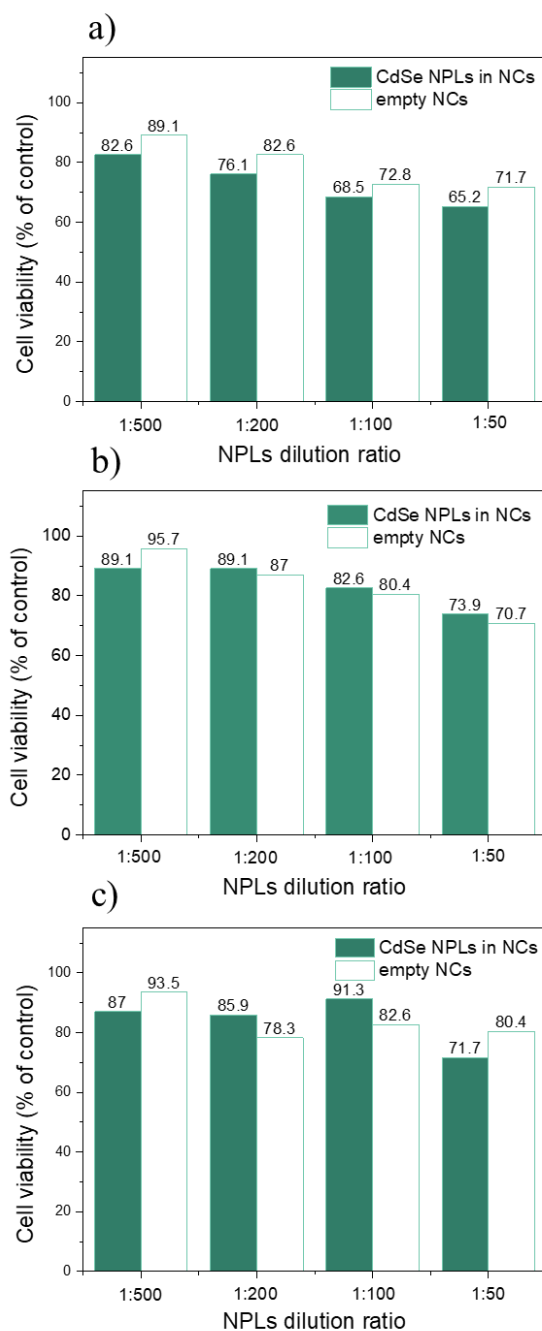
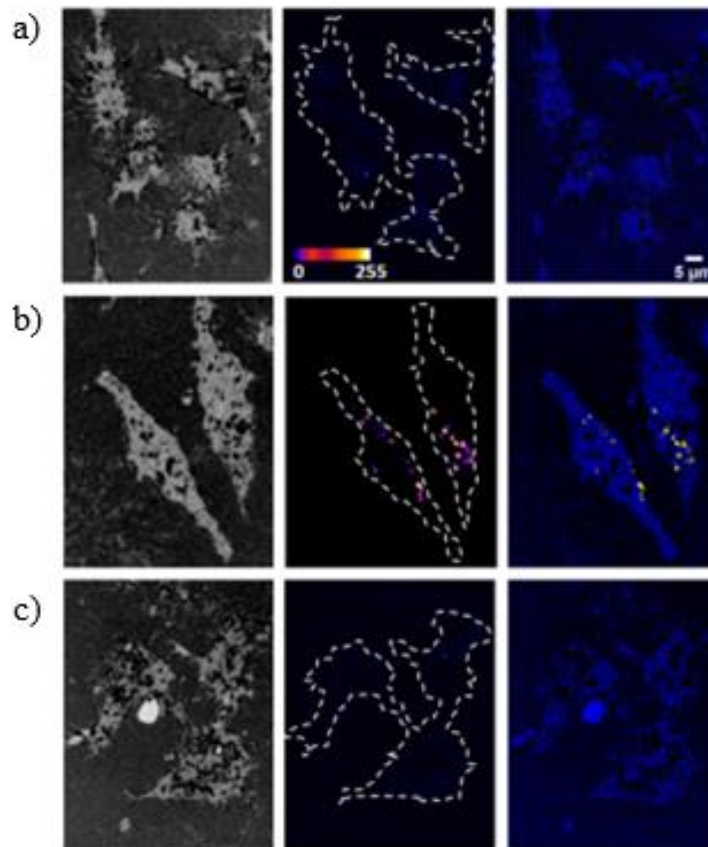


Figure 31 Cell viability after incubation with encapsulated CdSe NPLs and empty NCs tested on (a) HGF for 24 h, (b) MDAH-2774 for 24 h and (c) MDAH-2774 for 48 h (based on Nawrot et al. [114]).

The possibility of applying the NPLs-loaded NCs in practice was studied through two-photon microscopic analysis (Figure 3232) on fibroblast cells. Again, despite 24 h incubation, the cells remain viable, proving the results of the above MTT assay.

Two-photon excitation allowed detection of NPLs emission, visible both in the middle panel and the in overlaid image. No additional stimulation was employed, but, interestingly, the plasma membrane was substantially attached with NCs and a part of the nanomaterial penetrated the cells that are observed in the cytoplasm. On the one hand, such penetration, which might be enhanced by electroporation, is promising for application in bioimaging. On the other hand though, if NPLs-loaded NCs were to be applied in the field, they require further functionalisation, for example with folic acid or galactose [117,118] to be more selective, or optimisation of the carrier size to penetrate only tumour cells omitting healthy tissues.



*Figure 32 Two-photon microscopy of fibroblasts (a) untreated, (b) incubated for 24 h with NPLs encapsulated in NCs and (c) incubated for 24 h with empty NCs. Cell outlines (white dashed lines) are based on the reflection channel. NPL channel presented in fire look-up table (middle panel) and in yellow in overlaid image (based on Nawrot et al. [112]).*

The functionalisation of CdSe NPLs by their encapsulation in polymeric NCs allowed their dispersion in an aqueous medium, preventing aggregation and precipitation in a range of temperature and pH conditions present in a human organism. High cells viability after incubation with the material indicates that the polymeric carrier prevents the diffusion of Cd<sup>2+</sup> inhibiting its toxic impact. Moreover, TPA cross-section and two-photon brightness was maintained at high level, which was determined not only using TPEE method but also was visible through a two-photon microscope.

#### 4.2.3.3. *Doping with noble metal ions*

Functionalisation may be performed not only to introduce desired properties but also to enhance the already existing ones. In this case, promising TPA cross-sections following by intense two-photon brightness were subjected to an attempt of further improvement. As described in *Theory* chapter, doping of QDs with copper ions [21] has been reported to increase QY. Such a phenomenon is likely to have consequences in higher two-photon brightness, therefore, the next research of this thesis focuses on doping CdSe NPLs with metal ions for improvement of their NLO behaviour. The following results were described in Nawrot et al., Spectrally Resolved Nonlinear Optical Properties of Doped *Versus* Undoped Quasi-2D Semiconductor Nanocrystals: Copper and Silver Doping Provokes Strong Nonlinearity in Colloidal CdSe Nanoplatelets, ACS Photonics. 9 (2022) 256–267.

The raw undoped and the functionalised doped materials form were received from Nanyang Technological University, Singapur. Concentrations of the dopant in the structure of NPLs were estimated by ICP:MS measurements as presented in Table 6.

Table 6 ICP:MS measurements-based estimation of doping levels with respect to cadmium quantity.

Sample	doping (%)	Error (%)
Ag-doped CdSe NPLs	0.4	±0.08
Ag-doped CdSe NPLs	1.2	±0.10
Cu-doped CdSe NPLs	0.5	±0.06
Cu-doped CdSe NPLs	1.1	±0.15

Hereinafter, the samples are named undoped, 0.4% Ag-doped, 1.2% Ag-doped, 0.5% Cu-doped and 1.1% Cu-doped 4.5 ML CdSe NPLs, with the average sizes of the samples determined from the TEM analysis (Figure 333 b,g-h) as 20 nm × 14 nm, 45 nm × 10 nm, 30 nm × 8 nm, 45 nm × 10 nm, and 45 nm × 10 nm, respectively.

First, an initial linear optical characterisation was performed. Doping neither changes the position nor alters the shape of the absorption spectra, as characteristic sharp peaks are observed with the first exciton peak at 512 nm and the second at 480 nm (Figure 333). The emission spectrum, similarly to undoped NPLs, displays a narrow peak with hardly visible Stokes shift. An additional broad band of lower energy appears in all spectra of doped samples, with maxima at ca. 600 nm and 700 nm for Ag-doped and Cu-doped NPLs, respectively. According to the literature [119], in case of both Ag and Cu ions, photoexcited holes are trapped by dopant states working as a mid-gap state during recombination. This explains a red-shifted emission (see *Excitation and following processes* section in *Theory* chapter) depending rather on the type of dopant than on its concentration.

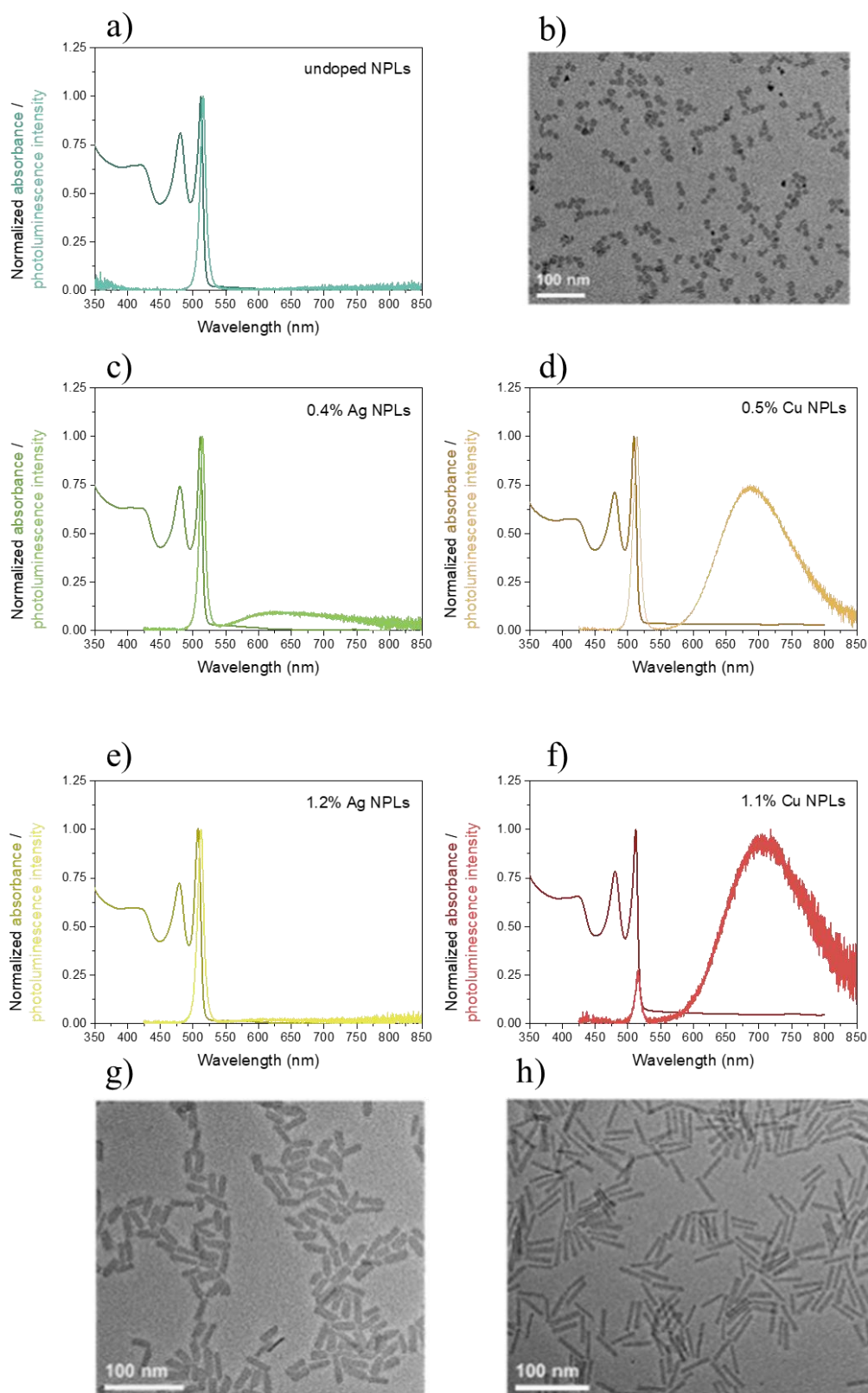


Figure 33 (a) Absorption and photoluminescence spectrum of undoped 4.5 ML CdSe NPLs upon excitation with 400 nm together with (b) TEM image of undoped 4.5 ML CdSe NPLs. Absorption and emission spectrum of 4.5 ML CdSe NPLs doped with (c) 0.4% Ag, (d) 0.5% Cu, (e) 1.2% Ag and (f) 1.1% Cu along with representative TEM images of (g) Ag-doped and (h) Cu-doped NPLs.

Photoluminescence decay times were measured with the streak camera and the curves were fitted with a double-component model, resulting in  $\tau_1 = 4.5 \text{ ns} \pm 0.4 \text{ ns}$  and  $\tau_2 = 20.7 \text{ ns} \pm 0.3 \text{ ns}$  for undoped NPLs excited with 400 nm. Table 7 and Table 8 present the impact of doping on influenced emission lifetimes. The photoluminescence of 0.4% Ag-doped NPLs is shorter in both decay phases with  $\tau_1 = 2.36 \text{ ns} \pm 0.01 \text{ ns}$  and  $\tau_2 = 17.96 \text{ ns} \pm 0.3 \text{ ns}$ . That may be attributed to additional defect states created by silver atoms. Silver may form isolated point defects and dope CdSe NPLs interstitially as  $\text{Ag}_i^+$  donor or substitutionally as  $\text{Ag}_{\text{Cd}}$  (either  $\text{Ag}_{\text{Cd}}^-$  or  $\text{Ag}_{\text{Cd}}^{2-}$ ) generating an acceptor-like defect. Moreover, it may induce formation of higher-order defects which involve charge-compensating pairs:  $\text{Ag}_{\text{Cd}}^- + \text{Ag}_i^+$ ,  $\text{Ag}_{\text{Cd}}^0 + \text{Ag}_i^0$  or  $\text{V}_{\text{Cd}}^{2-} + 2 \text{Ag}_i^+$ . However, further increasing the concentration of Ag ions does not result in even shorter lifetime but in elongation, as for 1.2% Ag-doped CdSe NPLs  $\tau_1 = 6.56 \text{ ns} \pm 0.05 \text{ ns}$  and  $\tau_2 = 33.56 \text{ ns} \pm 0.71 \text{ ns}$  were calculated. A probable explanation is connected with chemical potential as in heavy silver doped samples,  $\text{Ag}_{\text{Cd}}^{2-}$  defect types are present, rather than  $\text{Ag}_{\text{Cd}}^-$ , which may have decisive impact on relaxation rates and influence the ratio between substitutional and interstitial defects on NPLs. In the case of Cu-doped samples, such a behaviour is not observed and decay times shorten along with increasing dopant concentration. In contrast to silver,  $\text{Cu}^{2+}$  oxidation states are typically more preferred than  $\text{Cu}^+$ . It may have its reflexion on the charge of interstitial defects whereas strong acceptors may form at the cadmium substitutional sites This may explain preference of relaxation through copper states rather than Cd-Se-related antibonding states which shorten decay times. Similar tendencies, both for Ag-doped and Cu-doped samples, are observed in two-photon regime, confirming metal concentration and emission lifetime characteristics depending on metal type, suggesting the occurrence of different mechanisms.

*Table 7 Photoluminescence decay parameters estimated from streak camera spectra upon excitation with 400 nm.*

Sample	Exciton band maximum (nm)	Exciton band decay parameters					Defects band maximum (nm)	Defects band decay parameter (ns)
		(ns)	(ns)	A <sub>1</sub>	A <sub>2</sub>	(ns)		
<b>Undoped</b>	517.48	4.51 ±0.04	20.77 ±0.32	3.364e6 ±4.980e4	2.736e5 ±7.470e3	5.73 ±0.07	-	-
<b>0.4% Ag-doped</b>	513.70	2.36 ±0.01	17.96 ±0.30	1.262e7 ±2.214e5	2.256e5 ±4.681e3	2.63 ±0.01	594.03	68.69 ±6.62
<b>1.2% Ag-doped</b>	510.72	6.56 ±0.05	33.56 ±0.71	1.113e8 ±3.506e6	6.536e5 ±2.745e4	6.71 ±0.05	574.64	68.09 ±1.84
<b>0.5% Cu-doped</b>	517.02	2.07 ±0.03	0.31 ±1e-3	2.207e5 ±5.418e3	2.149e7 ±4.222e5	0.32 ±0.00	667.16	260.07 ±2.06
<b>1.1% Cu-doped</b>	525.17	0.10 ±1e-3	0.51 ±9e-3	1.257e6 ±2.657e4	9.915e4 ±2.832e3	0.12 ±0.00	676.12	390.68 ±8.91

Table 8 Photoluminescence decay parameters estimated from streak camera spectra upon excitation with 800 nm.

Sample	Exciton band maximum (nm)	Exciton band decay parameters		Defects band maximum (nm)	Defects band decay parameters (ns)
		(ns)	(ns)		
<b>Undoped</b>	520.67	1.68±0.02	14.87±0.21	-	-
<b>0.4% Ag-doped</b>	525.17	1.24±0.01	11.16±0.53	595.81	41.92±1.52
<b>1.2% Ag-doped</b>	523.83	5.07±0.07	35.17±2.09	580.56	52.95±3.14
<b>0.5% Cu-doped</b>	526.83	0.17±2e-3	0.94±0.05	664.94	282.73±20.62
<b>1.1% Cu-doped</b>	527.50	0.08±1e-3	0.42±0.01	676.34	384.88±41.43

The NPLs were characterized nonlinearly using the Z-scan method in the range of 625 nm to 1350 nm and representative open- and closed-aperture measurement traces are presented in Figure 344. A local maximum absorption was observed for all samples twice in this range, between 825 nm and 925 nm and between 1100 nm and 1225 nm (see

Figure 37). Doubled maximum may suggest the occurrence of TPA in the shorter wavelength range and three-photon absorption in the latter range.

In order to examine the hypothesis, graphs shapes were analysed according to a previously reported method [120], initially confirming the presence of two mechanisms. Moreover, photoluminescence of the samples excited with different laser beam powers was measured (Figure 355) and slopes values are, indeed, respectively, near 2 or 3.

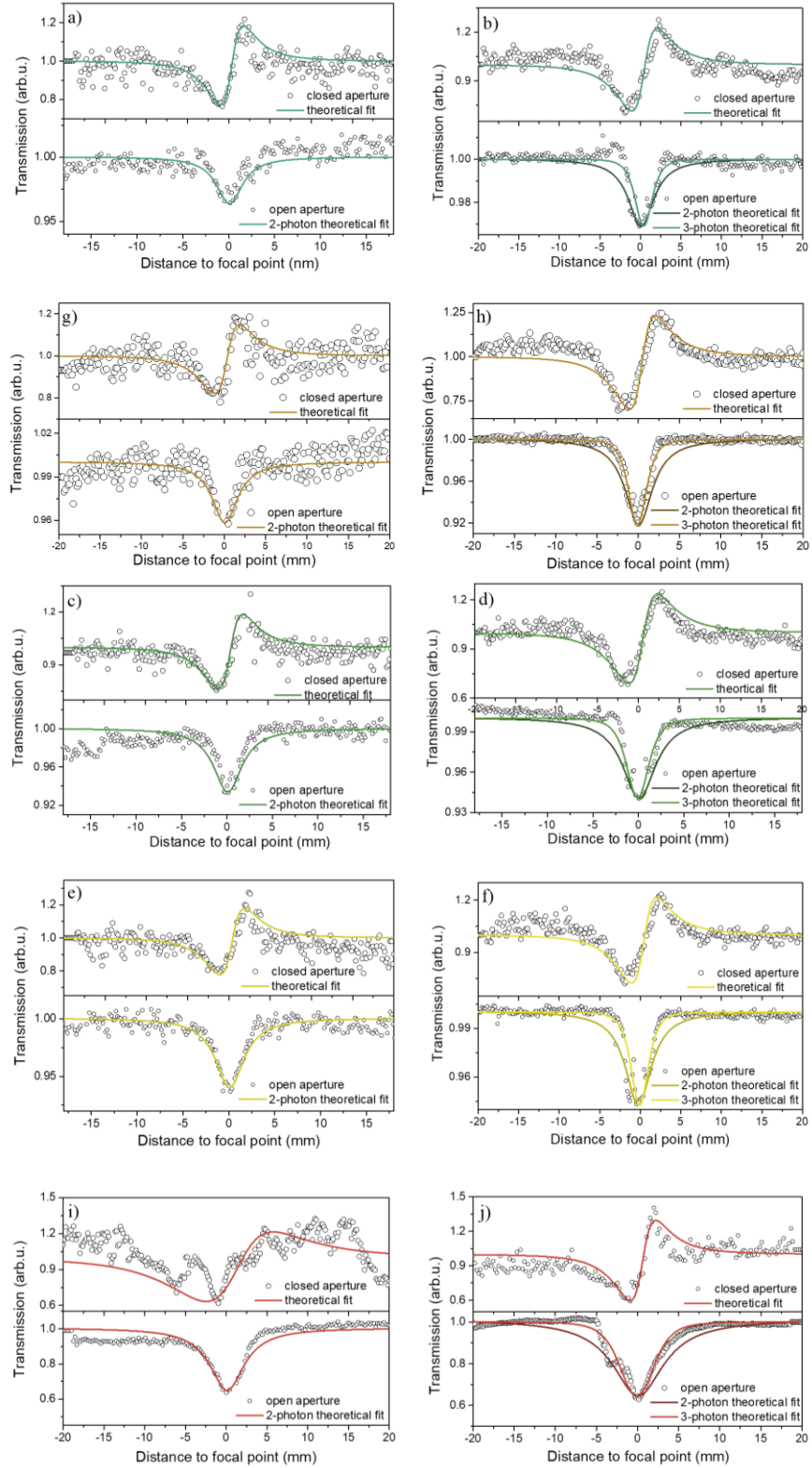
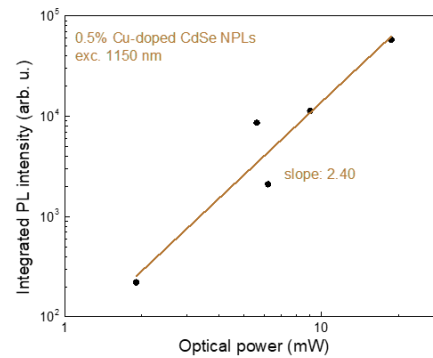
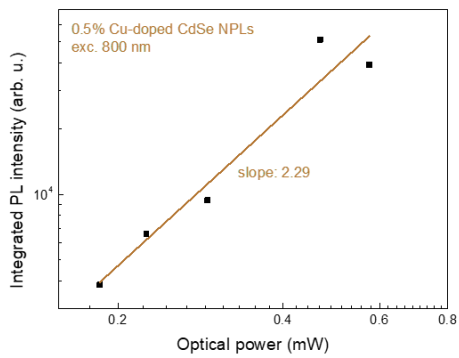
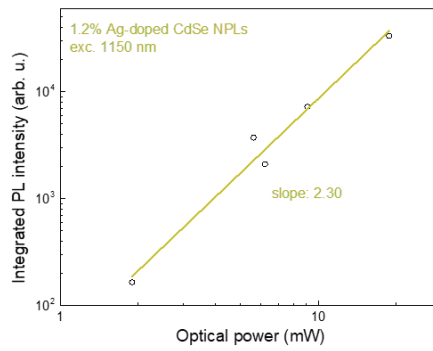
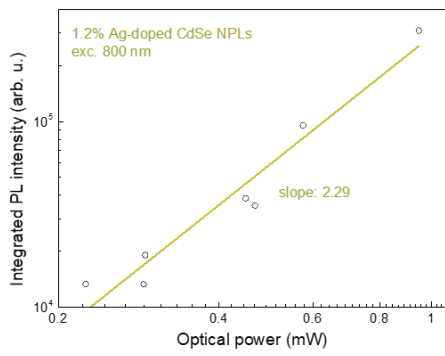
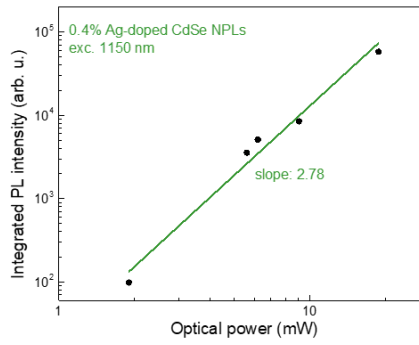
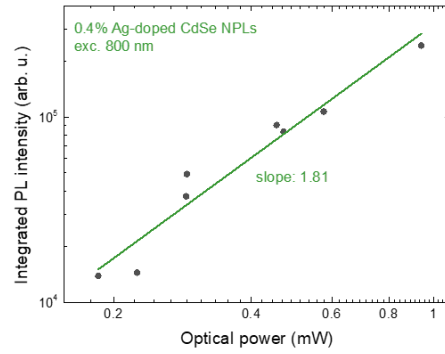
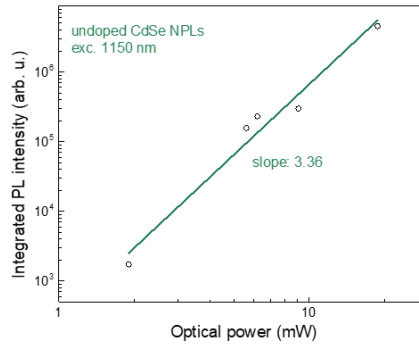
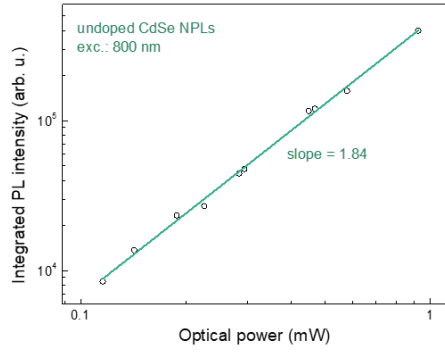


Figure 34 Open and closed-aperture Z-scan traces for (a-b) undoped, (c-d) 0.4% Ag-doped, (e-f) 1.2% Ag-doped, (g-h) 0.5% Cu-doped and (i-j) 1.1% Cu-doped 4.5 ML CdSe NPLs after excitation with 850 nm (left column) or with 1225 nm (right column).



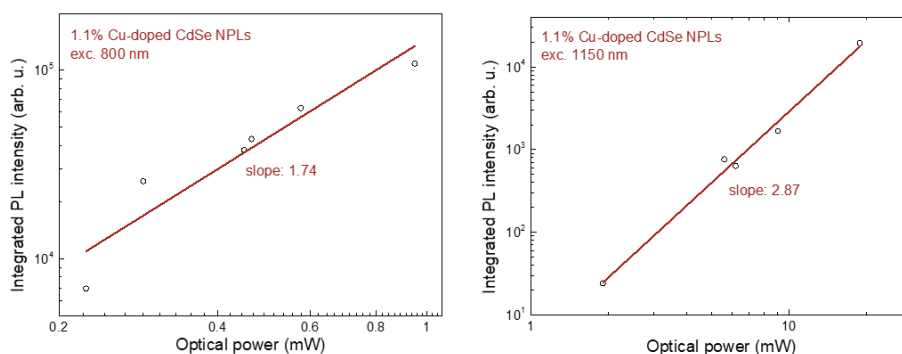


Figure 35 Dependence of PL intensity on laser beam power in logarithmic scale. Slope of the linear fits indicates the order of the multi-photon excitation process.

Excitation in both ranges results in emission presented in Figure 366 and in corresponding photographs where the formation of bright two- and three-photon excited photoluminescence spot may be observed.

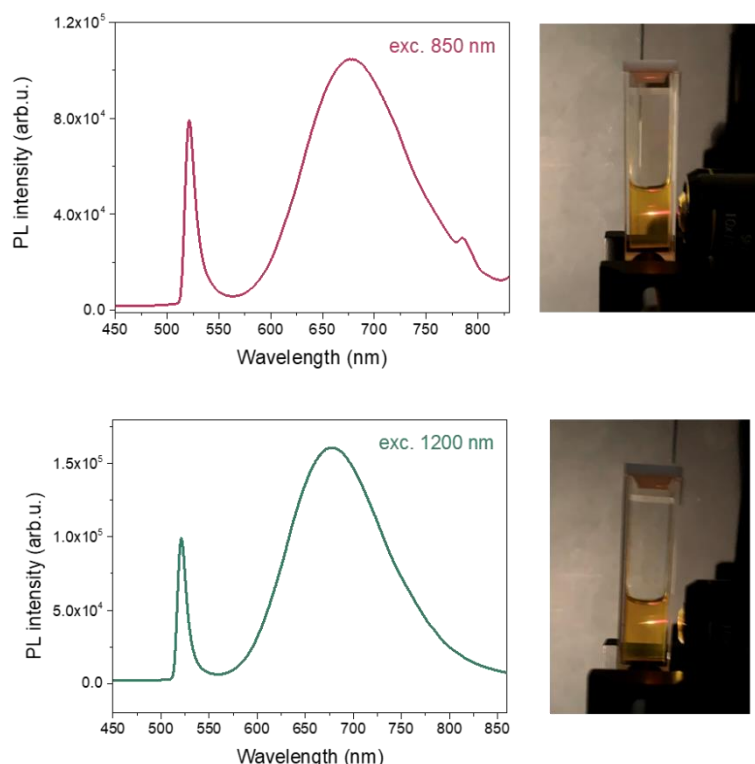


Figure 36 Representative photoluminescence spectra of 0.5% Cu-doped 4.5 ML CdSe NPLs upon excitation with 850 nm or 1200 nm along with corresponding photographs illustrating the formation of a bright two- and three-photon excited photoluminescence spot from a focused beam.

The data collected from the Z-scan measurement served for the calculation of TPA cross sections presented in respect of the wavelength as nonlinear absorption spectra (Figure 377). TPA and three-photon absorption peaks positions roughly correspond to doubled and tripled wavelengths of linear absorption peaks with typical blue-shifts [18,77].

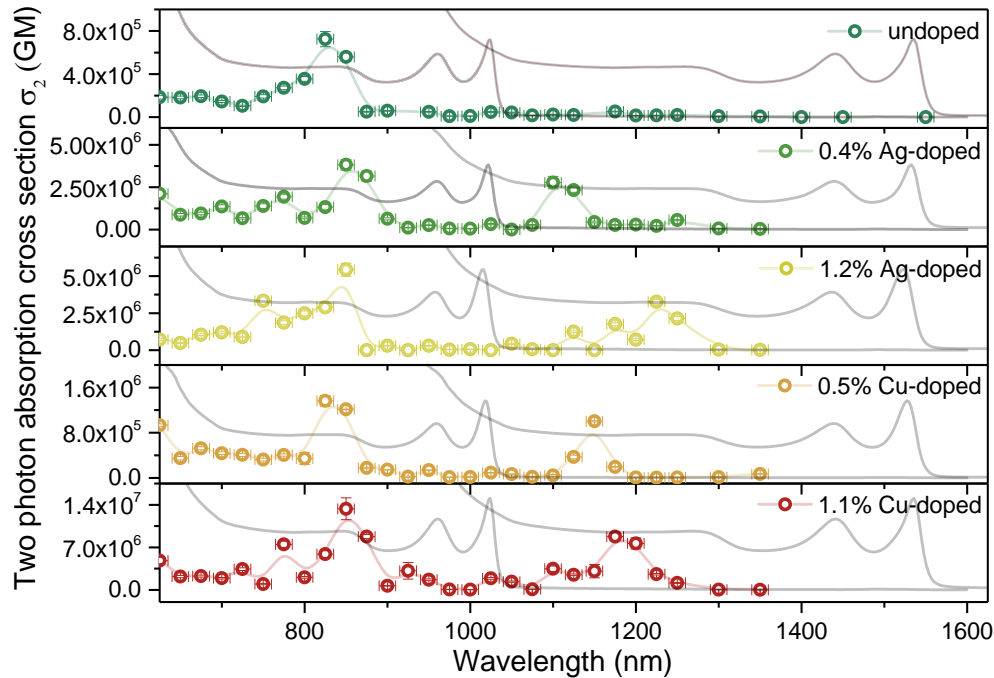


Figure 37 TPA cross section spectra of undoped, 0.4% Ag-doped, 1.2% Ag-doped, 0.5% Cu-doped and 1.1% Cu-doped 4.5 ML CdSe NPLs along with one-photon absorption spectra of doubled and tripled wavelength for comparison. Light colour lines are eye-guides (based on Nawrot et al. [5]).

The highest maximum TPA cross section was detected as  $7.25 \times 10^5$  GM for undoped NPLs (Table 9), which quite corresponds to the volume-dependence theory, although the value seems to be slightly inflated when compared to the values of a previous report.[6] This discrepancy may be attributed to possible differences in the amount or presence of defect depending on the synthesis protocols and their individual execution as well as to difference in measuring set-ups and laser working characteristics. An interesting fact is that TPA cross section of NPLs characterized for this work and the values of QRs measured using the same Z-scan set up [18] increase with volume despite dimensionality. Independently, the same tendency is visible in the results reported by Scott et al. [6] It confirms superlinearity of the relationship between volume of QRs and TPA cross section. However, such a tendency is specific only for strongly confined structures (of small

diameter), limiting flexibility in enhancing TPA cross section. In the case of NPLs, however, the potential is higher along with the possibility to lengthen two dimensions to increase TPA cross section for thin NPLs.

*Table 99 Maximum TPA cross sections together with volume- and mass-normalized factors and two-photon brightness of NPLs with different dopant levels and of different sizes (based on Nawrot et al. [5]).*

<b>4.5 ML CdSe NPLs</b>	<b>Area (nm<sup>2</sup>)</b>	<b>Wavelength (nm)</b>	<b><math>\sigma_2</math> (GM)</b>	<b><math>\sigma_2/M</math> (GM · mol·g<sup>-1</sup>)</b>	<b><math>\sigma_2/V</math> (GM · nm<sup>-3</sup>)</b>	<b><math>\sigma_2 \times QY</math> (GM)</b>
<b>Undoped</b>	132	825	$7.25 \times 10^5$ $\pm 7.01 \times 10^4$	1.31	$4.59 \times 10^3$	$1.60 \times 10^5$
<b>0.4% Ag-doped</b>	262	850	$3.82 \times 10^6$ $\pm 3.07 \times 10^5$	3.47	$1.21 \times 10^4$	$2.10 \times 10^6$
<b>1.2% Ag-doped</b>	210	850	$5.44 \times 10^6$ $\pm 4.34 \times 10^5$	6.17	$2.16 \times 10^4$	$3.26 \times 10^6$
<b>0.5% Cu-doped</b>	185	825	$1.36 \times 10^6$ $\pm 9.42 \times 10^4$	1.75	$6.12 \times 10^3$	$8.43 \times 10^5$
<b>1.1% Cu-doped</b>	213	850	$1.33 \times 10^7$ $\pm 1.79 \times 10^6$	14.8	$5.19 \times 10^4$	$9.98 \times 10^6$

The most promising TPA cross section detected in the present study is  $1.51 \times 10^7$  GM for 1.1% Cu-doped NPLs. It is worth noting that such enhanced nonlinear absorption was observed in relatively small NPLs. Compared to undoped NPLs of similar volume (Table 10), 1.1% Cu-doping allowed for more than 30 times enhanced TPA. For large NPLs even higher nonlinear absorption is expected. In fact, the doping was performed to enhance QY values and, thus indirectly, two-photon brightness but the enhancement is already present in the absorption abilities. A probable clue for explanation is that metal ions produce a resonant enhancement. Similar effects were discussed in respect of InAs/GaAs QDs by Li and Dagenais [121] and ZnSe QDs by Xing et al.[122] The synergistic effect of enhanced absorption and increased QY resulted in two-photon brightness  $\sigma_2 \times QY$  of up to  $9.98 \times 10^6$  GM, which is nearly two orders of magnitude higher than for typical undoped NPLs. Nonlinear absorption was presented as a molar-mass normalized parameter to allow comparison of material abilities and, additionally, as volume normalized absorption as

samples of different volumes are tabulated (Table and Table 99). However, the dependence between TPA and volume is not a linear function, rather a superlinear relation for such highly confined systems, thus, comparisons of any volume-dependent parameters should be done carefully with that in mind.

Table 10 NLO properties of CdSe NPs regarding their size and dimensionality.

CdSe NPs	Size (nm)	Volume (nm <sup>3</sup> )	$\lambda$ (nm)	$\sigma_2$ (GM)	$\sigma_2/M$ (GM · mol <sup>-1</sup> · g <sup>-1</sup> )	$\sigma_2/V$ (GM · nm <sup>-3</sup> )	$\sigma_2 \cdot QY$ (GM)	Reference
<b>QDs</b>	<b>Diameter</b>						<b>For assumed QY = 10%</b>	
	2.1	4.8	800	$1.44 \times 10^3$	0.08	297	$1.44 \times 10^2$	[6]
	2.7	10.3	800	$2.80 \times 10^5$	7.76	$2.7 \times 10^4$	$2.80 \times 10^4$	[6]
	3.2	17.1	800	$5.32 \times 10^3$	0.31	$1.1 \times 10^3$	$5.32 \times 10^2$	[6]
	3.2	17.1	800	$2.01 \times 10^4$	0.33	$1.2 \times 10^3$	$2.01 \times 10^3$	[77]
	4.2	38.8	970	$6.6 \times 10^4$	0.49	$1.7 \times 10^3$	$6.6 \times 10^3$	[77]
<b>QRs</b>	<b>Diameter × length</b>							
	3.1 × 7.1	54	725	$6.9 \times 10^4$	3.68	$1.3 \times 10^4$	-	[77]
	3.4 × 8.0	71	750	$1.33 \times 10^5$	5.23	$1.8 \times 10^4$	-	[77]
	3.7 × 10.7	115	750	$1.64 \times 10^5$	4.07	$1.42 \times 10^4$	-	[77]
	3 × 25	176	800	$1.45 \times 10^5$	2.34	$8.21 \times 10^3$	-	[6]
	4 × 16	200	800	$1.42 \times 10^5$	2.02	$7.07 \times 10^3$	-	[6]
<b>NPLs</b>	<b>Width × length</b>							
<b>3.5 ML</b>	5 × 5	22.5	800	$7.97 \times 10^3$	0.10	$3.54 \times 10^2$	- (up to $3.59 \times 10^3$ )	[6]
<b>3.5 ML</b>	11 × 17	168	800	$2.80 \times 10^5$	0.48	$1.66 \times 10^3$	- (up to $1.26 \times 10^5$ )	[6]

<b>4.5 ML</b>	8 × 16	153	800	$9.22 \times 10^4$	0.17	$6.00 \times 10^2$	- (up to $4.15 \times 10^4$ )	[6]
<b>4.5 ML</b>	10.2 × 12.8	157	825	$7.25 \times 10^5$	1.31	$4.59 \times 10^3$	$1.60 \times 10^5$	[5]
<b>4.5 ML</b>	8 × 32	307	800	$4.40 \times 10^5$	0.41	$1.27 \times 10^3$	- (up to $1.98 \times 10^5$ )	[6]
<b>4.5 ML</b>	13 × 26	406	800	$1.40 \times 10^6$	0.99	$3.45 \times 10^3$	- (up to $0.63 \times 10^6$ )	[6]
<b>4.5 ML</b>	23 × 27	745	800	$1.73 \times 10^6$	0.66	$2.32 \times 10^3$	- (up to $0.78 \times 10^5$ )	[6]
<b>5.5 ML</b>	22 × 82	2706	800	$4.89 \times 10^7$	5.16	$1.81 \times 10^3$	- (up to $2.2 \times 10^7$ )	[6]

Between 1100 nm and 1225 nm, a second local maximum is observed in nonlinear absorption spectra. It is plotted along with the first peak as “effective” values of  $\sigma_2$  (corresponding to light intensity of ca. 250 GW/cm<sup>2</sup>). However, as suggested by the red-shift and verified by the analysis of Z-scan traces shape (Figure 344), log-log intensity vs. laser power relationships (Figure 355) and confirmed visually by the shape of laser beam excited emission spots (Figure 366), the dominant effect in that part of spectrum are three-photon processes. In the case of undoped NPLs, the peak is hardly visible, while doping led to  $\sigma_3$  of from  $5.55 \times 10^{-75}$  cm<sup>6</sup>s<sup>2</sup> to  $4.11 \times 10^{-74}$  cm<sup>6</sup>s<sup>2</sup> (Table 10). To compare, the molar mass normalized three-photon absorption cross-section reaching up to  $4.58 \times 10^{-80}$  cm<sup>6</sup>s<sup>2</sup>mol × g<sup>-1</sup> exceeds more than twice  $\sigma_3/M$  of  $1.36 \times 10^{-82}$  cm<sup>6</sup>s<sup>2</sup> × g<sup>-1</sup>, calculated previously for CdSe QDs.[77] The results indicate that the material may be successfully excited with even further IR wavelengths (which, as a note, are in range of the second biological transmission window), what may find future applications, for instance, as a part of complex anti-counterfeiting inks.[27]

Table 10 Three-photon absorption cross section and molar mass-normalized factor of NPLs doped with different metal ions in different levels (based on Nawrot et al. [5]).

4.5 ML CdSe NPLs	Wavelength (nm)	$\sigma_3$ (cm <sup>6</sup> s <sup>2</sup> )	$\sigma_3/M$ (cm <sup>6</sup> s <sup>2</sup> mol × g <sup>-1</sup> )
<b>Undoped</b>	1025	$4.06 \times 10^{-76}$	$7.34 \times 10^{-81}$
<b>0.4% Ag-doped</b>	1100	$2.24 \times 10^{-74}$	$2.03 \times 10^{-80}$
<b>1.2% Ag-doped</b>	1225	$1.22 \times 10^{-74}$	$1.38 \times 10^{-80}$
<b>0.5% Cu-doped</b>	1150	$5.55 \times 10^{-75}$	$7.13 \times 10^{-81}$
<b>1.1% Cu-doped</b>	1175	$4.11 \times 10^{-74}$	$4.58 \times 10^{-80}$

To complete NLO characterisation, the data collected from CA Z-scan measurements was used to analyse nonlinear refraction of undoped and doped 4.5 ML CdSe NPLs. The results are presented in the form of wavelength-dependent nonlinear refractive cross section  $\sigma_R$  spectra (Figure 388) as this convenient parameter [123] allows for comparison with other materials similarly as in the case of  $\sigma_2$  parameter. Apart from anomalies appearing at the wavelengths of nonlinear absorption maxima, no unequivocal trends are observed in the spectra (Figure 38). The large scatter of the results,  $\sigma_R$  from  $-1.26 \times 10^7$  refractive GM (RGM) to  $3.39 \times 10^7$  RGM and extrapolated  $n_2$  from  $-9.95 \times 10^{-17}$  to  $3.03 \times 10^{-16}$  (Figure 399), is attributed to high disturbance of the signal caused by the solvent and the cuvette cell walls.

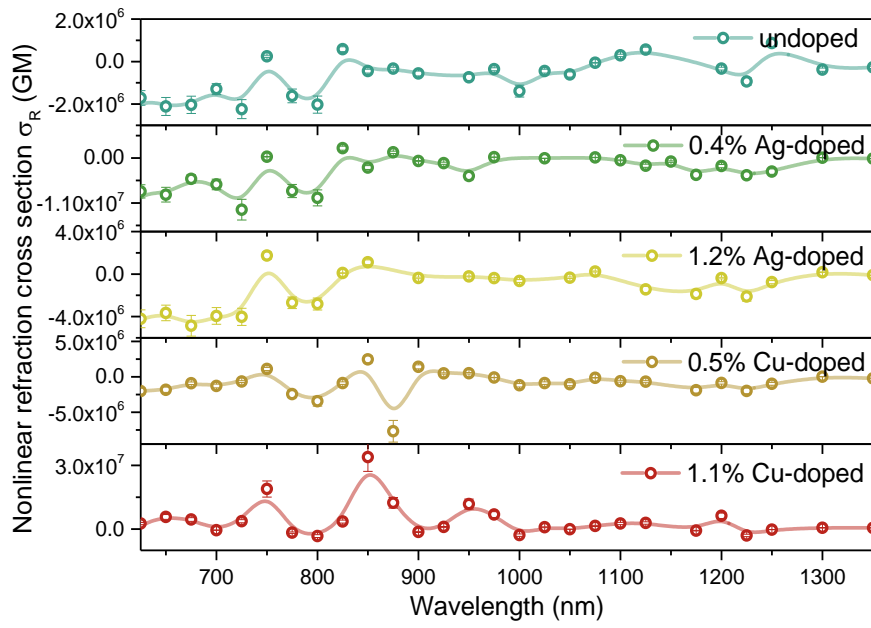


Figure 38 Nonlinear refraction cross section  $\sigma_R$  of undoped and doped NPLs. Lines are added to guide eye.

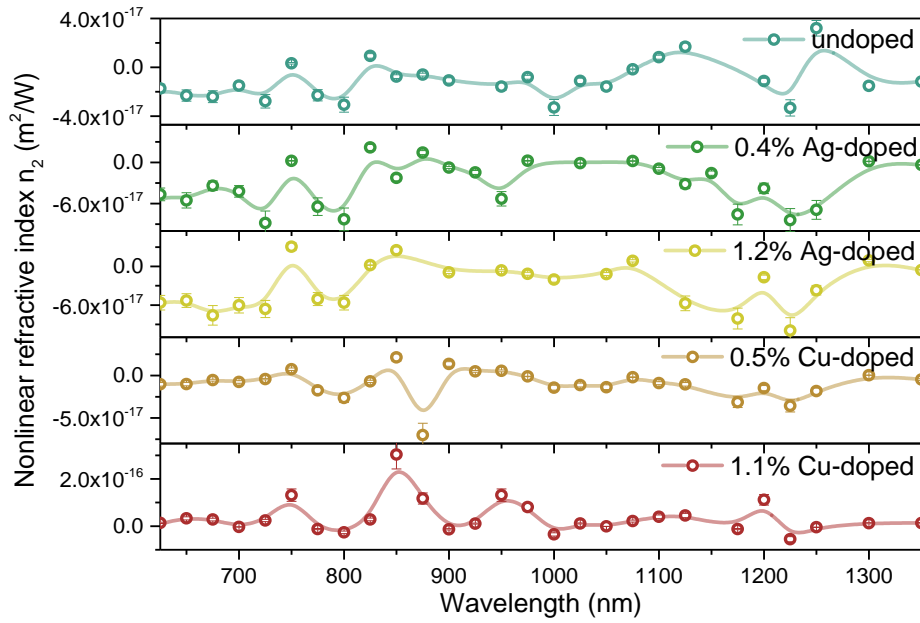


Figure 39 Nonlinear refractive index  $n_2$  of undoped and doped NPLs. Lines are added to guide eye.

Functionalisation of colloidal CdSe NPLs by doping with Ag and Cu ions resulted in enhancement of several optical parameters. With large TPA cross sections, they may serve as optical power limiters to decrease noise related to laser work or to protect sensitive sensors. As two- or three-photon excited, they produce high multiphoton brightness values, they may find applications in advanced anti-counterfeiting materials or, as the excitation ranges fall on first and second biological transmission windows, in complex multiphoton fluorescence microscopy for biological samples, even as two-band or two-colour PL markers.

## 5. CONCLUSION

As for their semiconducting and strong NLO properties together with high stability, resistance to photobleaching, high emission intensity and size-dependent optical behaviour, QDs are worth attention for application requiring separated electrons or holes and excitation within a red-shifted regime, at once or separately.

Photo-induced charge separation phenomenon was employed for hydrophilic penicillamine-capped CdS QDs and enhanced by embedment of gold nanostructures on their surface. Both reduction of MB, involving electrons, and degradation of BSA, that require the presence of positive charge, were observed to be photocatalysed by CdS-Au multifunctional nanohybrids. Although metal nanostructures are responsible for photoluminescence bleaching, it also generates a plasmon resonance effect, therefore optimisation of the amount of gold deposited on semiconductor nanostructures allowed for preservation of TPA and TPEE properties, keeping them at the level of  $15.8 \times 10^3$  GM and  $15.8 \times 10^2$  GM, respectively, making hydrophilic penicillamine-capped CdS-Au nanohybrids a model multifunctional nanomaterial for complex biological applications, for example, infra-red light-induced photodynamic therapy.

CdSe NPLs of three different thicknesses and several different aspect ratios were characterized confirming unique properties of 2D colloidal semiconductor nanomaterials including high emission intensity with strictly defined maximum positions and narrow peaks, short photoluminescence lifetimes, high values of exciton binding energies determined with a new method at the range of 130 – 230 meV, strong nonlinear absorption

even for relatively small NPLs measured as up to  $7.25 \times 10^5$  GM for the corresponding volume of merely  $132 \text{ nm}^2$ , followed by intense two-photon brightness and super-linear dependence between volume and TPA cross section. Encapsulation of 5.5 ML CdSe NPLs in polymeric carriers leads to hydrophilization and elimination of cytotoxicity with simultaneous preservation of optical activity, including the TPA cross section estimated as  $2.0 \times 10^8$  GM for NCs filled with NPLs and the two-photon brightness at the level of  $2.2 \times 10^7$  GM. The resulting material may serve as a model for biological applications, including bioimaging. The 4.5 ML CdSe NPLs were doped with copper and silver ions in different concentrations and subjected to Z-scan measurements. Both dopants presence resulted in increase in nonlinear absorption with the maximum TPA cross section calculated for 1.1% Cu-doped 4.5 ML CdSe NPLs as  $1.33 \times 10^7$  GM with the following two-photon brightness of  $9.98 \times 10^6$  GM, to my knowledge the highest values reported for 4.5 ML CdSe NPLs by now, exceeded only by nonlinear properties of 5.5 ML CdSe NPLs of far larger dimensions.[6] Moreover, pronounced three-photon absorption and three-photon excited emission were observed in 4.5 ML CdSe NPLs, with higher values in case of doped samples. High third-order nonlinear absorption is advantageous for applications requiring absorption in near infrared region, including encryption and medical fields. Doping may develop as a convenient way of enhancing absorption in QDs without enlarging their size with record values for 2D semiconductor nanomaterials.

The dissertation presents and discusses several issues at the intersection of nanophotonics and material science. It refers to the relation between structure and optical properties. Starting with the size effect, which in case of two-dimensional NPLs acts as the “thickness effect”, leading to stronger confinement in thinner NPLs, which manifests itself in emission blue-shift and higher EBE, advantageable e.g. for lasing. In case of dimensionality-dependent properties, higher-dimensional structures produce narrower and appearing in strictly defined positions emission spectra, making them more adequate for such applications as bioimaging in medical diagnosis, displaying in information technologies and sensing in military field. Again, 1D QRs and 2D NPLs exhibit higher EBE values than 0D QDs but are also characterized by superlinear volume-TPA cross section dependence and, in turn, the largest NPLs are exceptionally strong absorbers with the order of magnitude of TPA cross sections up to  $10^7$  GM. Further, the thesis demonstrates inventive ideas for functionalisation of semiconductor nanoparticles through incorporation, enhancement or inhibition of chosen properties. Introduction of new

functions was presented on the example of CdS-Au hydrophilic hybrid nanoparticles which are able to photocatalyse a reduction reaction and ROS generation and CdSe NPLs which gained hydrophilicity after encapsulation in polymeric NCs. Enhancement of TPA and two-photon brightness may be observed in NPLs doped with noble metal ions, where TPA cross section reach  $10^7$  GM, despite relatively small volume, and somehow in CdS-Au hybrid nanoparticles probably kept high due to plasmon resonance effect. Cytotoxicity of CdSe NPLs was inhibited by introduction of an encapsulating polymer barrier. SAs several characteristics may be modified in one nanomaterial to produce a multifunctional system, the number of combinations of properties possible to achieve in a semiconductor-based nanomaterial is significantly higher than the few examples described in this thesis and still waits to be designed and investigated.

## References

- [1] M.P. Moloney, J. Govan, A. Loudon, M. Mukhina, Y.K. Gun'ko, Preparation of chiral quantum dots, *Nature Protocols*. 10 (2015) 558–573.  
<https://doi.org/10.1038/nprot.2015.028>.
- [2] D. Wawrzyńczyk, Two-photon absorption in penicillamine capped CdS tetrapods, *Journal of Materials Chemistry C*. 5 (2017) 1724–1729.  
<https://doi.org/10.1039/C6TC05285A>.
- [3] K.C. Nawrot, D. Wawrzyńczyk, O. Bezkrovnyi, L. Kępiński, B. Cichy, M. Samoć, M. Nyk, Functional CdS-Au Nanocomposite for Efficient Photocatalytic, Photosensitizing, and Two-Photon Applications, *Nanomaterials*. 10 (2020) 715.  
<https://doi.org/10.3390/nano10040715>.
- [4] S.J. Zelewski, K.C. Nawrot, A. Zak, M. Gladysiewicz, M. Nyk, R. Kudrawiec, Exciton Binding Energy of Two-Dimensional Highly Luminescent Colloidal Nanostructures Determined from Combined Optical and Photoacoustic Spectroscopies, *J. Phys. Chem. Lett.* 10 (2019) 3459–3464.  
<https://doi.org/10.1021/acs.jpcllett.9b00591>.
- [5] K.C. Nawrot, M. Sharma, B. Cichy, A. Sharma, S. Delikanli, M. Samoć, H.V. Demir, M. Nyk, Spectrally Resolved Nonlinear Optical Properties of Doped *Versus* Undoped Quasi-2D Semiconductor Nanocrystals: Copper and Silver Doping Provokes Strong

- Nonlinearity in Colloidal CdSe Nanoplatelets, *ACS Photonics*. 9 (2022) 256–267.  
<https://doi.org/10.1021/acsp Photonics.1c01456>.
- [6] R. Scott, A.W. Achtstein, A. Prudnikau, A. Antanovich, S. Christodoulou, I. Moreels, M. Artemyev, U. Woggon, Two Photon Absorption in II–VI Semiconductors: The Influence of Dimensionality and Size, *Nano Letters*. 15 (2015) 4985–4992.  
<https://doi.org/10.1021/acs.nanolett.5b00966>.
- [7] J. Hulla, S. Sahu, A. Hayes, Nanotechnology: History and future, *Hum Exp Toxicol*. 34 (2015) 1318–1321. <https://doi.org/10.1177/0960327115603588>.
- [8] G. Doria, J. Conde, B. Veigas, L. Giestas, C. Almeida, M. Assunção, J. Rosa, P.V. Baptista, Noble Metal Nanoparticles for Biosensing Applications, *Sensors*. 12 (2012) 1657–1687. <https://doi.org/10.3390/s120201657>.
- [9] M. Notarianni, K. Vernon, A. Chou, M. Aljada, J. Liu, N. Motta, Plasmonic effect of gold nanoparticles in organic solar cells, *Solar Energy*. 106 (2014) 23–37.  
<https://doi.org/10.1016/j.solener.2013.09.026>.
- [10] M. Fleischer, A. Weber-Bargioni, M.V.P. Altoe, A.M. Schwartzberg, P.J. Schuck, S. Cabrini, D.P. Kern, Gold Nanocone Near-Field Scanning Optical Microscopy Probes, *ACS Nano*. 5 (2011) 2570–2579. <https://doi.org/10.1021/nn102199u>.
- [11] T. Grosjes, D. Barchiesi, Gold Nanoparticles as a Photothermal Agent in Cancer Therapy: The Thermal Ablation Characteristic Length, *Molecules*. 23 (2018) 1316.  
<https://doi.org/10.3390/molecules23061316>.
- [12] Q.A. Pankhurst, J. Connolly, S.K. Jones, J. Dobson, Applications of magnetic nanoparticles in biomedicine, *J. Phys. D: Appl. Phys.* 36 (2003) R167–R181.  
<https://doi.org/10.1088/0022-3727/36/13/201>.
- [13] O.D. Neikov, N.A. Yefimov, Nanopowders, in: *Handbook of Non-Ferrous Metal Powders*, Elsevier, 2019: pp. 271–311. <https://doi.org/10.1016/B978-0-08-100543-9.00009-9>.
- [14] Y. Kang, Z. Song, X. Jiang, X. Yin, L. Fang, J. Gao, Y. Su, F. Zhao, Quantum Dots for Wide Color Gamut Displays from Photoluminescence to Electroluminescence, *Nanoscale Res Lett*. 12 (2017) 154.  
<https://doi.org/10.1186/s11671-017-1907-1>.
- [15] R. Ding, Y. Chen, Q. Wang, Z. Wu, X. Zhang, B. Li, L. Lin, Recent advances in quantum dots-based biosensors for antibiotic detection, *Journal of Pharmaceutical Analysis*. (2021) S2095177921000885. <https://doi.org/10.1016/j.jpha.2021.08.002>.

- [16] J. Dana, P. Maity, H.N. Ghosh, Hot-electron transfer from the semiconductor domain to the metal domain in CdSe@CdS{Au} nano-heterostructures, *Nanoscale*. 9 (2017) 9723–9731. <https://doi.org/10.1039/C7NR02232H>.
- [17] G.S. He, B.A. Reinhardt, J.C. Bhatt, A.G. Dillard, G.C. Xu, P.N. Prasad, Two-photon absorption and optical-limiting properties of novel organic compounds, *Opt. Lett.* 20 (1995) 435. <https://doi.org/10.1364/OL.20.000435>.
- [18] M. Nyk, J. Szeremeta, D. Wawrzynczyk, M. Samoc, Enhancement of Two-Photon Absorption Cross Section in CdSe Quantum Rods, *J. Phys. Chem. C*. 118 (2014) 17914–17921. <https://doi.org/10.1021/jp501843g>.
- [19] J.D. Bhawalkar, N.D. Kumar, C.-F. Zhao, P.N. Prasad, Two-Photon Photodynamic Therapy, *Journal of Clinical Laser Medicine & Surgery*. 15 (1997) 201–204. <https://doi.org/10.1089/clm.1997.15.201>.
- [20] P. Gupta, M. Ramrakhiani, Influence of the Particle Size on the Optical Properties of CdSe Nanoparticles, *TONANOJ*. 3 (2009) 15–19. <https://doi.org/10.2174/1874140100903010015>.
- [21] S. Wageh, A.A. Al-Ghamdi, A.A. Al-Zahrani, H. Driss, High quantum yield Cu doped CdSe quantum dots, *Mater. Res. Express*. 6 (2019) 0850d4. <https://doi.org/10.1088/2053-1591/ab268f>.
- [22] S. Ithurria, M.D. Tessier, B. Mahler, R.P.S.M. Lobo, B. Dubertret, A.I.E. Efros, Colloidal nanoplatelets with two-dimensional electronic structure, *Nature Materials*. 10 (2011) 936–941.
- [23] K. Wu, Z. Chen, H. Lv, H. Zhu, C.L. Hill, T. Lian, Hole Removal Rate Limits Photodriven H<sub>2</sub> Generation Efficiency in CdS-Pt and CdSe/CdS-Pt Semiconductor Nanorod–Metal Tip Heterostructures, *J. Am. Chem. Soc.* 136 (2014) 7708–7716. <https://doi.org/10.1021/ja5023893>.
- [24] N. Waiskopf, Y. Ben-Shahar, U. Banin, Photocatalytic Hybrid Semiconductor-Metal Nanoparticles; from Synergistic Properties to Emerging Applications, *Adv. Mater.* 30 (2018) 1706697. <https://doi.org/10.1002/adma.201706697>.
- [25] E. Hemmer, A. Benayas, F. Légaré, F. Vetrone, Exploiting the biological windows: current perspectives on fluorescent bioprobes emitting above 1000 nm, *Nanoscale Horiz.* 1 (2016) 168–184. <https://doi.org/10.1039/C5NH00073D>.
- [26] U. Bazylińska, S. Drozdek, M. Nyk, J. Kulbacka, M. Samoć, K.A. Wilk, Core/Shell Quantum Dots Encapsulated in Biocompatible Oil-Core Nanocarriers as

- Two-Photon Fluorescent Markers for Bioimaging, *Langmuir*. 30 (2014) 14931–14943. <https://doi.org/10.1021/la504558z>.
- [27] M.A. Antoniak, D. Wawrzyńczyk, J.K. Zaręba, M. Samoć, M. Nyk, Spectrally resolved two-photon absorption properties and switching of the multi-modal luminescence of NaYF<sub>4</sub>:Yb,Er/CdSe hybrid nanostructures, *J. Mater. Chem. C*. 6 (2018) 5949–5956. <https://doi.org/10.1039/C8TC00969D>.
- [28] G.S. He, K.-T. Yong, Q. Zheng, Y. Sahoo, A. Baev, A.I. Ryasnyanskiy, P.N. Prasad, Multi-photon excitation properties of CdSe quantum dots solutions and optical limiting behavior in infrared range, *Opt. Express*. 15 (2007) 12818. <https://doi.org/10.1364/OE.15.012818>.
- [29] J.R. Lakowicz, *Principles of fluorescence spectroscopy*, 3rd ed, Springer, New York, 2006.
- [30] N.S. Makarov, M. Drobizhev, A. Rebane, Two-photon absorption standards in the 550-1600 nm excitation wavelength range, *Opt. Express*. 16 (2008) 4029. <https://doi.org/10.1364/OE.16.004029>.
- [31] M. Sheik-Bahae, A.A. Said, T.-H. Wei, D.J. Hagan, E.W. Van Stryland, Sensitive measurement of optical nonlinearities using a single beam, *IEEE J. Quantum Electron*. 26 (1990) 760–769. <https://doi.org/10.1109/3.53394>.
- [32] M. Reed, J. Randall, R. Aggarwal, R. Matyi, T. Moore, A. Wetsel, Observation of discrete electronic states in a zero-dimensional semiconductor nanostructure, *Phys. Rev. Lett*. 60 (1988) 535–537. <https://doi.org/10.1103/PhysRevLett.60.535>.
- [33] D. Bera, L. Qian, T.-K. Tseng, P.H. Holloway, Quantum Dots and Their Multimodal Applications: A Review, *Materials*. 3 (2010) 2260–2345. <https://doi.org/10.3390/ma3042260>.
- [34] P. Mushonga, M.O. Onani, A.M. Madiehe, M. Meyer, Indium Phosphide-Based Semiconductor Nanocrystals and Their Applications, *Journal of Nanomaterials*. 2012 (2012) 1–11. <https://doi.org/10.1155/2012/869284>.
- [35] X. Peng, L. Manna, W. Yang, J. Wickham, E. Scher, A. Kadavanich, A.P. Alivisatos, Shape control of CdSe nanocrystals, *Nature*. 404 (2000) 59–61. <https://doi.org/10.1038/35003535>.
- [36] K. Yu, J. Ouyang, Md.B. Zaman, D. Johnston, F.J. Yan, G. Li, C.I. Ratcliffe, D.M. Leek, X. Wu, J. Stupak, Z. Jakubek, D. Whitfield, Single-Sized CdSe Nanocrystals with Bandgap Photoemission via a Noninjection One-Pot Approach, *J. Phys. Chem. C*. 113 (2009) 3390–3401. <https://doi.org/10.1021/jp809990a>.

- [37] B. Kim, K. Kim, S. Woo, K. Jang, T. Lee, W. Kim, 11-4: Novel Switching Display using R/G/B Quantum Rods for Wide Color Gamut, *SID Symposium Digest of Technical Papers*. 49 (2018) 112–114. <https://doi.org/10.1002/sdtp.12495>.
- [38] B. Ji, Y.E. Panfil, N. Waiskopf, S. Remennik, I. Popov, U. Banin, Strain-controlled shell morphology on quantum rods, *Nat Commun*. 10 (2019) 2. <https://doi.org/10.1038/s41467-018-07837-z>.
- [39] S. Ithurria, B. Dubertret, Quasi 2D Colloidal CdSe Platelets with Thicknesses Controlled at the Atomic Level, *J. Am. Chem. Soc.* 130 (2008) 16504–16505. <https://doi.org/10.1021/ja807724e>.
- [40] J.M. Ha, S.H. Hur, A. Pathak, J.-E. Jeong, H.Y. Woo, Recent advances in organic luminescent materials with narrowband emission, *NPG Asia Mater.* 13 (2021) 53. <https://doi.org/10.1038/s41427-021-00318-8>.
- [41] T.J. Fountaine, S.M. Wincovitch, D.H. Geho, S.H. Garfield, S. Pittaluga, Multispectral imaging of clinically relevant cellular targets in tonsil and lymphoid tissue using semiconductor quantum dots, *Mod Pathol*. 19 (2006) 1181–1191. <https://doi.org/10.1038/modpathol.3800628>.
- [42] D.F. King, W.A. Radford, E.A. Patten, R.W. Graham, T.F. McEwan, J.G. Vodicka, R.E. Bornfreund, P.M. Goetz, G.M. Venzor, S.M. Johnson, J.E. Jensen, B.Z. Nosh, J.A. Roth, 3<sup>rd</sup> generation 1280 x 720 FPA development status at Raytheon Vision Systems, in: B.F. Andresen, G.F. Fulop, P.R. Norton (Eds.), Orlando (Kissimmee), FL, 2006: p. 62060W. <https://doi.org/10.1117/12.673241>.
- [43] M.F. Prodanov, V.V. Vashchenko, A.K. Srivastava, Progress toward blue-emitting (460–475 nm) nanomaterials in display applications, *Nanophotonics*. 10 (2021) 1801–1836. <https://doi.org/10.1515/nanoph-2021-0053>.
- [44] J.-W. Lim, S.U. Son, E.-K. Lim, Recent Advances in Bioimaging for Cancer Research, in: M.S. Ghamsari (Ed.), *State of the Art in Nano-Bioimaging*, InTech, 2018. <https://doi.org/10.5772/intechopen.72725>.
- [45] S.M. Geyer, J.M. Scherer, F.B. Jaworski, M.G. Bawendi, Multispectral imaging via luminescent down-shifting with colloidal quantum dots, *Opt. Mater. Express*. 3 (2013) 1167. <https://doi.org/10.1364/OME.3.001167>.
- [46] M.S. Dresselhaus, G. Chen, M.Y. Tang, R.G. Yang, H. Lee, D.Z. Wang, Z.F. Ren, J.-P. Fleurial, P. Gogna, New Directions for Low-Dimensional Thermoelectric Materials, *Adv. Mater.* 19 (2007) 1043–1053. <https://doi.org/10.1002/adma.200600527>.

- [47] A.C. Bartnik, A.I. Efros, W.-K. Koh, C.B. Murray, F.W. Wise, Electronic states and optical properties of PbSe nanorods and nanowires, *Phys. Rev. B.* 82 (2010) 195313. <https://doi.org/10.1103/PhysRevB.82.195313>.
- [48] R. Scott, A.W. Achtstein, A.V. Prudnikau, A. Antanovich, L.D.A. Siebbeles, M. Artemyev, U. Woggon, Time-Resolved Stark Spectroscopy in CdSe Nanoplatelets: Exciton Binding Energy, Polarizability, and Field-Dependent Radiative Rates, *Nano Letters.* 16 (2016) 6576–6583.
- [49] J. Hu, L. Li, W. Yang, L. Manna, L. Wang, A.P. Alivisatos, Linearly Polarized Emission from Colloidal Semiconductor Quantum Rods, *Science.* 292 (2001) 2060–2063. <https://doi.org/10.1126/science.1060810>.
- [50] G. Jia, Y. Pang, J. Ning, U. Banin, B. Ji, Heavy-Metal-Free Colloidal Semiconductor Nanorods: Recent Advances and Future Perspectives, *Adv. Mater.* 31 (2019) 1900781. <https://doi.org/10.1002/adma.201900781>.
- [51] W.U. Huynh, J.J. Dittmer, A.P. Alivisatos, Hybrid Nanorod-Polymer Solar Cells, *Science.* 295 (2002) 2425–2427. <https://doi.org/10.1126/science.1069156>.
- [52] R. Costi, A.E. Saunders, E. Elmaleh, A. Salant, U. Banin, Visible Light-Induced Charge Retention and Photocatalysis with Hybrid CdSe–Au Nanodumbbells, *Nano Letters.* 8 (2008) 637–641. <https://doi.org/10.1021/nl0730514>.
- [53] C.M. Wolff, P.D. Frischmann, M. Schulze, B.J. Bohn, R. Wein, P. Livadas, M.T. Carlson, F. Jäckel, J. Feldmann, F. Würthner, J.K. Stolarczyk, All-in-one visible-light-driven water splitting by combining nanoparticulate and molecular co-catalysts on CdS nanorods, *Nat Energy.* 3 (2018) 862–869. <https://doi.org/10.1038/s41560-018-0229-6>.
- [54] S. Christodoulou, J.I. Climente, J. Planelles, R. Brescia, M. Prato, B. Martín-García, A.H. Khan, I. Moreels, Chloride-Induced Thickness Control in CdSe Nanoplatelets, *Nano Lett.* 18 (2018) 6248–6254. <https://doi.org/10.1021/acs.nanolett.8b02361>.
- [55] A.H. Khan, R. Brescia, A. Polovitsyn, I. Angeloni, B. Martín-García, I. Moreels, Near-Infrared Emitting Colloidal PbS Nanoplatelets: Lateral Size Control and Optical Spectroscopy, *Chem. Mater.* 29 (2017) 2883–2889. <https://doi.org/10.1021/acs.chemmater.6b05111>.
- [56] W. Koh, N.K. Dandu, A.F. Fidler, V.I. Klimov, J.M. Pietryga, S.V. Kilina, Thickness-Controlled Quasi-Two-Dimensional Colloidal PbSe Nanoplatelets, *J. Am. Chem. Soc.* 139 (2017) 2152–2155. <https://doi.org/10.1021/jacs.6b11945>.

- [57] A. Reichhelm, R. Hübner, C. Damm, K. Nielsch, A. Eychmüller, Increasing the Diversity and Understanding of Semiconductor Nanoplatelets by Colloidal Atomic Layer Deposition, *Phys. Status Solidi RRL*. 14 (2020) 2000282.  
<https://doi.org/10.1002/pssr.202000282>.
- [58] F. Wang, Y. Wang, Y.-H. Liu, P.J. Morrison, R.A. Loomis, W.E. Buhro, Two-Dimensional Semiconductor Nanocrystals: Properties, Templated Formation, and Magic-Size Nanocluster Intermediates, *Acc. Chem. Res.* 48 (2015) 13–21.  
<https://doi.org/10.1021/ar500286j>.
- [59] L. Liu, Z. Zhuang, T. Xie, Y.-G. Wang, J. Li, Q. Peng, Y. Li, Shape Control of CdSe Nanocrystals with Zinc Blende Structure, *J. Am. Chem. Soc.* 131 (2009) 16423–16429. <https://doi.org/10.1021/ja903633d>.
- [60] C. Schliehe, B.H. Juarez, M. Pelletier, S. Jander, D. Greshnykh, M. Nagel, A. Meyer, S. Foerster, A. Kornowski, C. Klinke, H. Weller, Ultrathin PbS Sheets by Two-Dimensional Oriented Attachment, *Science*. 329 (2010) 550–553.  
<https://doi.org/10.1126/science.1188035>.
- [61] Y. Chen, D. Chen, Z. Li, X. Peng, Symmetry-Breaking for Formation of Rectangular CdSe Two-Dimensional Nanocrystals in Zinc-Blende Structure, *J. Am. Chem. Soc.* 139 (2017) 10009–10019. <https://doi.org/10.1021/jacs.7b04855>.
- [62] J.S. Son, X.-D. Wen, J. Joo, J. Chae, S. Baek, K. Park, J.H. Kim, K. An, J.H. Yu, S.G. Kwon, S.-H. Choi, Z. Wang, Y.-W. Kim, Y. Kuk, R. Hoffmann, T. Hyeon, Large-Scale Soft Colloidal Template Synthesis of 1.4 nm Thick CdSe Nanosheets, *Angew. Chem. Int. Ed.* 48 (2009) 6861–6864.  
<https://doi.org/10.1002/anie.200902791>.
- [63] S. Ithurria, G. Bousquet, B. Dubertret, Continuous Transition from 3D to 1D Confinement Observed during the Formation of CdSe Nanoplatelets, *J. Am. Chem. Soc.* 133 (2011) 3070–3077. <https://doi.org/10.1021/ja110046d>.
- [64] A. Riedinger, F.D. Ott, A. Mule, S. Mazzotti, P.N. Knüsel, S.J.P. Kress, F. Prins, S.C. Erwin, D.J. Norris, An intrinsic growth instability in isotropic materials leads to quasi-two-dimensional nanoplatelets, *Nature Mater.* 16 (2017) 743–748.  
<https://doi.org/10.1038/nmat4889>.
- [65] Y. Jiang, W.-S. Ojo, B. Mahler, X. Xu, B. Abécassis, B. Dubertret, Synthesis of CdSe Nanoplatelets without Short-Chain Ligands: Implication for Their Growth Mechanisms, *ACS Omega*. 3 (2018) 6199–6205.  
<https://doi.org/10.1021/acsomega.8b01006>.

- [66] N. Castro, C. Bouet, S. Ithurria, N. Lequeux, D. Constantin, P. Levitz, D. Pontoni, B. Abécassis, Insights into the Formation Mechanism of CdSe Nanoplatelets Using in Situ X-ray Scattering, *Nano Lett.* 19 (2019) 6466–6474.  
<https://doi.org/10.1021/acs.nanolett.9b02687>.
- [67] D.P. Morgan, C.J.A. Maddux, D.F. Kelley, Transient Absorption Spectroscopy of CdSe Nanoplatelets, *J. Phys. Chem. C.* 122 (2018) 23772–23779.  
<https://doi.org/10.1021/acs.jpcc.8b07733>.
- [68] W. Cho, S. Kim, I. Coropceanu, V. Srivastava, B.T. Diroll, A. Hazarika, I. Fedin, G. Galli, R.D. Schaller, D.V. Talapin, Direct Synthesis of Six-Monolayer (1.9 nm) Thick Zinc-Blende CdSe Nanoplatelets Emitting at 585 nm, *Chemistry of Materials.* 30 (2018).
- [69] R.W. Meulenbergh, J.R.I. Lee, A. Wolcott, J.Z. Zhang, L.J. Terminello, T. van Buuren, Determination of the Exciton Binding Energy in CdSe Quantum Dots, *ACS Nano.* 3 (2009) 325–330.
- [70] Y.S. Park, D.C. Reynolds, Exciton Structure in Photoconductivity of CdS, CdSe, and CdS: Se Single Crystals, *Phys. Rev.* 132 (1963) 2450–2457.  
<https://doi.org/10.1103/PhysRev.132.2450>.
- [71] R. Benchamekh, N.A. Gippius, J. Even, M.O. Nestoklon, J.-M. Jancu, S. Ithurria, B. Dubertret, A.I.L. Efros, P. Voisin, Tight-binding calculations of image-charge effects in colloidal nanoscale platelets of CdSe, *Phys. Rev. B.* 89 (2014) 035307.  
<https://doi.org/10.1103/PhysRevB.89.035307>.
- [72] A.W. Achtstein, A. Schliwa, A. Prudnikau, M. Hardzei, M.V. Artemyev, C. Thomsen, U. Woggon, Electronic Structure and Exciton–Phonon Interaction in Two-Dimensional Colloidal CdSe Nanosheets, *Nano Lett.* 12 (2012) 3151–3157.  
<https://doi.org/10.1021/nl301071n>.
- [73] G.H.V. Bertrand, A. Polovitsyn, S. Christodoulou, A.H. Khan, I. Moreels, Shape control of zincblende CdSe nanoplatelets, *Chem. Commun.* 52 (2016) 11975–11978.  
<https://doi.org/10.1039/C6CC05705E>.
- [74] G. Ramakrishna, O. Varnavski, J. Kim, D. Lee, T. Goodson, Quantum-Sized Gold Clusters as Efficient Two-Photon Absorbers, *J. Am. Chem. Soc.* 130 (2008) 5032–5033. <https://doi.org/10.1021/ja800341v>.
- [75] U. Resch-Genger, M. Grabolle, S. Cavaliere-Jaricot, R. Nitschke, T. Nann, Quantum dots versus organic dyes as fluorescent labels, *Nat Methods.* 5 (2008) 763–775. <https://doi.org/10.1038/nmeth.1248>.

- [76] J. Nam, N. Won, J. Bang, H. Jin, J. Park, S. Jung, S. Jung, Y. Park, S. Kim, Surface engineering of inorganic nanoparticles for imaging and therapy, *Advanced Drug Delivery Reviews*. 65 (2013) 622–648.  
<https://doi.org/10.1016/j.addr.2012.08.015>.
- [77] M. Nyk, D. Wawrzyńczyk, J. Szeremeta, M. Samoć, Spectrally resolved size-dependent third-order nonlinear optical properties of colloidal CdSe quantum dots, *Applied Physics Letters*. 100 (2012) 041102. <https://doi.org/10.1063/1.3679381>.
- [78] D. Wawrzyńczyk, J. Szeremeta, M. Samoć, M. Nyk, Third-Order Nonlinear Optical Properties of Infrared Emitting PbS and PbSe Quantum Dots, *The Journal of Physical Chemistry C*. 120 (2016) 21939–21945.  
<https://doi.org/10.1021/acs.jpcc.6b05956>.
- [79] A.M. Smith, M.C. Mancini, S. Nie, Second window for in vivo imaging, *Nature Nanotech.* 4 (2009) 710–711. <https://doi.org/10.1038/nnano.2009.326>.
- [80] N. Chen, Y. He, Y. Su, X. Li, Q. Huang, H. Wang, X. Zhang, R. Tai, C. Fan, The cytotoxicity of cadmium-based quantum dots, *Biomaterials*. 33 (2012) 1238–1244.  
<https://doi.org/10.1016/j.biomaterials.2011.10.070>.
- [81] C.A.M. Bonilla, M.-H.T. Flórez, D.R. Molina Velasco, V.V. Kouznetsov, Surface characterization of thiol ligands on CdTe quantum dots: analysis by <sup>1</sup>H NMR and DOSY, *New J. Chem.* 43 (2019) 8452–8458. <https://doi.org/10.1039/C8NJ05914D>.
- [82] N. Tomczak, R. Liu, J.G. Vancso, Polymer-coated quantum dots, *Nanoscale*. 5 (2013) 12018. <https://doi.org/10.1039/c3nr03949h>.
- [83] T. Delgado-Pérez, L.M. Bouchet, M. de la Guardia, R.E. Galian, J. Pérez-Prieto, Sensing Chiral Drugs by Using CdSe/ZnS Nanoparticles Capped with *N*-Acetyl- L -Cysteine Methyl Ester, *Chem. Eur. J.* 19 (2013) 11068–11076.  
<https://doi.org/10.1002/chem.201300875>.
- [84] A. Ben Moshe, D. Szwarcman, G. Markovich, Size Dependence of Chiroptical Activity in Colloidal Quantum Dots, *ACS Nano*. 5 (2011) 9034–9043.  
<https://doi.org/10.1021/nn203234b>.
- [85] S.D. Elliott, M.P. Moloney, Y.K. Gun'ko, Chiral Shells and Achiral Cores in CdS Quantum Dots, *Nano Lett.* 8 (2008) 2452–2457. <https://doi.org/10.1021/nl801453g>.
- [86] Y. Li, Y. Zhou, H.-Y. Wang, S. Perrett, Y. Zhao, Z. Tang, G. Nie, Chirality of Glutathione Surface Coating Affects the Cytotoxicity of Quantum Dots, *Angew. Chem. Int. Ed.* 50 (2011) 5860–5864. <https://doi.org/10.1002/anie.201008206>.

- [87] X. Feng, W. Ji, Shape-dependent two-photon absorption in semiconductor nanocrystals, *Opt. Express*. 17 (2009) 13140. <https://doi.org/10.1364/OE.17.013140>.
- [88] W. Sheng, S. Kim, J. Lee, S.-W. Kim, K. Jensen, M.G. Bawendi, In-Situ Encapsulation of Quantum Dots into Polymer Microspheres, *Langmuir*. 22 (2006) 3782–3790. <https://doi.org/10.1021/la051973l>.
- [89] A.R. Edmund, S. Kambalapally, T.A. Wilson, R.J. Nicolosi, Encapsulation of cadmium selenide quantum dots using a self-assembling nanoemulsion (SANE) reduces their in vitro toxicity, *Toxicology in Vitro*. 25 (2011) 185–190. <https://doi.org/10.1016/j.tiv.2010.10.017>.
- [90] J.A. Nagy, S.-H. Chang, A.M. Dvorak, H.F. Dvorak, Why are tumour blood vessels abnormal and why is it important to know?, *Br J Cancer*. 100 (2009) 865–869. <https://doi.org/10.1038/sj.bjc.6604929>.
- [91] T. Mangeolle, I. Yakavets, N. Lequeux, T. Pons, L. Bezdetnaya, F. Marchal, The targeting ability of fluorescent quantum dots to the folate receptor rich tumors, *Photodiagnosis and Photodynamic Therapy*. 26 (2019) 150–156. <https://doi.org/10.1016/j.pdpdt.2019.03.010>.
- [92] C. Yang, N. Ding, Y. Xu, X. Qu, J. Zhang, C. Zhao, L. Hong, Y. Lu, G. Xiang, Folate receptor-targeted quantum dot liposomes as fluorescence probes, *Journal of Drug Targeting*. 17 (2009) 502–511. <https://doi.org/10.1080/10611860903013248>.
- [93] S. Naskar, A. Schlosser, J.F. Miethe, F. Steinbach, A. Feldhoff, N.C. Bigall, Site-Selective Noble Metal Growth on CdSe Nanoplatelets, *Chemistry of Materials*. 27 (2015) 3159–3166. <https://doi.org/10.1021/acs.chemmater.5b01110>.
- [94] M. Sharma, K. Gungor, A. Yeltik, M. Olutas, B. Guzelurk, Y. Kelestemur, T. Erdem, S. Delikanli, J.R. McBride, H.V. Demir, Near-Unity Emitting Copper-Doped Colloidal Semiconductor Quantum Wells for Luminescent Solar Concentrators, *Adv. Mater*. 29 (2017) 1700821. <https://doi.org/10.1002/adma.201700821>.
- [95] R.W. Meulenberg, T. van Buuren, K.M. Hanif, T.M. Willey, G.F. Strouse, L.J. Terminello, Structure and Composition of Cu-Doped CdSe Nanocrystals Using Soft X-ray Absorption Spectroscopy, *Nano Lett*. 4 (2004) 2277–2285. <https://doi.org/10.1021/nl048738s>.
- [96] D. Morgan, D.F. Kelley, Role of Surface States in Silver-Doped CdSe and CdSe/CdS Quantum Dots, *J. Phys. Chem. C*. 122 (2018) 10627–10636. <https://doi.org/10.1021/acs.jpcc.8b02776>.

- [97] J.E. Govan, E. Jan, A. Querejeta, N.A. Kotov, Y.K. Gun'ko, Chiral luminescent CdS nano-tetrapods, *Chem. Commun.* 46 (2010) 6072.  
<https://doi.org/10.1039/c0cc00930j>.
- [98] J. Szeremeta, M. Nyk, D. Wawrzynczyk, M. Samoc, Wavelength dependence of nonlinear optical properties of colloidal CdS quantum dots, *Nanoscale*. 5 (2013) 2388. <https://doi.org/10.1039/c3nr33860f>.
- [99] J. He, J. Mi, H. Li, W. Ji, Observation of Interband Two-Photon Absorption Saturation in CdS Nanocrystals, *J. Phys. Chem. B.* 109 (2005) 19184–19187.  
<https://doi.org/10.1021/jp0534028>.
- [100] X. Li, J. van Embden, J.W.M. Chon, M. Gu, Enhanced two-photon absorption of CdS nanocrystal rods, *Appl. Phys. Lett.* 94 (2009) 103117.  
<https://doi.org/10.1063/1.3100196>.
- [101] N. Waiskopf, Y. Ben-Shahar, M. Galchenko, I. Carmel, G. Moshitzky, H. Soreq, U. Banin, Photocatalytic Reactive Oxygen Species Formation by Semiconductor–Metal Hybrid Nanoparticles. Toward Light-Induced Modulation of Biological Processes, *Nano Lett.* 16 (2016) 4266–4273.  
<https://doi.org/10.1021/acs.nanolett.6b01298>.
- [102] E. Shaviv, O. Schubert, M. Alves-Santos, G. Goldoni, R. Di Felice, F. Vallée, N. Del Fatti, U. Banin, C. Sönnichsen, Absorption Properties of Metal–Semiconductor Hybrid Nanoparticles, *ACS Nano*. 5 (2011) 4712–4719.  
<https://doi.org/10.1021/nn200645h>.
- [103] B.T. Diroll, D.V. Talapin, R.D. Schaller, Violet-to-Blue Gain and Lasing from Colloidal CdS Nanoplatelets: Low-Threshold Stimulated Emission Despite Low Photoluminescence Quantum Yield, *ACS Photonics*. 4 (2017) 576–583.  
<https://doi.org/10.1021/acsp Photonics.6b00890>.
- [104] S. Delikanli, B. Guzelturk, P.L. Hernández-Martínez, T. Erdem, Y. Kelestemur, M. Olutas, M.Z. Akgul, H.V. Demir, Continuously Tunable Emission in Inverted Type-I CdS/CdSe Core/Crown Semiconductor Nanoplatelets, *Adv. Funct. Mater.* 25 (2015) 4282–4289. <https://doi.org/10.1002/adfm.201500403>.
- [105] H. Woznica, M. Banski, A. Podhorodecki, CdS Dots, Rods and Platelets—How to Obtain Predefined Shapes in a One-Pot Synthesis of Nanoparticles, *Materials*. 14 (2021) 476. <https://doi.org/10.3390/ma14030476>.
- [106] M.D. Tessier, P. Spinicelli, D. Dupont, G. Patriarche, S. Ithurria, B. Dubertret, Efficient Exciton Concentrators Built from Colloidal Core/Crown CdSe/CdS

- Semiconductor Nanoplatelets, *Nano Lett.* 14 (2014) 207–213.  
<https://doi.org/10.1021/nl403746p>.
- [107] M. Dufour, E. Izquierdo, C. Livache, B. Martinez, M.G. Silly, T. Pons, E. Lhuillier, C. Delerue, S. Ithurria, Doping as Strategy to Tune Color of 2D colloidal Nanoplatelets, *ACS Applied Materials & Interfaces.* 11 (2019) 10128–10134.
- [108] A.A. Mitioglu, P. Plochocka, Á. Granados del Aguila, P.C.M. Christianen, G. Deligeorgis, S. Anghel, L. Kulyuk, D.K. Maude, Optical Investigation of Monolayer and Bulk Tungsten Diselenide ( $\text{WSe}_2$ ) in High Magnetic Fields, *Nano Lett.* 15 (2015) 4387–4392. <https://doi.org/10.1021/acs.nanolett.5b00626>.
- [109] A.V. Stier, K.M. McCreary, B.T. Jonker, J. Kono, S.A. Crooker, Exciton diamagnetic shifts and valley Zeeman effects in monolayer  $\text{WS}_2$  and  $\text{MoS}_2$  to 65 Tesla, *Nature Communications.* 7 (2016) 1–8.
- [110] M.D. Tessier, C. Javaux, I. Maksimovic, V. Lorient, B. Dubertret, Spectroscopy of Single CdSe Nanoplatelets, *ACS Nano.* 6 (2012) 6751–6758.  
<https://doi.org/10.1021/nn3014855>.
- [111] M. Olutas, B. Guzelturk, Y. Kelestemur, A. Yeltik, S. Delikanli, H.V. Demir, Lateral Size-Dependent Spontaneous and Stimulated Emission Properties in Colloidal CdSe Nanoplatelets, *ACS Nano.* 9 (2015) 5041–5050.  
<https://doi.org/10.1021/acs.nano.5b01927>.
- [112] M.A. Antoniak, U. Bazylińska, D. Wawrzyńczyk, M. Ćwierzona, S. Maćkowski, D. Piątkowski, J. Kulbacka, M. Nyk, Enhancing optical functionality by co-loading  $\text{NaYF}_4:\text{Yb,Er}$  and CdSe QDs in a single core-shell nanocapsule, *J. Mater. Chem. C.* 8 (2020) 14796–14804. <https://doi.org/10.1039/D0TC03538F>.
- [113] M.A. Antoniak, J. Grzyb, M. Nyk, Preserved two-photon optical properties of hydrophilic proteins-conjugated quantum dots, *Journal of Luminescence.* 209 (2019) 57–60. <https://doi.org/10.1016/j.jlumin.2019.01.029>.
- [114] K.C. Nawrot, J.K. Zareba, M. Toporkiewicz, G. Chodaczek, D. Wawrzyńczyk, J. Kulbacka, U. Bazylińska, M. Nyk, Polymeric Nanocarriers with Luminescent Colloidal Nanoplatelets as Hydrophilic and Non-Toxic Two-Photon Bioimaging Agents, *IJN. Volume 16* (2021) 3649–3660. <https://doi.org/10.2147/IJN.S298300>.
- [115] M.A. Antoniak, R. Pązik, U. Bazylińska, K. Wiwatowski, A. Tomaszewska, M. Kulpa-Greszta, J. Adamczyk-Grochala, M. Wnuk, S. Maćkowski, A. Lewińska, M. Nyk, Multimodal polymer encapsulated CdSe/ $\text{Fe}_3\text{O}_4$  nanoplatfrom with improved biocompatibility for two-photon and temperature stimulated bioapplications,

- Materials Science and Engineering: C. 127 (2021) 112224.  
<https://doi.org/10.1016/j.msec.2021.112224>.
- [116] X. Wang, J. Hao, J. Cheng, J. Li, J. Miao, R. Li, Y. Li, J. Li, Y. Liu, X. Zhu, Y. Liu, X.W. Sun, Z. Tang, M.-H. Delville, T. He, R. Chen, Chiral CdSe nanoplatelets as an ultrasensitive probe for lead ion sensing, *Nanoscale*. 11 (2019) 9327–9334.  
<https://doi.org/10.1039/C8NR10506E>.
- [117] S. Mansouri, Y. Cuie, F. Winnik, Q. Shi, P. Lavigne, M. Benderdour, E. Beaumont, J.C. Fernandes, Characterization of folate-chitosan-DNA nanoparticles for gene therapy, *Biomaterials*. 27 (2006) 2060–2065.  
<https://doi.org/10.1016/j.biomaterials.2005.09.020>.
- [118] T.H. Kim, I.K. Park, J.W. Nah, Y.J. Choi, C.S. Cho, Galactosylated chitosan/DNA nanoparticles prepared using water-soluble chitosan as a gene carrier, *Biomaterials*. 25 (2004) 3783–3792.  
<https://doi.org/10.1016/j.biomaterials.2003.10.063>.
- [119] H.D. Nelson, S.O.M. Hinterding, R. Fainblat, S.E. Creutz, X. Li, D.R. Gamelin, Mid-Gap States and Normal vs Inverted Bonding in Luminescent Cu<sup>+</sup> - and Ag<sup>+</sup> - Doped CdSe Nanocrystals, *J. Am. Chem. Soc.* 139 (2017) 6411–6421.  
<https://doi.org/10.1021/jacs.7b01924>.
- [120] M. Samoc, J.P. Morrall, G.T. Dalton, M.P. Cifuentes, M.G. Humphrey, Two-Photon and Three-Photon Absorption in an Organometallic Dendrimer, *Angew. Chem.* 119 (2007) 745–747. <https://doi.org/10.1002/ange.200602341>.
- [121] M. Dagenais, Non-resonant below-bandgap two-photon absorption in quantum dot solar cells, *Appl. Phys. Lett.* 106 (2015) 171101. <https://doi.org/10.1063/1.4919381>.
- [122] G. Xing, W. Ji, Y. Zheng, J.Y. Ying, Two- and three-photon absorption of semiconductor quantum dots in the vicinity of half of lowest exciton energy, *Appl. Phys. Lett.* 93 (2008) 241114. <https://doi.org/10.1063/1.3049132>.
- [123] M. Balu, L.A. Padilha, D.J. Hagan, E.W. Van Stryland, S. Yao, K. Belfield, S. Zheng, S. Barlow, S. Marder, Broadband Z-scan characterization using a high-spectral-irradiance, high-quality supercontinuum, *J. Opt. Soc. Am. B.* 25 (2008) 159.  
<https://doi.org/10.1364/JOSAB.25.000159>.

## Appendix (Achievements)

### Publications included in PhD thesis

1. Nawrot K.C., Wawrzyńczyk D., Bezkravnyi O., Kępiński L., Cichy B., Samoć M., Nyk M., Functional CdS-Au Nanocomposite for Efficient Photocatalytic, Photosensitizing, and Two-Photon Applications, *Nanomaterials*. 10 (2020) 715. <https://doi.org/10.3390/nano10040715>.
2. Zelewski S.J., Nawrot K.C., Żak A., Gladysiewicz M., Nyk M., Kudrawiec R., Exciton Binding Energy of Two-Dimensional Highly Luminescent Colloidal Nanostructures Determined from Combined Optical and Photoacoustic Spectroscopies, *J. Phys. Chem. Lett.* 10 (2019) 3459–3464. <https://doi.org/10.1021/acs.jpcclett.9b00591>.
3. Nawrot K.C., Zareba J.K., Toporkiewicz M., Chodaczek G., Wawrzyńczyk D., Kulbacka J., Bazylińska U., Nyk M., Polymeric Nanocarriers with Luminescent Colloidal Nanoplatelets as Hydrophilic and Non-Toxic Two-Photon Bioimaging Agents, *Int J Nanomedicine*. Volume 16 (2021) 3649–3660. <https://doi.org/10.2147/IJN.S298300>.
4. Nawrot K.C., Sharma M., Cichy B., Sharma A., Delikanli S., Samoć M., Demir H.V., Nyk M., Spectrally Resolved Nonlinear Optical Properties of Doped *Versus* Undoped Quasi-2D Semiconductor Nanocrystals: Copper and Silver Doping Provokes Strong Nonlinearity in Colloidal CdSe Nanoplatelets, *ACS Photonics*. 9 (2022) 256–267. <https://doi.org/10.1021/acsphotonics.1c01456>

### Publications not included in PhD thesis

1. Ośmiałowski, B. Petrusевич E.F., Nawrot K.C., Paszkiewicz B.K., Nyk M., Zielak J., Jędrzejewska B., Luis J.M., Jacquemin D., Zaleśny R., Tailoring the nonlinear absorption of

fluorescent dyes by substitution at a boron center, *Journal of Materials Chemistry C*, 9 (2021) 6225-6233

2. Nawrot K.C., Nyk M., Encapsulated quantum dots as biocompatible imaging agents for cancer diagnosis, *Optoelectronics and Microsystems: proceedings of 2017 International Students and Young Scientists Workshop: 8-10 September 2017, Szklarska Poręba, Poland, Wydawnictwo GMORK*, (2018) 47-52.

## Conference presentations

1. Nawrot K.C., Nyk M., Encapsulated quantum dots as biocompatible imaging agents for cancer diagnosis, 2017 International Students and Young Scientists Workshop, 2017, Szklarska Poręba (oral presentation)

2. Nawrot K.C., Żak A., Nyk M., "Potential bioimaging agents for cancer diagnosis in form of highly efficient semiconductor nanoplatelets", XXIIIrd International Krutyn Summer School "Advanced Lanthanide Molecules and Materials for Bioimaging and Medical Diagnostics: State of the Art", 2018, Krutyń (poster)

3. Chachuła M., Nawrot K.C., Wawrzyńczyk D., Nyk M., "Interaction between penicillamine-stabilized CdS nanotetrapods and gold nanostructures", 11th International Conference on Nanophotonics, 2018, Wrocław (poster)

4. Nawrot K.C., Wawrzyńczyk D., Nyk M., Applications of the charge transfer phenomenon occurring in hybrid semiconductor-metal nanosystems, 2018 International Students and Young Scientists Workshop "Optoelectronics and Microsystems Packaging", 2018, Drezno (oral presentation)

5. Nawrot K.C., Wawrzyńczyk D., Bezkrovnyi O., Kępiński L., Cichy B., Samoć M., Nyk M., CdS-Au Nanocomposite for Efficient Photocatalytic and Photosensitizing Applications, PhoBia Annual Nanophotonics International Conference (PANIC), 2019, Wrocław (oral presentation)

6. Nawrot K.C., Bazylińska U., Nyk M., Preserved optical properties and reduced toxicity of colloidal semiconductor nanoplatelets encapsulated in polymeric nanospheres, 5th International Workshop on Nano and Bio-Photonics, 2019, Saint-Nectaire (Francja) (oral presentation)

7. Nawrot K.C., Wawrzyńczyk D., Nyk M., Multifunctional CdS-Au nanocomposite, PANIC, 2020, Wrocław (oral presentation)
8. Nawrot K.C., Bazylińska U., Kulbacka J., Nyk M., Fluorescent polymeric nanocarriers of low cytotoxicity for two-photon bioimaging, 4th International Wrocław Scientific Meetings, 2020, Wrocław (oral presentation)
9. Nawrot K.C., Nyk M., How to introduce fluorescent nanoparticles into a biological system?, PhoBiA Annual Nanophotonics International Conference, 2021, Wrocław (oral presentation)